

# **Swarm Carrier: An Autonomous, Multi-vehicle System Capable of Deploying and Recovering Groups of sUAS**

**MEIE 4701/4702**

## **Technical Design Report**

### **Swarm Carrier: An Autonomous, Multi-vehicle System Capable of Deploying and Recovering Groups of sUAS**

**Fall Report 2**

**Design Advisor: Professor Mehdi Abedi**

#### **Design Team**

**John Buczek, Joshua Field,  
Erik Little, Blake McHale,  
Noah Ossanna, Michael Tang**

**December 10, 2021**

**Department of Mechanical and Industrial Engineering**

**College of Engineering, Northeastern University**

**Boston, MA 02115**

# **Swarm Carrier: An Autonomous, Multi-vehicle System Capable of Deploying and Recovering Groups of sUAS**

## **Design Team**

**John Buczek, Joshua Field,  
Erik Little, Blake McHale,  
Noah Ossanna, Michael Tang**

## **Design Advisor**

**Professor Mehdi Abedi**

## **Abstract**

The purpose of the Swarm Carrier capstone is to design, manufacture, and demonstrate a system to deploy and recover several small unmanned aerial systems (sUASs) from a carrier unmanned aerial system (UAS). Development for this capstone focused on achieving system-level functionality defined by a full-circle test of deployment, recovery, and mission execution. Hardware developments concern finite element analysis (FEA) of UAS designs, system validation tests, and subsequent design iterations of the Carrier Drone, Swarm Drones, and Multidrop Bay. Software development focuses on behavior trees, autonomous landings, Drop Mode, and collaborative swarm control. The concept of the Swarm Carrier system and its sub-components originated from research conducted by AerospaceNU. Building upon this, Capstone-specific development involved final prototypes and integration as well as system-level software development to achieve the full test. The end goal of Swarm Carrier was to demonstrate the possibility of a deployable, multi-vehicle robotic system. The system-level test demonstrated use of off the shelf (OTS) controllers, software packages, and composite airframe design to accomplish a novel approach to enhancing the operational capabilities of unmanned aerial vehicles (UAVs).

# Contents

<b>1</b>	<b>Acronyms</b>	<b>7</b>
<b>2</b>	<b>Acknowledgements</b>	<b>9</b>
<b>3</b>	<b>Introduction</b>	<b>9</b>
3.1	Problem Statement . . . . .	9
3.2	Goals . . . . .	9
3.3	UAS Definition . . . . .	10
3.4	Constraints . . . . .	10
3.5	Concept Development . . . . .	11
3.5.1	Swarm UAS Applications . . . . .	11
3.5.2	Swarm UAS Limitations . . . . .	12
3.5.3	Solutions to Limitations . . . . .	12
<b>4</b>	<b>Background</b>	<b>12</b>
4.1	Existing Technologies . . . . .	12
4.2	Key Theories . . . . .	15
4.2.1	Co-Axial Motor Thrust Loss . . . . .	15
4.2.2	Propulsion Systems . . . . .	16
4.2.3	Airframe Design . . . . .	16
4.2.4	ArUco Markers . . . . .	18
4.2.5	Behavior Trees . . . . .	19
4.3	Previous Work . . . . .	20
4.3.1	Swarm Drones . . . . .	20
4.3.2	Drop Mode . . . . .	25
4.3.3	Multidrop Bay . . . . .	27
4.3.4	Carrier Drone . . . . .	30
4.3.5	Companion Computing . . . . .	31
4.3.6	Simulation . . . . .	34
4.3.7	Path Planning . . . . .	34
4.4	Regulations . . . . .	35
<b>5</b>	<b>Designs</b>	<b>36</b>
5.1	Flowchart Overview . . . . .	36
5.2	Swarm Carrier System Level Objective Re-evaluations . . . . .	40
5.3	Carrier Drone . . . . .	42
5.3.1	Cable Tensioning . . . . .	48
5.3.2	Carbon Fiber Tolerance Stackup Issues . . . . .	53
5.3.3	Carbon Fiber Material Evaluation . . . . .	53
5.3.4	Motor Mount Design . . . . .	54
5.3.5	Carrier Drone Battery Mechanism . . . . .	57
5.3.6	Motor Configuration . . . . .	60

5.3.7	Power Distribution . . . . .	64
5.3.8	FEA of Carrier Drone . . . . .	65
5.4	Behavior Trees . . . . .	66
5.5	Drop Mode . . . . .	68
5.6	Precision Landing . . . . .	68
5.7	Multidrop Bay . . . . .	71
5.7.1	Multidrop Bay Lattice and Connector Optimization . . . . .	73
5.7.2	Multidrop Bay Connections to Carrier Drone . . . . .	75
5.7.3	Landing Guides . . . . .	85
5.7.4	Actuators . . . . .	95
5.8	Swarm Drone V3 Design . . . . .	98
5.9	Simulation . . . . .	103
5.10	Visualization . . . . .	106
5.11	Design Validation . . . . .	109
5.11.1	Thrust Tests . . . . .	109
5.11.2	Precision Land . . . . .	110
5.11.3	Motor Kill Test . . . . .	114
5.11.4	Drop Mode Test . . . . .	118
5.11.5	Carrier Drone V1 Air Frame Test . . . . .	121
5.11.6	Carrier Drone V3 Air Frame Test . . . . .	127
5.11.7	Multi-system Integration Tests . . . . .	131
5.12	Design Review: MassDOT . . . . .	136
5.13	Final Design . . . . .	137
5.14	Regulations . . . . .	138
<b>6</b>	<b>Conclusions</b>	<b>138</b>
<b>7</b>	<b>Intellectual Property</b>	<b>140</b>
7.1	Description of Problem . . . . .	140
7.2	Proof of Concept . . . . .	140
7.3	Progress to Date . . . . .	141
7.4	Individual Contributions . . . . .	143
7.5	Future Work . . . . .	143
<b>8</b>	<b>References</b>	<b>144</b>

## List of Figures

1	Multicopter vs. Fixed Wing Capability [1]	10
2	Multicopter deployment and recovery method [2]	13
3	Fixed wing swarm deployment and recovery method [3]	14
4	Single, coaxial, and parallel motor mounting configurations [4]	16
5	Industry airframe design example: Freefly Systems Alta X [5]	17
6	Example ArUco pose estimation [6]	18
7	Example Behavior Tree vs. finite-state machine (FSM) design [7]	19
8	Swarm Drone V1	22
9	Waterjet-cut carbon fiber components	23
10	Swarm Drone V2	24
11	Swarm Drone V2.0 fleet of six vehicles	25
12	Octocopter with three FPV quadcopters for the initial test of Drop Mode	26
13	Drop Mode testing	27
14	Early Drone Drop Mechanism Prototype	28
15	Multidrop Bay V2	29
16	Carrier Drone proof of concept	30
17	Carrier Drone scale model	31
18	Corner connector design progression	31
19	Example of QGroundControl GUI [8]	32
20	Communication framework between Pixhawk 4 (PX4) and Robot Operating System 2 (ROS2) [9]	33
21	coverage path planning (CPP)	35
22	High level task flowchart	37
23	System flowchart	39
24	System level objective re-evaluation weighted decision matrix	41
25	Carrier Drone V1	43
26	Carrier Drone V2 CAD	44
27	Carrier Drone V3 CAD	45
28	Overview of frame member reuse between V1 and V3	46
29	Carrier Drone Design Progression	47
30	Carrier Drone V3 tensioning schemes	49
31	Carrier Drone cable tensioning	50
32	Cable tension clamp to Carrier Drone	51
33	Field assembly of the Carrier Drone	52
34	Carrier Drone Motor Mount	55
35	Final Carrier Drone Mount	56
36	Battery mechanism	58
37	Location of the battery mechanism (highlighted blue) on the Carrier Drone V3	59
38	Coaxial thrust test results	61
39	Experimental results design decisions	62
40	Prediction design decisions	63
41	Carrier Drone V3 theoretical flight time calculation	64

42	Power distribution printed circuit board (PCB)	65
43	High-level precision land behavior tree	67
44	Precision landing in simulation	70
45	ArUco landing array V2	71
46	Multidrop Bay V3	72
47	Multidrop Bay V2-V3 connector iterations	73
48	Multidrop Bay V3 connector configuration	74
49	Aligned interface clamp between Carrier Drone and Multidrop Bay	76
50	Hyperbolic profile of clamp	77
51	Real life application of clamp to frame	78
52	Offset between Multidrop and Carrier frames	79
53	Unaligned interface clamp	80
54	Real life application of clamp to frame	81
55	Deflection of bottom of Multidrop Bay	82
56	Fix to Multidrop Bay rigidity using cable tensioning	83
57	Cable tensioning to fix Multidrop Bay sagging	84
58	Landing guide designs for Swarm Drone reintegration	86
59	Landing Guides	88
60	Top down view of old and new guides	89
61	Accuracy calculations for autonomous landing	90
62	Top down view of Multidrop Bay with new guides	91
63	Side view showing interference gap between propellers and top of guides	92
64	Revised ArUco target placement: Multidrop Bay	93
65	ArUco design iterations	94
66	Motorized Linkages	96
67	Anti-jam spacer on the Multidrop bay's actuators	97
68	Swarm Drone V3 CAD	99
69	Swarm Drone V3 motor mount with collision sensing	100
70	Swarm Drone contact sensing schematic	101
71	Second contact sensor iteration: compliant, damping geometry	102
72	Custom Swarm Drone in simulation	104
73	Custom Carrier Drone V2 in simulation	104
74	Custom Carrier Drone V3 in simulation	105
75	ROSBoard running in simulation	107
76	Foxglove running in simulation	108
77	RCbenchmark S1780 Motor Thrust Test Stand with Coaxial Configuration	109
78	Flowchart: Precision landing test in a Multidrop Bay	111
79	Swarm Drone performing a precision landing during testing	113
80	Swarm Drone performing a precision landing on Carrier Drone	113
81	Contact sensing test: failed motor kill	115
82	Contact sensing test: successful motor kill	117
83	Drop mechanism utilized for the Drop Mode test	119
84	Drop mechanism interfaced with the Swarm Drone	119
85	Drop Mode test overview	120

86	Wall Drop Mode test long exposure . . . . .	121
87	Examples of damage to the Carrier Drone V1 (Post Crash) . . . . .	123
88	Carrier Drone V1 successful hover . . . . .	124
89	Pixhawk 4 flight logs for Carrier Drone V1 quadcopter hover test . . . . .	126
90	Tethered Carrier Drone flight test . . . . .	128
91	Untethered Carrier Drone Test . . . . .	129
92	Team picture: Carrier Drone V3 maiden flight . . . . .	130
93	Carrier Drone hovering with two Swarm Drones . . . . .	132
94	Carrier Drone loaded before flight tests . . . . .	133
95	Drop deployment of a single Swarm Drone from the Carrier Drone . . . . .	134
96	Long exposure of the Swarm Drone deploying from the Carrier Drone . . . . .	135
97	CAD of completed system . . . . .	137
98	Completed system . . . . .	138

**List of Tables**

2	Related Patents . . . . .	14
3	IP team member contributions . . . . .	143

# 1 Acronyms

<b>ACP</b>	ANSYS Composite PrepPost 65
<b>AMA</b>	Academy for Model Aeronautics 9, 138
<b>AUW</b>	all-up weight 10, 16, 25, 52
<b>CNC</b>	computerized numerical control 30, 31, 52, 53, 84
<b>CPP</b>	coverage path planning 4, 34, 35
<b>DDD</b>	data-driven decision 110
<b>DFM</b>	design for manufacturing 18, 21
<b>EMI</b>	electromagnetic interference 112
<b>ESC</b>	electronic speed controller 54, 64, 65
<b>FAA</b>	Federal Aviation Administration 9, 10, 35
<b>FC</b>	flight controller 26, 27, 53, 125
<b>FEA</b>	finite element analysis 1, 65
<b>FMU</b>	Flight Management Unit 98
<b>FPV</b>	first person view 26
<b>FSM</b>	finite-state machine 4, 19
<b>GPIO</b>	general-purpose input/output 69, 101, 114
<b>GPS</b>	Global Positioning System 20, 34, 68, 103, 106, 112
<b>GUI</b>	graphical user interface 31, 106, 139
<b>HITL</b>	Hardware-in-the-Loop 34
<b>I2C</b>	Inter-integrated Circuit 38, 95
<b>IMU</b>	inertial measurement unit 26, 34, 103, 106
<b>MassDOT</b>	Massachusetts Department of Transportation 36, 138
<b>OTS</b>	off the shelf 1, 20, 30, 131
<b>PCB</b>	printed circuit board 5, 18, 21, 64, 65
<b>PDB</b>	power distribution board 18
<b>PID</b>	proportional-integral-derivative 68
<b>PX4</b>	Pixhawk 4 4, 20, 26, 31–34, 68, 98, 103, 121
<b>RGB-D</b>	Red Green Blue Depth 103
<b>ROS2</b>	Robot Operating System 2 4, 18, 32–34, 66, 95, 103, 106, 114, 116
<b>RTPS</b>	Real Time Publisher Subscriber 31, 32

**SAR** search and rescue 34  
**SITL** Software-in-the-Loop 34  
**SOP** standard operating procedure 110  
**sUAS** small unmanned aerial system 1, 10, 11, 25–27, 30, 35, 42, 127

**UAS** unmanned aerial system 1, 9, 10, 12–16, 18, 26, 27, 30, 35, 36, 38, 60, 64, 118, 127, 138

**UAV** unmanned aerial vehicle 1, 10, 11, 34, 35

**UGV** unmanned ground vehicle 11

**URDF** Unified Robot Description Format 103

## **2 Acknowledgements**

The Swarm Carrier team would like to thank its advisor, Professor Abedi for providing improved direction and critiques towards the quality of presentations of complex systems. Alongside faculty members, Alexander Wittich (Assistant Director of Northeastern's Risk Services) consistently expedited the team's requests for vehicle tests. His work allowed for the validation of the Swarm Carrier system within a realistic timeframe. The team would like to specifically express its gratitude towards Professor Gouldstone for his incredibly active role in the years leading up to and during the culmination of Swarm Carrier as a Capstone project. Lastly, for her review of many documents, critiques of presentations, and overall oversight of the program, recognition of Professor Smyser is required. Her extensive feedback elevated the team's communication skills and made the concepts of the project understandable to wider audiences.

Swarm Carrier originated from years of research and development by dozens of students within Northeastern University's aerospace engineering club: AerospaceNU (AIAA). The team wishes to express its appreciation towards the club's members, advisors, and numerous E-Boards since 2017 that were instrumental in the genesis of this project.

The project's success is also attributed to collaboration with other capstone teams, notably Forest Sensor Drone. From exchange of information to shared design use and testing transportation, they propelled the timelines of Swarm Carrier forward.

Outside of Northeastern University members, the Swarm Carrier team would like to express its thanks towards Noel Zamot, Rob Knochenhauer, and other members of the MassDOT. From their review of the system, the team gained invaluable connections to high-level Federal Aviation Administration (FAA) and Academy for Model Aeronautics (AMA) representatives and insight into the most up to date drone regulations.

## **3 Introduction**

### **3.1 Problem Statement**

The problem statement for this Capstone Project is to design, manufacture, and test a system capable of deploying and recovering a swarm of multirotor UAS.

### **3.2 Goals**

The goal of this capstone is a proof of concept for a swarm UAS deployment and recovery system. Success metrics can be broken down into the individual subsystem tasks of deploying and recovering UAS. The primary objectives are successful subsystem tests for aerially deploying a singular Swarm Drone and recovering a single Swarm Drone in separate tests. Following the confirmation of these subsystems, a full deployment and recovery test of a single Swarm Drone was performed. Finally, after successful single Swarm Drone testing, full Swarm Drone payload testing was performed to fully confirm the functionality of the deployment and recovery system.

### 3.3 UAS Definition

UAV are defined as un-piloted flight systems that consist of a vehicles and their associated sensors, payloads, propulsion. The distinction between sUAS and UAS is driven by weight requirements dictated by the FAA. For vehicles below 55 lb all-up weight (AUW) on takeoff, the distinction of sUAS is officially recognized. Correspondingly, vehicles over 55 lb are defined as UAS and require special flight approval. Fig. 1 below breaks down sUAS and UAS into broad categories of multirotors and fixed wing vehicles. Multirotors are defined by vehicles that use electronically-controlled brushless motors to adjust attitude in flight and provide lift. In comparison, fixed wing vehicles use an airfoil and control surfaces for thrust and attitude adjustments, respectively. These differences define key strengths and weaknesses of each vehicle such as comparisons between flight time, maneuverability, and payload capability [1].



Figure 1: Multirotor vs. Fixed Wing Capability [1]

Of the comparisons listed above, capabilities relating to control precision, payload capability, and flight time are the most critical for multi-vehicle systems. For such applications, multirotors have the benefit of increased fidelity of control but suffer from shorter flight times. Fixed wing vehicles have greater range but are larger and far less maneuverable than the former vehicle type [1]. The purpose of the Swarm Carrier system is to combine the strengths of these vehicles to create a multirotor system capable of longer mission duration and high fidelity tasks such as deployment and recovery.

### 3.4 Constraints

Prior to this project, some work had been done towards the development of a swarm of sUAS. While Section 4.3 outlines the previous work in greater detail, this section provides the physical constraints for this design of a system to deploy and recover a swarm of UAS. From previous work, it is known that the Swarm Drones each weigh approximately 2.3kg with a maximum flight time of 9 minutes. A total of 3 Swarm Drones was deployed and recovered. Both the Carrier Drone and

all the Swarm Drones were fully autonomous and require synchronous communication both inter-drone and with the ground station for system monitoring. Finally, the Carrier Drone was required to have a minimum flight time of 15 minutes with the full payload of all Swarm Drones. This final constraint is to ensure sufficient flight time for all the Swarm Drones to be deployed.

### 3.5 Concept Development

The above goals originated from the fact that alongside many applications of UAV are limitations in range, effectiveness, and payload capacity. Many tasks need to be performed quickly, precisely, and over unknown terrain which are demanding feats for any *individual* flight system. However, by combining multiple vehicles to accomplish goals, mission capabilities can be increased by distributing the demands of tasks across multiple agents. This section outlines example use cases, their limitations, and the solution of Swarm Carrier: a multi-vehicle systems to accomplish tasks more quickly.

#### 3.5.1 Swarm UAS Applications

Applications of single and multi-vehicle drone systems largely involve time-sensitive or large area coverage missions. The motive for these is the increased efficiency associated with UAV over unmanned ground vehicle (UGV) or manned operations. Current applications include search and rescue in spatially denied or large environments, wildfire detection, Naloxone delivery, and geological surveying. [10] describes applications of UAV to autonomously recognize injured personnel and deliver medical supplies. Their investigation provides an excellent example of automation of search and rescue to remove survivability barriers. Such barriers include the limited response times of volunteer rescue teams and the legal ramifications of parks or property owners having to publicly declare lost individuals. Furthermore, [11] provides an outline of a drone-system to monitor wildfires faster than existing satellite methods with the goal of limiting human intervention. Specifically, they formulate a variety of collaborative drone behaviors, such as leaders and zones of occupation, to efficiently search an area with multiple vehicles. In addition to wilderness operations, [12] performed a case study on the use of drones to deliver Naloxone to overdose victims faster than manned methods. Naloxone is a nasal medication administered to victims of opioid overdose that if performed rapidly, can save the life on an individual. Results showed that the use of sUAS drastically decreased the time interval required between 9-1-1 calls and antidote administration. Lastly, a study performed by [13] found that UAV can be applied for precise coastal surveying missions with equivalent accuracy to existing methods and easier implementation.

From the analysis of the above sources, it should be understood that the mission of a UAV is directly a function of payload. For time-sensitive and area coverage use cases, rescue versus delivery versus data collection are all dictated by what the system carries. Studies also outlined the greater efficiency of task completion using one or multiple UAV. Based on the assumption of vehicle modularity and known benefits of multiple vehicles from research, it was affirmed that any of the above tasks could be optimized, in terms of efficiency, speed, and simplicity, using a rapidly deployable group of multiple sUAS.

### 3.5.2 Swarm UAS Limitations

While there are endless applications for swarms of multirotor UAS, the main reason that they are not prevalent today is because of flight time limitations. Flight time  $t_f$  can be calculated as:

$$t_f = \frac{E_T}{P_T}. \quad (1)$$

Where  $E_T$  is the total energy capacity ( $J$ ) on board the UAS and  $P_T$  is the total power consumption ( $W$ ) of the UAS. For multirotor UAS, typical flight times are below 45 minutes and decrease with additional payload weight [14]. For a swarm of UAS, total flight time becomes more of an issue when the swarm needs to traverse to a target region before performing their application.

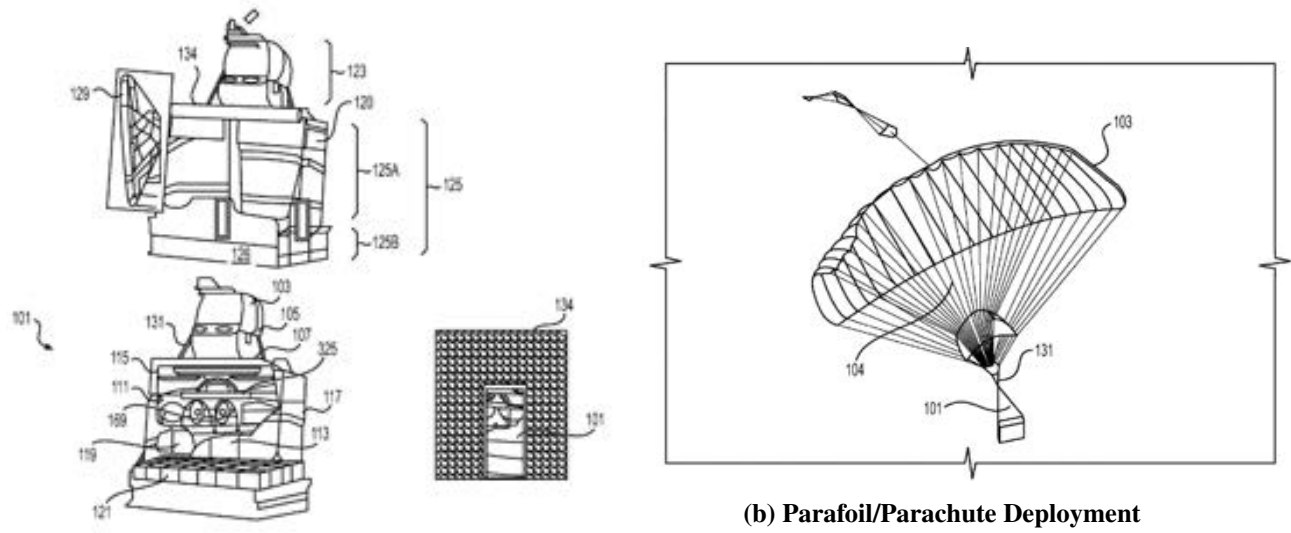
### 3.5.3 Solutions to Limitations

There are numerous ways to increase the flight time of a UAS. The easiest is to increase the battery capacity with a larger battery. However, increasing the battery also increases the overall drone weight and causes the motors to draw more power [14]. Other solutions include increasing individual drone sizes as larger multirotor UAS can typically fly for longer at the same payload weight. This may not be possible if the Swarm Drone size is a constraint due to their application. Another possible solution is to incorporate on-board power generation. Current solar technologies unfortunately are insufficient for sustained multirotor flight and gasoline generation requires a significantly larger airframe. The solution that this work focuses on is the use of the Swarm Carrier system. It consists of a large aerial vehicle that acts as a mobile carrier for smaller, deployable vehicles. The rest of this report will elaborate on this system in great detail, starting context on UAS provided in Section 4.

## 4 Background

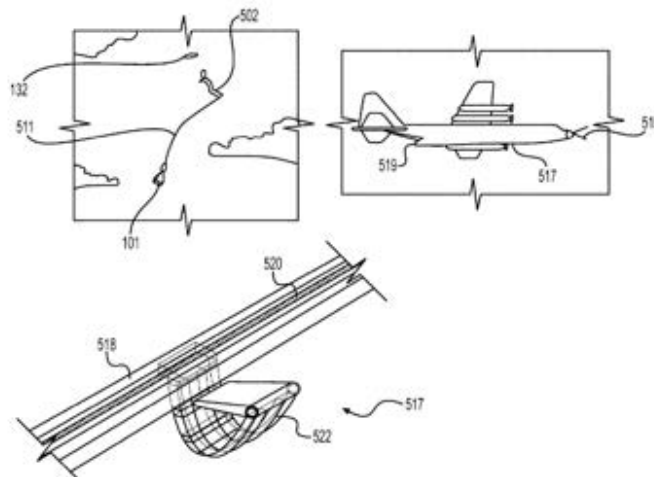
### 4.1 Existing Technologies

Existing patents and technology were researched in order to determine novelty and assist in the brainstorming process. Both fixed wing and multirotor patents were considered due to the greater number of fixed wing UAS deployment and recovery methods. The only method found for deploying and recovering multirotors specifically was in [2] which outlined the process of using a cargo plane to aerially drop a packaged multirotor. Once the package was dropped, a parafoil or parachute would deploy and guide the UAS safely to the ground. Once landed, the package would open and deploy the UAS. The recovery system outlined in [2] involved a grappling cable that the cargo plane would snare to recover the UAS. Figure 2 displays the UAS package, parafoil deployment, and grapple recovery from [2]. This and several other patents use a grapple hook and line or similar methods to recover drones. This method was deemed insufficient for swarm applications as it would require at least one grapple line and hook per drone or would require a human operator to reset the apparatus between drone recoveries.



(a) Packaged UAS

(b) Parafoil/Parachute Deployment



(c) Cable grapple snare recovery

Figure 2: Multirotor deployment and recovery method [2]

Another patent similar to the solution proposed in this paper for UAS deployment and recovery was [3]. In [3], an airborne runway underneath the fuselage of a manned plane was used to both deploy and recover fixed wing UAS. The fuselage of the manned plane would act as a storage hanger with an elevator to the lower runway. Thus multiple UAS could be deployed and recovered. Figure 3 displays the deployment and recovery method from [3]. This runway method of recovery was deemed impossible for multirotors as they typically cannot achieve air speeds comparable to manned aircraft and the drones in this scheme would need to fly faster than the manned aircraft in order to land.

Table 2 compares the solution presented in this work to the existing patents regarding the deployment and recovery of UAS. The criteria compared includes the UAS type being recovered or deployed, the number of UAS affected, the carrier vehicle extending the UAS range, the deployment method, and the recovery method. The vast majority of discovered works were designed for

fixed wing UAS due to multirotors only being developed recently [15]. The only works found developing a deployment or recovery method specifically for multirotor UAS was [2]. The number of UAS deployed or recovered was recorded as the vast majority of systems are only capable of deploying or recovering a single UAS without the need for human resetting of their respective mechanisms. The only works found developing multi-UAS deployment or recovery systems were [16, 3]. The inclusion of both the deployment and recovery methods stems from many of the existing patents either only presenting a solution to deploy or only a system to recover their respective UAS. The method for deployment, storage, and recovery of UAS presented in this paper is unique and novel.

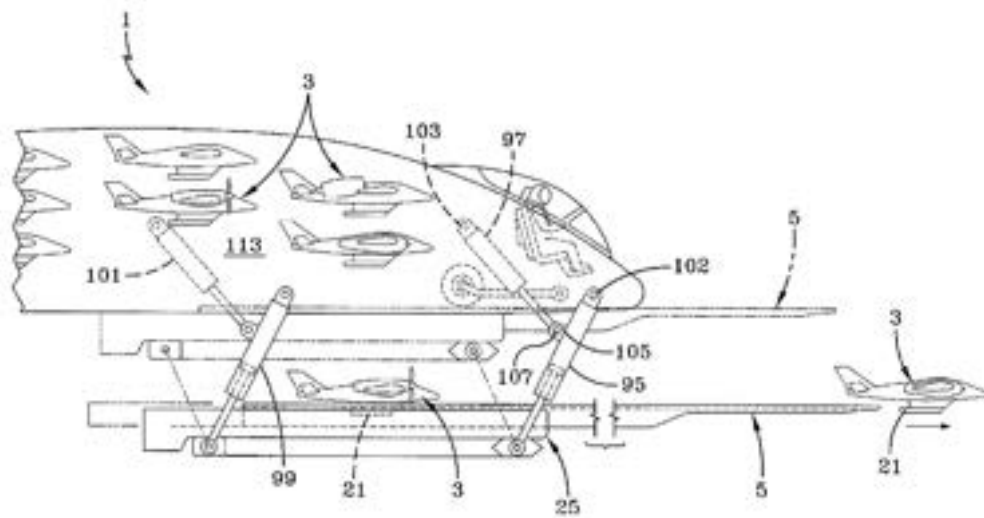


Figure 3: Fixed wing swarm deployment and recovery method [3]

Table 2: Related Patents

Patent	UAS Type	Num. UAS	Carrier Vehicle	Deployment Method	Recovery Method
[17]	Fixed Wing	1	Ship	-	Horizontal Net
[18]	Fixed Wing	1	Ship	-	Vert. Line Hook
[19]	Fixed Wing	1	-	-	Vertical Net
[20]	Fixed Wing	1	Aircraft	-	Aircraft External Arms
[21]	Fixed Wing	1	-	-	Horiz. Line Hook
[22]	Fixed Wing	1	Multirotor	Airdrop	Aerial Interception
[23]	Fixed Wing	1	Rover	Landing Pad	Landing Pad
[24]	Fixed Wing	1	Ship	Latching Cable	Latching Cable
[25]	Fixed Wing	1	Blimp	-	Engagement Cage
[26]	Fixed Wing	1	-	-	Pneumatic Net
[27]	Fixed Wing	1	Ship	-	Horizontal Net
[28]	Fixed Wing	1	Ship	-	Arm Hook Snag
[29]	Fixed Wing	1	-	-	Arresting Hook
[16]	Fixed Wing	> 1	Aircraft	Missile	-
[3]	Fixed Wing	> 1	Airplane	Airborne Runway	Airborne Runway
[2]	Multirotor	1	Airplane	Parachute Airdrop	Cable Snag Aircraft
<b>this work</b>	Multirotor	> 1	Multirotor	Tube Airdrop	Aerial Landing Pad

## 4.2 Key Theories

The design and development of a multi-vehicle UAS demands mastery of theories of propulsion, airframe design, computer vision, and autonomous decision making. In the pursuit of the Swarm Carrier system, extensive research and experimentation was performed to validate key methodologies such as those relating to motor configuration and flight algorithms. Subsequent sections show the results of these efforts and represent crucial methodologies that were leveraged to develop the project.

### 4.2.1 Co-Axial Motor Thrust Loss

One of the key issues in designing a multirotor UAS is the choice of propulsion system. The original quadcopter design from the 2000s has since been incorporated into various other solutions from tricopters to dodecaopters and beyond [15]. In addition to different numbers of motors, new mounting methods have been attempted. Other than single motor mounting, another popular motor mounting technique is the coaxial motor mounting. Fig. 4 displays the top, side, and isometric views for single, coaxial, and parallel motor mountings. For coaxial motors, two oppositely rotating rotors are mounted such that the central orthogonal axes of the rotors are colinear and the rotors are separated by a planar distance ( $D_P$ ). Similarly, the parallel motor mounting configuration involves two oppositely rotating rotors positioned such that the orthogonal axes of the rotors are parallel and separated by an axial distance ( $D_A$ ). For both coaxial and parallel mounting configurations it is common to rotate the rotors in opposite directions to equalize the momentum of the platform [4]. The benefits of coaxial and parallel mounting in multirotors is that they increase the overall thrust output of the multirotor with minimal increase in overall vehicle size. They allow for more compact vehicle designs and increased payload capacities. The drawback of coaxial and parallel mounting with overlapping rotors is that motor thrust to electrical power efficiency decreases. For coaxial mounting, the *upper* motor has a thrust to electrical power output consistent with that of a single motor, but the *lower* motor operates in the output airflow of the *upper* motor and has a significantly worse thrust to electrical power output than the single motor configuration. This is due to the *lower* motor spinning in turbulent air that already has a significant velocity. Since the air already has a velocity, the spinning *lower* propeller induced less velocity and thus less force onto the turbulent air thus producing lower upward thrust force for the same electrical power input. In experiments, this phenomenon has recorded an average motor thrust loss of up to 23% [4, 30, 31]. In studies, it has been found that increasing the planar distance does not significantly affect the coaxial motor thrust loss. Parallel mounting with overlapping propellers also causes thrust loss, but increasing the axial distance of the motors reduces thrust loss [30, 31].

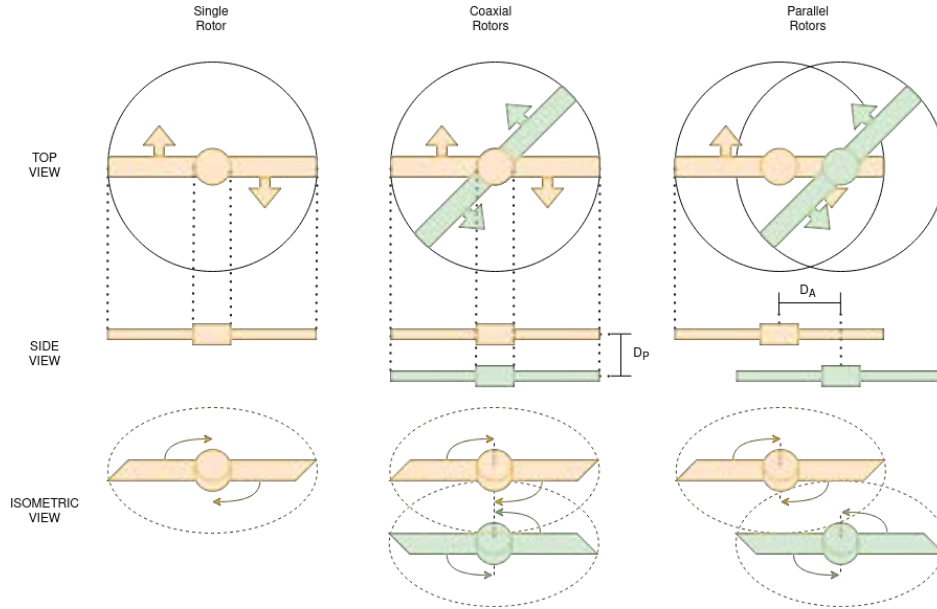


**Figure 4: Single, coaxial, and parallel motor mounting configurations [4]**

#### 4.2.2 Propulsion Systems

The method for choosing the motors, propellers, and batteries for a UAS can be determined from the desired application of the UAS. Design methodologies similar to those listed in [14] are used where the wireless systems, computational needs, payload, and desired flight time are first determined. From the needed electronics, the computational power  $P_C$  (W), Radio Power  $P_R$  (W), and payload power  $P_P$  (W) can be determined. The flight time in Eqn. 1 can be expanded as:

$$t_f = \frac{E_T}{P_F + P_C + P_R + P_P + P_{loss}}. \quad (2)$$

Where  $P_F$  is the power required to keep the UAS airborne (W) and  $P_{loss}$  is the lost power (W). From [14], assuming that the lost power is significantly less than the other powers, UAS flight time can be approximated as:

$$t_f \approx \frac{0.8Batt_{Wh}}{n * P_m(AUW/n) + P_C + P_R + P_P}. \quad (3)$$

Where  $Batt_{Wh}$  is the carried battery energy capacity (J),  $n$  is the number of motors,  $P_m(kgf)$  is the individual motor electrical power consumption (W) as a function of motor thrust (kgf), and  $AUW$  is the total AUW of the UAS and all attached items \*prior to takeoff (kg). Once the airframe is either chosen or designed, then the iterative method of choosing propellers, motors, and batteries outlined in [14] can be used to determine the overall flight time of the system.

#### 4.2.3 Airframe Design

To implicate motor configurations of propulsion systems outlined in sections 4.2.1 and 4.2.2, UAS require airframes that are both lightweight and inflexible. These must withstand the reaction forces

from motor impulses, steady state thrust output, and external forces such as wind to constrain deformation and be durable. To do so, the most common materials employed are woven carbon fiber sheets and tubes, injection molded plastic, 3D printed nylon alloys, and small aluminum parts in highly critical areas. Fig. 5 below shows an example of composite and molded airframe design by Freefly Systems for cinematography robotics. By leveraging carbon fiber laminate and machined components, the AltaX can achieve over 30 minutes of flight time with a payload of 10 lbs [5].



**Figure 5: Industry airframe design example: Freefly Systems Alta X [5]**

Due to the high ultimate strengths associated with these materials, static failure, in an ideal design, is far less likely during normal operation than damage resulting from vibration. As such, the engineer must mitigate elastic deformations in order to prevent high frequency oscillations from propagating through the frame and to critical inertial sensors. Methods to accomplish this include developing vibration-damped mounts for key components, utilizing thread-lock or nyloc hardware, and using a combination of airframe members in tension and compression to distribute load without flexing. Cable tensioning is also a common method for the development of larger UAS to prevent deformations without added weight from additional rigid members. Furthermore, simplicity of design is critical for optimizing cost and manufacturability. Carbon fiber is specifically costly and difficult to machine which necessitates airframes to be developed with a design for manufacturing (DFM) focus. Integration of electronics also becomes a challenge, especially for heavy-lift vehicles that require high steady-state current consumption. For this, custom designed power distribution boards (PDBs) and PCBs can be developed to simplify and easily integrate peripherals.

#### 4.2.4 ArUco Markers

ArUco markers are simple, matrix based fiducial markers that are easy for cameras to detect and compute a relative 3D pose. They are easy to view by using common computer vision techniques such as corner detection. This is why they are built from black and white squares. There are other popular visual fiducial marker systems such as Apriltags and ARtags. However, the ArUco system was chosen as its detection library has been built into the OpenCV, an open source computer vision library, making it easy to use with Python and subsequently ROS2. Additionally, the ArUco library makes use of error detection and correction techniques when decoding detected markers [6]. An example of marker detection and pose estimation is in Fig. 6.

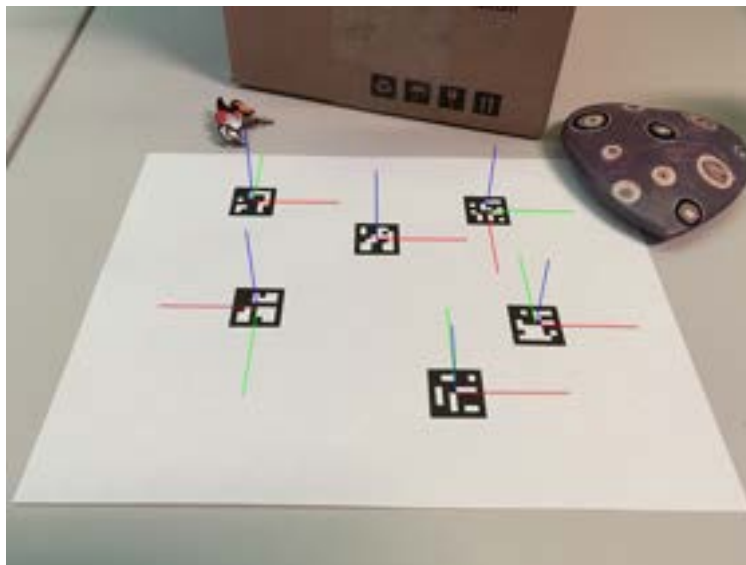
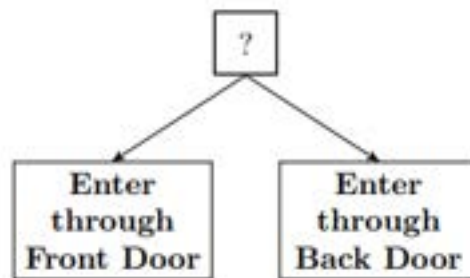


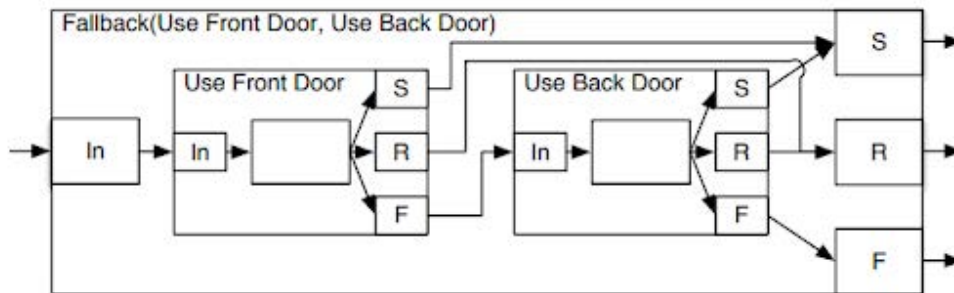
**Figure 6: Example ArUco pose estimation [6]**

#### 4.2.5 Behavior Trees

Behavior trees were used for high level mission architecture. Behavior trees are essentially hierarchical state machines. They have been used extensively in video game artificial intelligence as well as robotics and allow for reactive, modular missions to be executed. The most common comparison is to FSM. However, behavior trees are more expressive and easier to read or create due to the semantic meaning behind their structure. They are read left to right and top-down and contain modular logic blocks that enforce complex control flows. FSM can encapsulate the same logic of a behavior tree but it can get tedious quickly, as shown in Fig. 7. When constructing a behavior tree, the user does not have to define logic for success, running, or failure end conditions [7].



(a) Behavior Tree for entering a room



(b) FSM for entering a room

Figure 7: Example Behavior Tree vs. FSM design [7]

### 4.3 Previous Work

The Swarm Carrier system originated from a cluster of research projects called Northeastern UAV (NUAV). These were founded and lead by the authors of this paper as a project in 2018 within Northeastern University’s aerospace club AerospaceNU (AeroNU) with the goal of exposing students to drone and robotics research. Swarm Carrier emerged in 2019 as the main initiative of the project with substantial following in both hardware and software domains. Since 2019, the authors investigated a variety of methods to achieve the project’s goal such as compact drone design, drop and landing payloads, sensor selection, autonomy development, and economic manufacturing routes. This section outlines the results of research which were early prototypes of Swarm Carrier’s subsystems and flight algorithms. In Section 5, these independent prototypes are extensively iterated and subject to integration within the larger Swarm Carrier system.

#### 4.3.1 Swarm Drones

Independently, designing and developing drones is relatively easy with many solutions built off commercial platforms and widely accessible documentation. However, the integration of both of these functionalities in a custom system is far less trivial, especially when sizing constraints exist. Commercial solutions such as those by DJI and Skydio offer excellent flight performance, sensors and on-board computation but are prohibitive at \$13,000 – \$20,000 per vehicle [32], [33]. This solution drives many companies to develop their own vehicles capable of fitting a certain envelop while also allowing for custom software development [34]. Due to cost constraints and the niche operational requirements of Swarm Carrier, development of a custom vehicle, the Swarm Drone, was similarly pursued.

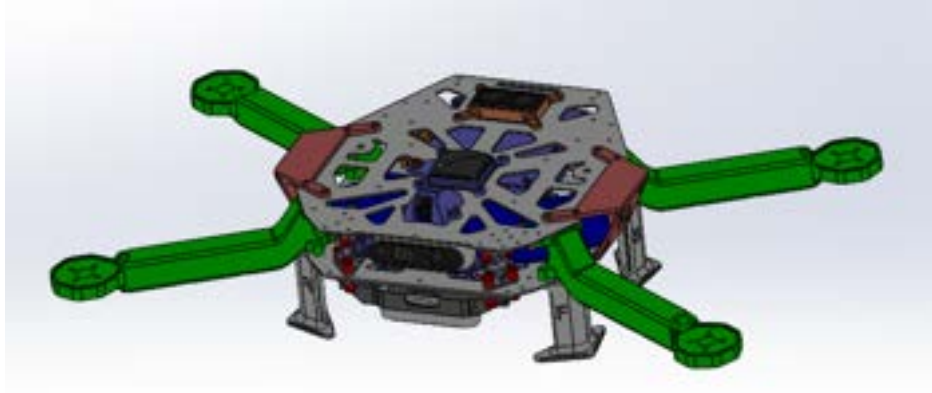
The previous development of the Swarm Drones was the most important foundational element of the Swarm Carrier system. As the agents meant to test flight algorithms and perform autonomous missions, early Swarm Drone prototypes were compact quadcopters. These combined Global Positioning System (GPS) based navigation with an on-board flight computer to facilitate advanced capabilities. To accomplish a variety of missions, they required a PX4 flight controller, Nvidia Jetson Nano computer, GPS, camera, and various other power distribution electronics. With these requirements, spatial constraints rapidly prevailed, so compact designs that retained required functionality were a critical point of research leading up to summer 2021.

In addition to their autonomous requirement, the Swarm Drones were developed with the notion that one day, they would have to be compatible with a deployment and reintegration mechanism. In order to remain future proof in this regard, the Swarm Drones needed to be as compact in one axis as possible with little to no external sensors that might be subject to damage during interactions with this mechanism. Therefore, research shifted to custom airframes that were specifically designed to house the electronics that the goal autonomy required. The reintegration mechanism is discussed in depth in Section 4.3.3.

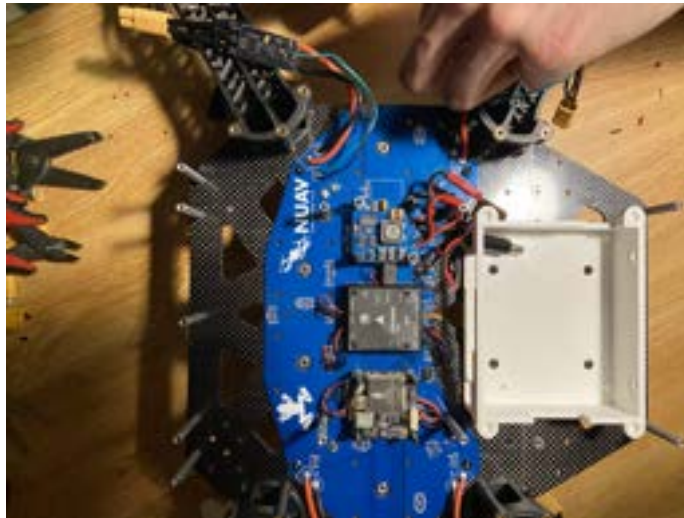
The first iteration, titled Swarm Drone V1, was developed specifically around OTS electronics to accomplish autonomous tasks. To meet future unknown methods of deployment, the overall vehicle’s height was minimized in order to make them ”stackable” in deployment mechanisms. Fig. 8 and Fig. 9 show early iterations of the Swarm Drone V1 that utilized waterjet carbon fiber as a rapid manufacturing process. The design also utilized 3D printed polycarbonate arms (shown

in green) and a custom PCB (shown in blue) to organize electronics and sensors.

The prototype represented a substantial progression toward better DFM methods but was ultimately a failure due to poor handling and durability, short flight time, and being too large in the direction of its planar axes. Subsequent iterations, embodied as the Swarm Drone V2, sought to further decrease form factor and weight to increase flight time with an equivalent feature set. Shown in Fig. 10a, the Swarm Drone V2's notable improvements were a symmetric design and more compact PCB that increased vehicle performance and flight time respectively. The images below show the elimination of all unnecessary space in the design as well as a flight test that proved more stable than the V1 design.



(a) V1 CAD model



(b) V1 flight electronics



(c) V1 initial prototype

Figure 8: Swarm Drone V1



**Figure 9: Waterjet-cut carbon fiber components**



**(a) V2 CAD model**



**(b) V2 flight electronics**



**(c) V2 prototype flight test**

**Figure 10: Swarm Drone V2**

Similar to the V1, the Swarm Drone V2 utilized mostly carbon fiber construction to be as light weight and inflexible as possible. It successfully increased flight times to approximately nine minutes and decreased AUW to under 2.5 kg. The V2 design was deemed functional enough to scale production to an additional five vehicles to make up the rest of the swarm. Fig. 11 below shows an image of all 6 of the early Swarm Drone V2 prototypes.



**Figure 11: Swarm Drone V2.0 fleet of six vehicles**

While successful, the V2 design was still not sufficient to properly interface with the emerging deployment and recovery concepts. Furthermore, requirements for electronics changed due to software developments towards newer flight controller firmware. As a result of these emerging requirements, a final V3 version of the Swarm Drone was established as a subsequent goal in order to meet new software and sensing requirements. Development of the V3 Swarm Drone is elaborated upon in Section 5.8.

#### 4.3.2 Drop Mode

Drop Mode is a flight mode that could detect when an sUAS has experienced a vertical free fall, arm the motors mid-air to stabilize the vehicle, and then hover in position. The original autonomy solution for the V1 was to have the Swarm Drones in "stabilized" flight mode, which automatically tried to level the drone with the horizon when the vehicle is armed. Of the numerous concerns about the validity of this procedure, one was the ability of the Swarm Drones to operate under

the downwash of the Carrier Drone. Another concern was the height necessary to allow for the Swarm Drones to catch themselves. In order to answer these concerns, a Tarot Ironman 1000 sUAS octocopter airframe was modified with an under slung payload rack to deploy first person view (FPV) quadcopters to test Drop Mode. The Tarot Ironman 1000 frame with three FPV quadcopters is shown mounted on initial payload rack system in Fig. 12 below.



**Figure 12: Octocopter with three FPV quadcopters for the initial test of Drop Mode**

This initial test concluded successfully with each of the FPV quadcopters stabilizing mid air before landing on the ground via pilot control. The test proved that the concept of Drop Mode was mechanically feasible and did not require any major hardware modifications to the Swarm Drones. Although from a software perspective, Drop Mode still had to overcome some significant barriers. The original Swarm Drones used in this initial test were manually piloted where humans visually determined when their Swarm Drone had been dropped. Many of these advanced features used in the Pixhawk 4 flight controller (FC) PX4 software also come with their own sets of preflight checks, safety parameters, and pre-requisites. One of the most important preflight checks was on the vehicle's inertial measurement unit (IMU), which detects if the sUAS is stationary when an arm command is sent. If the vehicle is experiencing any movement outside of a certain threshold, the FC rejects the arm command, which could prove catastrophic for the Swarm Drone being deployed. Although these preflight checks could be disabled, it would introduce unnecessary risk to change low level parameters in stock firmware. This resulted in the need for a more integrated solution for the Drop Mode configuration.

Following the successful manual control drop test, the preliminary autonomous drop testing began. Using a DJI F450 drone enabled with a PX4 flight controller, a confirmation test was performed to confirm that the "Drop Mode" aerial deployment provided by the ArduCopter flight firmware could aurally arm and stabilize a UAS after being dropped. The test performed is outlined in Fig. 13. First, the F450 was powered on at the top of a tall stadium wall and placed into the Drop

Mode flight mode (Fig. 13a). Next, while the propellers were not spinning, the F450 was pushed laterally such that it fell off of the wall (Fig. 13b). During the free-fall, the F450 tumbled and even completely inverted. Approximately 4 meters into free-fall the Drop Mode was initialized, the propellers began spinning and the onboard FC began stabilizing the UAS (Fig. 13b). The FC finally stabilized the UAS at an altitude approximately 30 meters below the drop point (Fig. 13d). Following stabilization, the UAS autonomously landed itself, which showed that the vehicle was ready to perform any subsequent autonomous behaviors after its aerial deployment.



**(a) Drop Mode enabled before deployment**

**(b) Drone is dropped off the edge of the wall**

**(c) Drop Mode initializes, motors spin**

**(d) Drone stabilizes**

**Figure 13: Drop Mode testing**

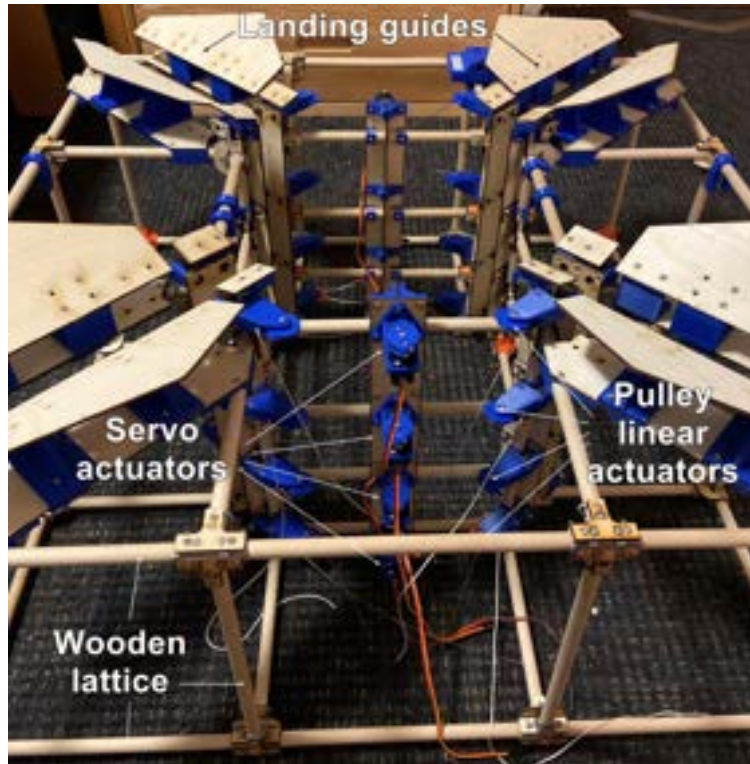
### 4.3.3 Multidrop Bay

In parallel to the developments of the Swarm Drone V1 (Section 4.3.1), concept research for deployment and reintegration mechanisms began in 2019. Initially, work focused solely on the deployment aspect with constraints requiring a payload that could drop multiple drones while taking up minimal space. Progress was catalyzed by the V1 mechanism shown in Fig. 14 below and mounted to a vehicle above in Fig. 12. The orange 3D printed geometries shown in these images passively locked into the frames of sUAS which are released by servos.

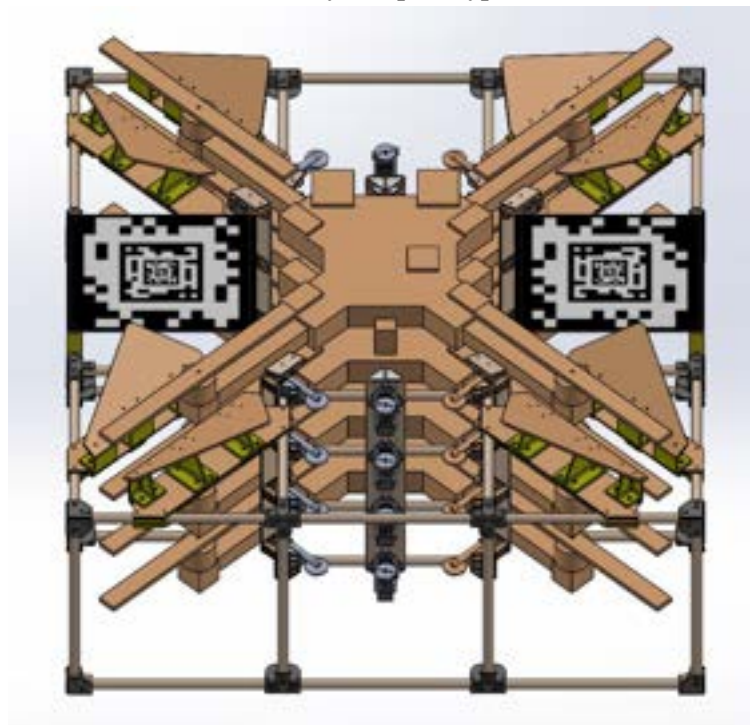
In 2020, reintegration was prioritized as a design constraint. With this, the initial concept of the Multidrop Bay was created. Functionally, it was a payload with a large central void that would allow for drones to land on top of, pass through, and be dropped out of the bottom of a carrier vehicle. It was prototyped as a wooden lattice structure with levels of actuators that acted as an active, gravity-fed deployment mechanism for the mentioned Swarm Drones. Design iterations also involved research into light weight, pulley-based linear actuators as well as geometries on the top of the lattice for passively aligning Swarm Drone propellers during landings. These concepts all resulted in the Multidrop Bay V2 assembly and CAD shown in Fig. 15a. The blue 3D printed parts illustrate the mentioned linear actuators that control the passage and selective deployment of Swarm Drones through the payload.



**Figure 14: Early Drone Drop Mechanism Prototype**



(a) Physical prototype



(b) CAD render

Figure 15: Multidrop Bay V2

The Multidrop Bay V2 used tension cables and pulleys to actuate the levels within the lattice of the design. These worked for actuation, though the assembly of the Multidrop Bay was difficult as each member required custom tuning and wire tensioning to work consistently. There were also issues with the manufacturing process of the frame. Due to having many connectors, the frame required hundreds of precision-drilled holes for assembly. Despite careful jiggling during drilling, tolerance stack up errors accumulated, resulting in inconsistency in key dimensions, causing jamming when the Swarm Drones dropped between levels. Lastly, the corner connectors between the circular frame members did not have a common design, leading to a high amount of unique parts. All of these issues were noted for the future design and assembly of the Multidrop V3. To help with the assembly of the future Multidrop V3 with assembly in carbon fiber, a custom 3-axis computerized numerical control (CNC) was developed to reliably and accurately drill holes in the frame to attach connectors to. Subsequent improvements are discussed in detail within Section 5.7.

#### 4.3.4 Carrier Drone

The proof of concept for the Carrier Drone used an OTS Tarot Iron Man 1000 sUAS octocopter frame, shown in Fig. 16. This frame was left mostly stock, with modifications made to outfit the on board Pixhawk flight controller, as well as the initial Multidrop Bay proof of concept. This was the same frame used in the Drop Mode test outlined in Section 4.3.2.



(a) Physical prototype in the field



(b) CAD render

**Figure 16: Carrier Drone proof of concept**

After tests with the proof of concept Carrier Drone were completed, work began on designing a new frame that was both compatible with the ongoing development of the Multidrop Bay, as well as perform functionally as a UAS. To test and validate the new Carrier Drone, a 1:2 scale model was created shown in Fig. 17. Instead of using carbon fiber, the frame members were made out of wood and the connectors were largely 3D printed. This allowed for cheap and quick manufacturing, as it was purely for validation of flight characteristics of the frame.



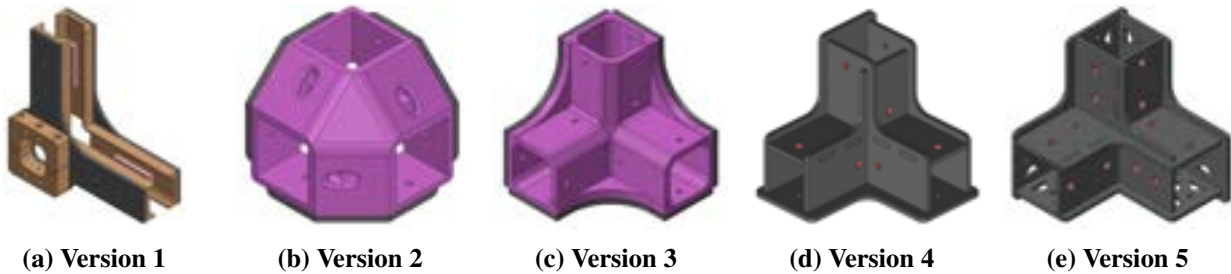
(a) Completed model in field



(b) In flight

Figure 17: Carrier Drone scale model

From this data, the full scale version of the Carrier Drone was designed using square carbon fiber tubes and carbon fiber plates for the connectors. The custom 3-axis CNC used in the assembly of the Multidrop V3 was also used to drill out the members of the frame of the Carrier Drone. Due to the geometry of the frame, many different types of connectors are required to hold the carbon fiber tubes together. These connectors went through many stages of development, gradually moving away from laser-cut wood and 3D prints to only carbon fiber plates to optimize weight and structural strength. One of these progressions is shown in Fig. 18.



(a) Version 1

(b) Version 2

(c) Version 3

(d) Version 4

(e) Version 5

Figure 18: Corner connector design progression

#### 4.3.5 Companion Computing

Companion computing is a general solution to vehicle control. It provides an interface to the PX4 flight controller running the PX4 software stack and generalizes a lot of the interactions to allow for a fully autonomous system with custom implementations. The way PX4 is implemented, it can be interfaced through a few systems: QGroundControl, MAVLink, and Real Time Publisher Subscriber (RTPS). QGroundControl is a high level graphical user interface (GUI) and it allows for users to create custom paths and see real time debugging (Fig. 19). MAVLink is a lower level interface where pre-defined messages can be sent over the network and then processed. This is actually what QGroundControl uses in the back-end. RTPS is the lowest level interface to PX4. It is similar to MAVLink in that it is sent over the network, however, it by-passes the pre-processing that occurs with MAVLink and directly communicates to PX4.



**Figure 19: Example of QGroundControl GUI [8]**

This project is using RTPS since it natively communicates with ROS2, allowing for easily building custom commands, and has significantly higher rates of communication (up to 500 Hz). ROS2 is an open source project commonly used in industry for controlling robotics. This project utilizes ROS2 for all of its communication and debugging. A diagram showing how PX4 and ROS2 communicate with each other can be seen in Fig. 20.

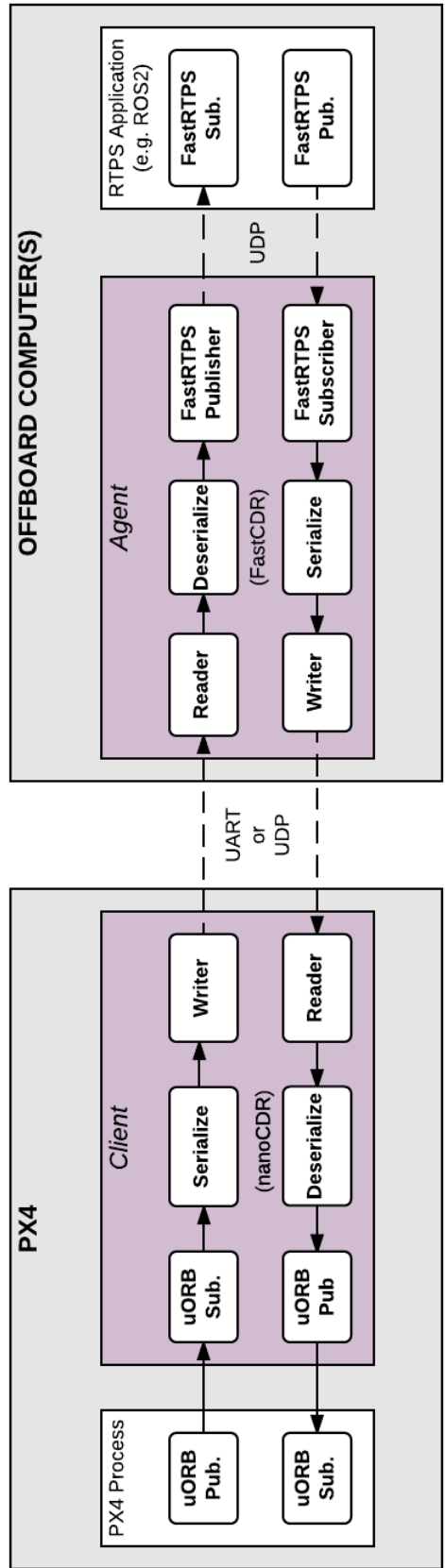


Figure 20: Communication framework between PX4 and ROS2 [9]

Using the tools mentioned previously, companion computing was built with an abstract interface for commanding positions and velocities to the vehicle. It also outputs relevant information of the vehicle state, such as GPS status, position, and orientation. This prior work established a strong foundation for capstone. As part of capstone, the goals changed to establishing a more consistent communication framework, making it easily accessible and testable via a custom shell interface, extending support to control multi-vehicles, and improving upon the fail-safes for control commands.

The flight controller used is running PX4, as stated before, but there was initially another option for control called ArduPilot. There was initial testing using ArduPilot, but it was decided that PX4 supported a better interface for ROS2 and also had a more active community of developers. All problems that were run into when using PX4 were directly solved by talking with the people who wrote the software. Discussions were done through various resources, such as Slack and the PX4 discussion website. Even in cases where this project needed to implement custom solutions, such as Drop Mode, advice was received from those resources.

#### 4.3.6 Simulation

To ensure that every autonomous action was working as intended the team used both Software-in-the-Loop (SITL) and Hardware-in-the-Loop (HITL). These two approaches were previously explored by the team and allowed for the rapid testing and validation of the flight software without waiting for possible hardware or manufacturing delays. Additionally this gave the team confidence in the validity of the software before all physical flight tests.

The SITL approach encompasses using the Gazebo open source robotics simulator with a custom built environment. Within Gazebo each sensor on the drone is simulated in software (i.e PX4 controller, GPS, Realsense camera, IMU, etc.) such that there is a 1:1 match with the real world. In testing, the team has found that in the field the main difference between Gazebo and the real world is additional sensor noise. Gazebo is designed to work with ROS2 so it makes the development process as smooth as possible. With ROS2, it is possible to spawn as many drones as desired, and the launch process for the simulation has been setup in a way to support multi-vehicle simulation testing.

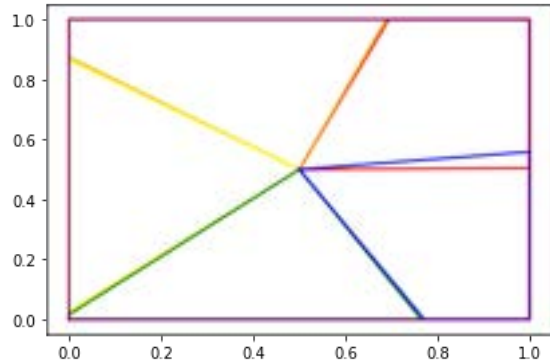
HITL is a simulation mode where the software is running on a physical PX4 flight controller. However, the drone is still simulated in Gazebo. This allows for the verification of the PX4 firmware without having to physically fly the drone, and is usually the last step before actual field testing.

#### 4.3.7 Path Planning

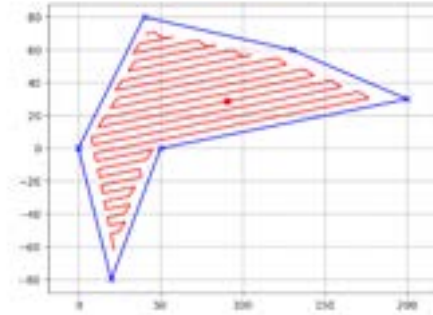
As noted in the Swarm Application Section (3.5.1), collaborative UAV swarms have been used for efficient search of an area. A stretch goal of the this project would be do demonstrate various collaborative search algorithms using the entire system.

To accomplish the task of a search and rescue (SAR) mission (step 5 in Fig. 22) with a deployed swarm of UAVs the team is researching CPP techniques for UAVs [35]. As the focus of this project is the deployment and recovery system, the actual SAR mission scope was limited. The planned scope would be to utilize approximate cellular decomposition within a known search area,

divide it into  $n$  polygons for  $n$  drones (Fig. 21a) and to test various CPP algorithms (Fig. 21b i.e. lawnmower, spiral etc.) These were early examples implemented in Python using the Shapely math library as a proof of concept for the algorithms.



(a) Polygon division example



(b) Lawnmower coverage path planning example

Figure 21: CPP

#### 4.4 Regulations

In the United States the FAA distinguishes UAV primarily based on their intended usage and weight class. The two categories of UAV operations are 14 CFR Part 107 and 49 U.S.C. 44809. 14 CFR Part 107, or more typically abbreviated as Part 107, are the regulations that dictate commercial operations of sUAS systems. This includes, but is not limited to, speed, altitude, pilot to vehicle ratio, and mission objective. 49 U.S.C. 44809 or the exception for limited recreational operations of unmanned aircraft, establishes regulations for purely recreational sUAS and UAS system operations. These regulations are much less restrictive than Part 107, allowing hobbyists and novices to continue their past time without significant overhead rules.

Although recreational regulations apply to both sUAS and UAS operations, Part 107 regulations are bound to sUAS operations only. Commercial UAS operations have much stricter system of evaluation before any flight operations can be conducted. There are currently two pathways, as of the time of writing, type certification and 49 U.S.C. 44807, Special Authority for Certain Unmanned Systems, also known as Section 44807 [36]. Type certification is an intense FAA design review process that seeks to verify and validate a UAS design to the same set of standards that conventional manned aircraft are held to [37]. The Section 44807 is on case by case basis waiver given to organizations that can demonstrate safe operations in national airspace and are in the best interests of the public. This is a very broad definition that allows the FAA to control who exactly has the ability to conduct commercial UAS operations. The result of this is a very difficult to enter procedure process that requires insider connections to initiate communication with the appropriate FAA officials.

The initial approach of Swarm Carrier capstone to legally operate was to register the Carrier Drone and the Swarm Drones as Part 107 sUAS. This would elevate the legitimacy of the system and increase the testing location operations as a commercial system. The problem though was

as an overall system, the Carrier Drone and the Swarm Drones would be over the 55 lb limit and be classified as an UAS. This meant that the group had to go through one of the two routes to obtain UAS operation permissions, as explained previously. This proved to be a significant bottle neck within the time constraints of the capstone project. As even with connections and regular meetings with the Massachusetts Department of Transportation (MassDOT), the project was unable to guarantee test site to operate legally. This led the capstone to take a different path to operate the system legally which is discussed in detail in 5.14.

## **5 Designs**

### **5.1 Flowchart Overview**

The original system functional flowchart is shown in Fig. 22. A Carrier UAS will contain one Multidrop payload bay of three Swarm Drones. The developed deployment and recovery system will function as such:

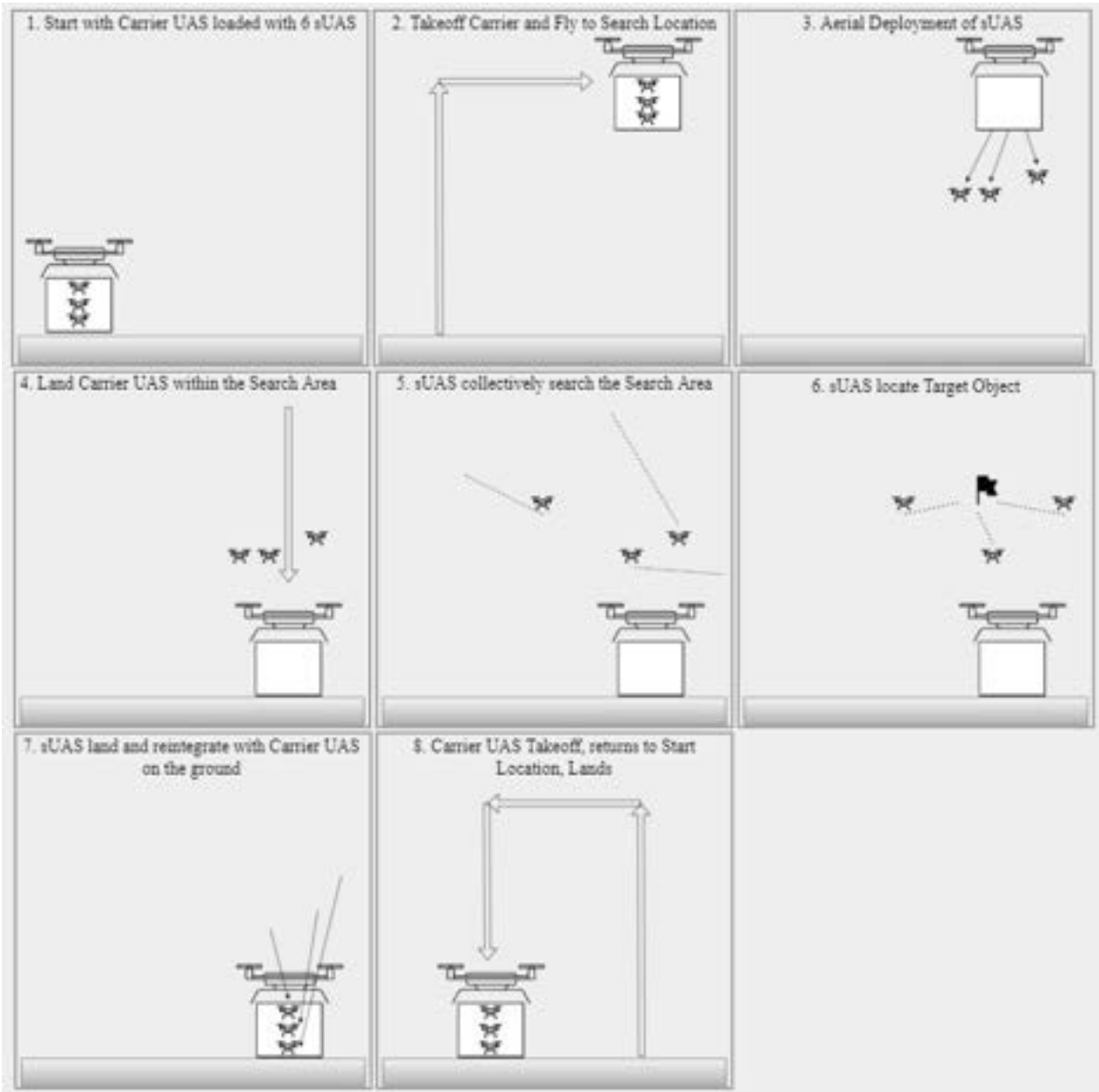


Figure 22: High level task flowchart

1. The Carrier UAS loaded with three Swarm Drones will start at its designated starting location.
2. The Carrier UAS will take off vertically to its designated drop altitude of 30 meters. The Carrier UAS will then traverse horizontally to the designated Search Location.
3. The Carrier UAS will deploy each Swarm Drone individually; dropping each out of the bottom of its multidrop bay.
4. Once all the Swarm Drones have been deployed, the Carrier UAS will land.
5. The Swarm Drones will then begin their mission. For this project, the designated mission is an area search.
6. The Swarm Drone mission will reach its end conditions. For this project, either the target will be located or the Swarm Drones exhaust their flight time.
7. Each Swarm Drone will sequentially land and reintegrate with the Carrier UAS.
8. Once all the Swarm Drones have been recovered, the Carrier UAS will takeoff vertically to its return altitude of 10 meters then traverse horizontally to its starting location. Once at the starting location, the Carrier UAS will land.

Due to the high complexity of deployment and recovery as well as the distributed nature of the control scheme, subsystem communication is required. Fig. 23 displays the subsystems and their communications. The Swarm Drones and Carrier UAS communicate with one another over a WiFi connection. For this Capstone Project, a single ground mounted TP-Link router is used to connect all the drones and the ground control system via an offline connection with static IP addresses. The Carrier UAS communicates via the Multidrop Bay via an Inter-integrated Circuit (I2C) connection to control the servo actuation. The feedback that the Swarm Drones receive from the Multidrop Bay comes from a contact sensing pad that acts as a hard stop, telling the Swarm Drones to stop motor spinning once triggered.

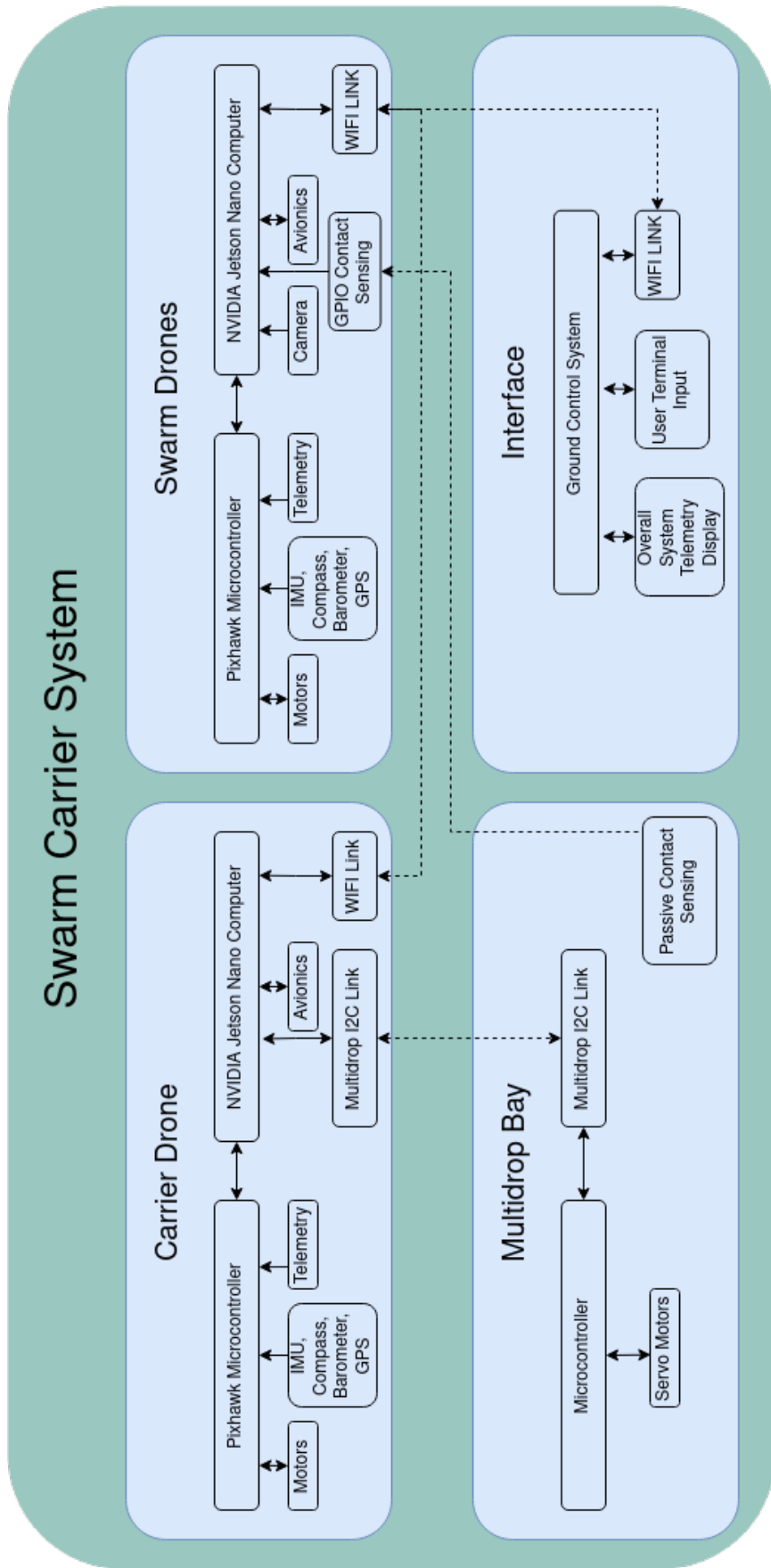


Figure 23: System flowchart

## **5.2 Swarm Carrier System Level Objective Re-evaluations**

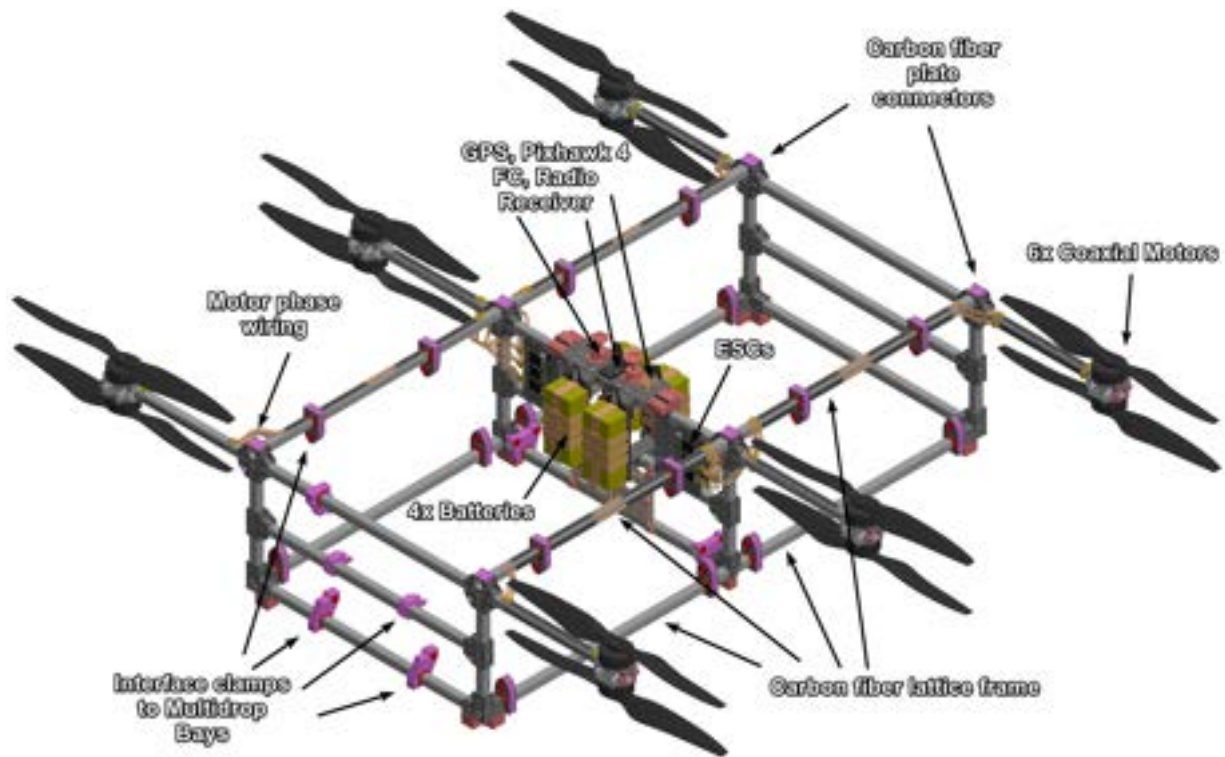
Before the beginning of Capstone II in the fall, the group met to evaluate the capability of the project to meet the original high level task flowchart objectives. This evaluation arose from the idea that certain subsystems and tasks could be removed while accomplishing the problem statement. A weighted decision matrix was created to decide the direction the project would take in the fall. Different configuration of the Carrier Drone, Multidrop Bay, and the Swarm Drones were considered in this decision matrix with four final combinations evaluated. Based on the criteria laid out for the decision matrix, the conclusion drawn was that the Carrier Drone would have a decacopter layout with a single Multidrop Bay, and three Swarm Drones would be used in the final system level test. This analysis drove the Carrier Drone V2 design, shown in the Carrier Drone 5.3 section. The Multidrop Bay V3 would remain the same, while three Swarm Drones be converted to their final V3 design. A figure of the weighted decision matrix used to guide the project's direction is shown in Fig. 24. Sections 5.3, 5.7, and 5.8 below discuss the progression of the Carrier Drone, Swarm Drones, and Multidrop Bay respectively. It should also be noted that the Carrier Drone V2 did not become the final design, which is detailed further in Section 5.3.

Final System Options			Weights (1:poor-10:best)									
Carrier Configuration	Number of Swarms	Number of Multidrop bays	Frog Outfitting	Capstone Fulfillment	Redesign Risk	Assembly Time	Drill Time	Cost	Flight Safety	Swarm Capability	Totals	
Decacopter	6	2	3	8.75	5	3.25	3.25	2.25	9.25	10	255.375	
Decacopter	3	1	6.5	8	5.5	6	6	4.75	7.75	5	276.1875	
Dodecacopter	6	2	3	4.5	7.75	5.5	5.5	6.5	5.5	8.25	230.8125	
Dodecacopter	3	1	6.5	3.75	8.5	8.75	9.25	9	5	3.5	270.4375	

Figure 24: System level objective re-evaluation weighted decision matrix

### **5.3 Carrier Drone**

Within the Swarm Carrier system, the original Carrier Drone design was an ultra-heavy lift airframe responsible for carrying a group of up to six sUAS (Swarm Drones) within the mentioned Multidrop Bay payloads. It had a 2500 mm x 2500 mm (motor to motor diagonal distance) dodeca-copter constructed from a carbon fiber laminate matrix. The frame itself weights just 9.5 kg despite its large size. The scope of the Carrier Drone's development encompasses continued frame design, payload interface, electronics routing, power electronics testing, and flight trials. Fig. 25 below shows an early render of the Carrier Drone and the assembly of the frame.



(a) Carrier Drone V1 CAD



(b) Carrier Drone V1 Airframe Prototype  
 Figure 25: Carrier Drone V1

The design of the Carrier Drone has undergone two version iterations since its original design at the end of Capstone I. The V2 design of the airframe sought to create a planar configuration of a decacopter vehicle in order to have a more efficient design by avoiding propeller overlap. This airframe boasted a much larger size, having a 3400 mm x 3400 mm (motor to motor diagonal distance), which dwarfed the previous airframe's size. Problems arose after the initial quadcopter test of the Carrier Drone V1, which revealed that the frame dynamically deflected during operation. The frame not only deflected upwards with the thrust, but twisted torsionally, which was especially apparent on unsupported members such as the cantilever beams that supported the motors of the Carrier Drone V1. A visualization of this deformation can be seen below in Fig. 88. This cantilever design of the airframe proved to be a much larger concern than originally thought, which made the group rethink how it would move forward with its new designs. Due to its longer cantilever design, the planar Carrier Drone V2 design was deemed too much of a risk with its extremely long cantilever members. An image of the V2 design in CAD is shown in Fig. 26.



**Figure 26: Carrier Drone V2 CAD**

The Carrier Drone V3 design arose after the scope of the project was adjusted. It became apparent that a more conventional design was necessary to make the Carrier Drone feasible within the timeline of Capstone II. The design shifted to a more conventional octocopter design that the group had experience with operating previously. In addition, since only a single Multidrop Bay was necessary for the final design, the footprint of the frame was significantly reduced from the V2 design. The Carrier Drone V3 Cad is shown below in Fig. 27.

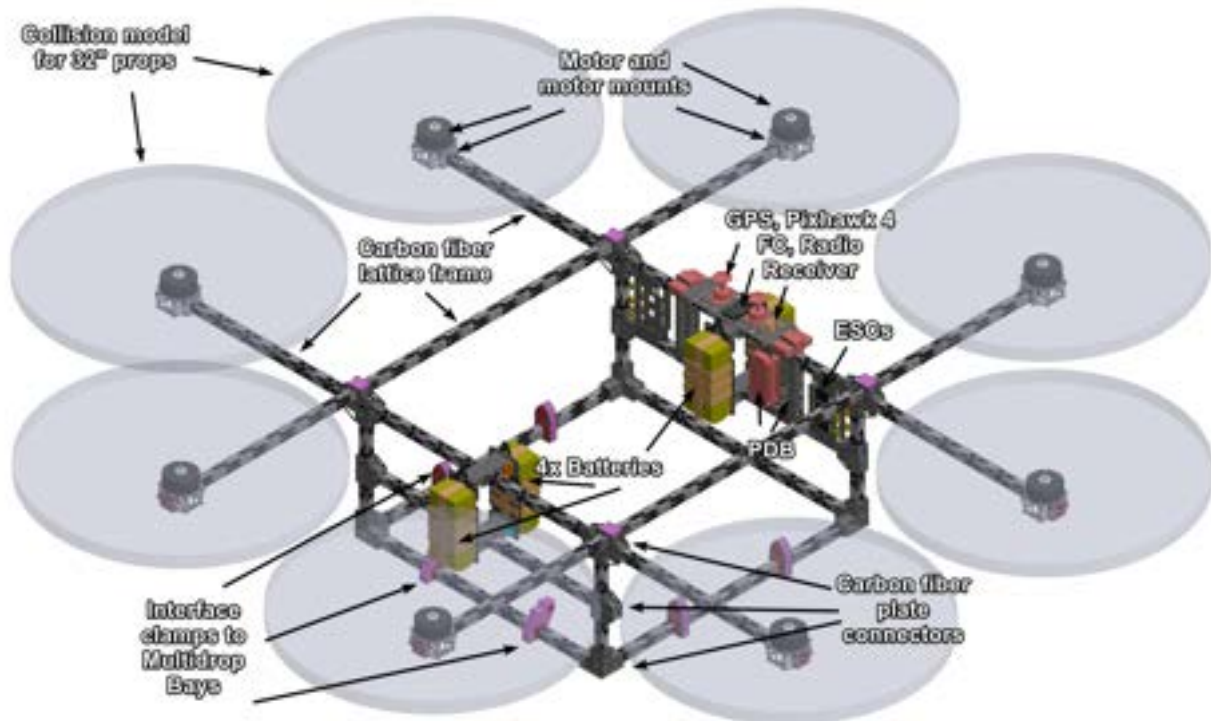
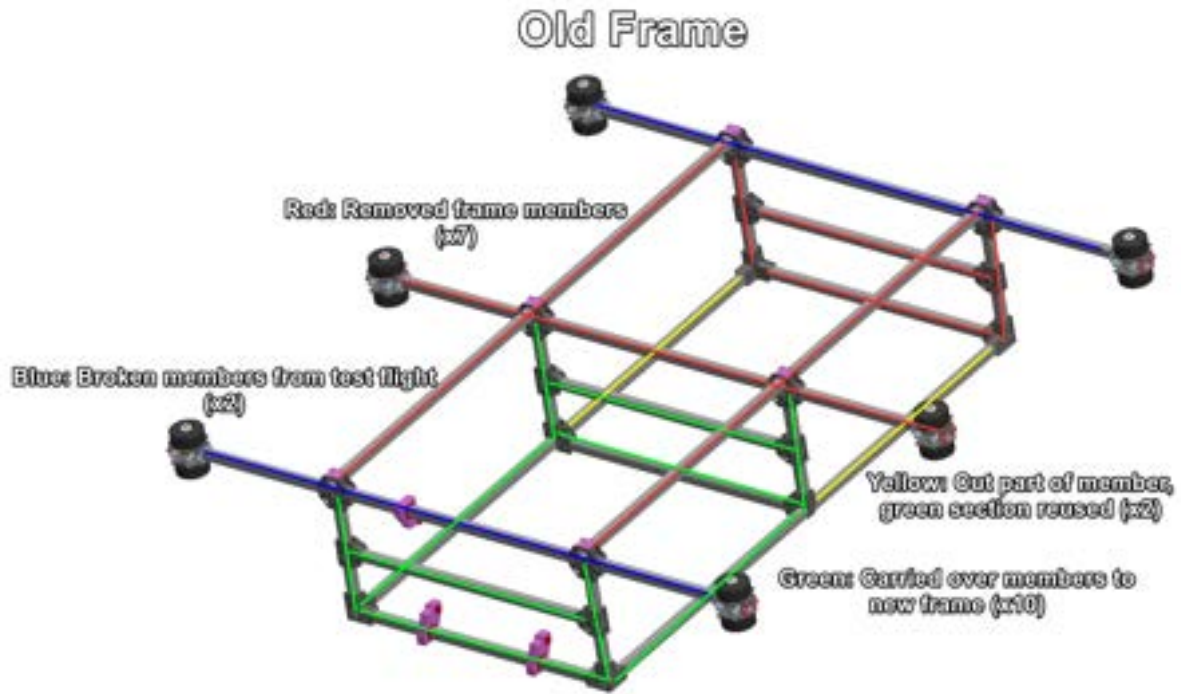
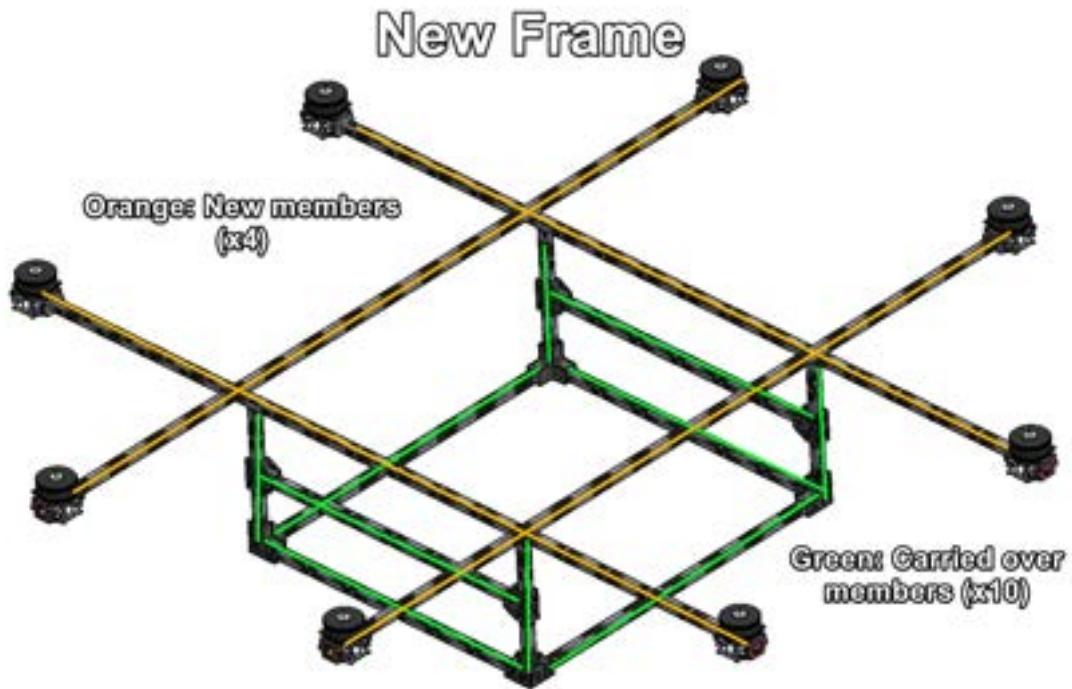


**Figure 27: Carrier Drone V3 CAD**

The Carrier Drone V3 drone was a modification and a simplification from the V1 design, with the Multidrop Bay and Swarm Drones remaining unaffected. This allowed for heavy reuse of carbon frame members, especially those on the lower part of the frame built around the Multidrop Bay. New tube lengths were required to accommodate for the new octocopter design, shown below in Fig. 28. The progression of the V1 through V3 design of the Carrier Drone's is also below shown in Fig. 29.



(a) Carrier Drone V1 frame members



(b) Carrier Drone V3 frame members

Figure 28: Overview of frame member reuse between V1 and V3

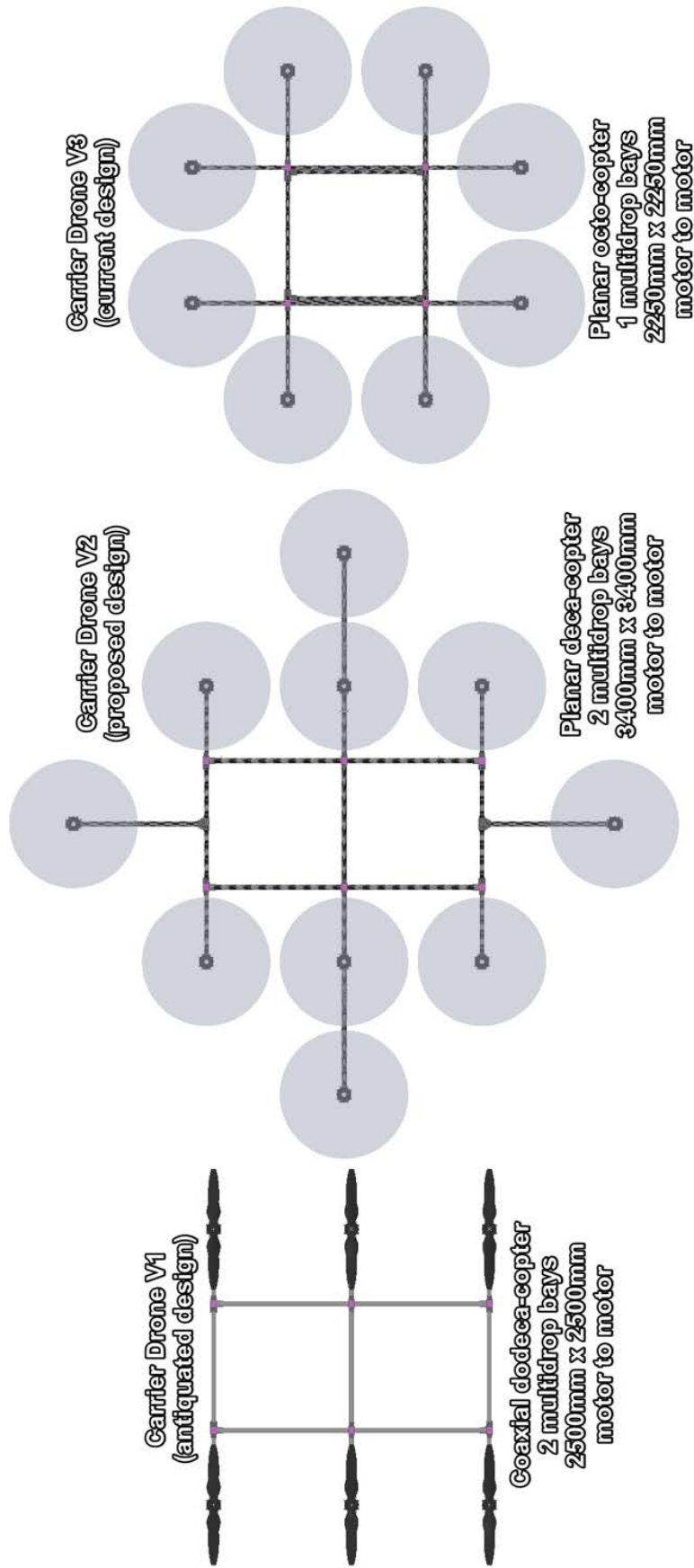
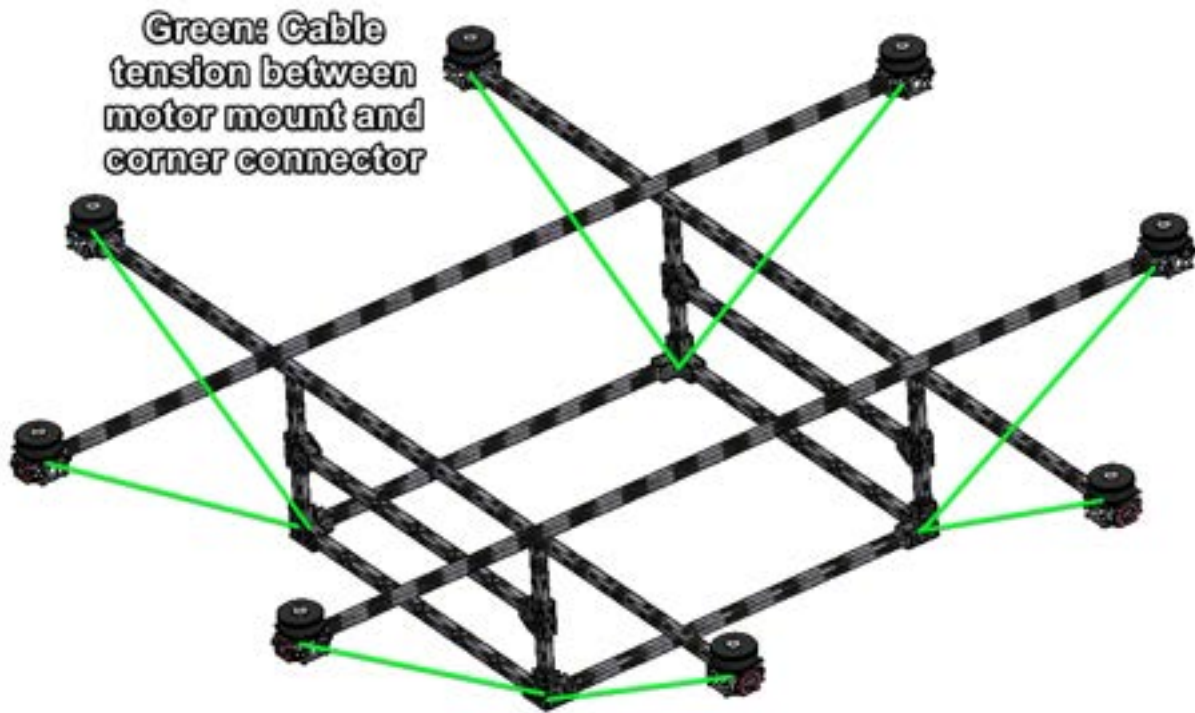


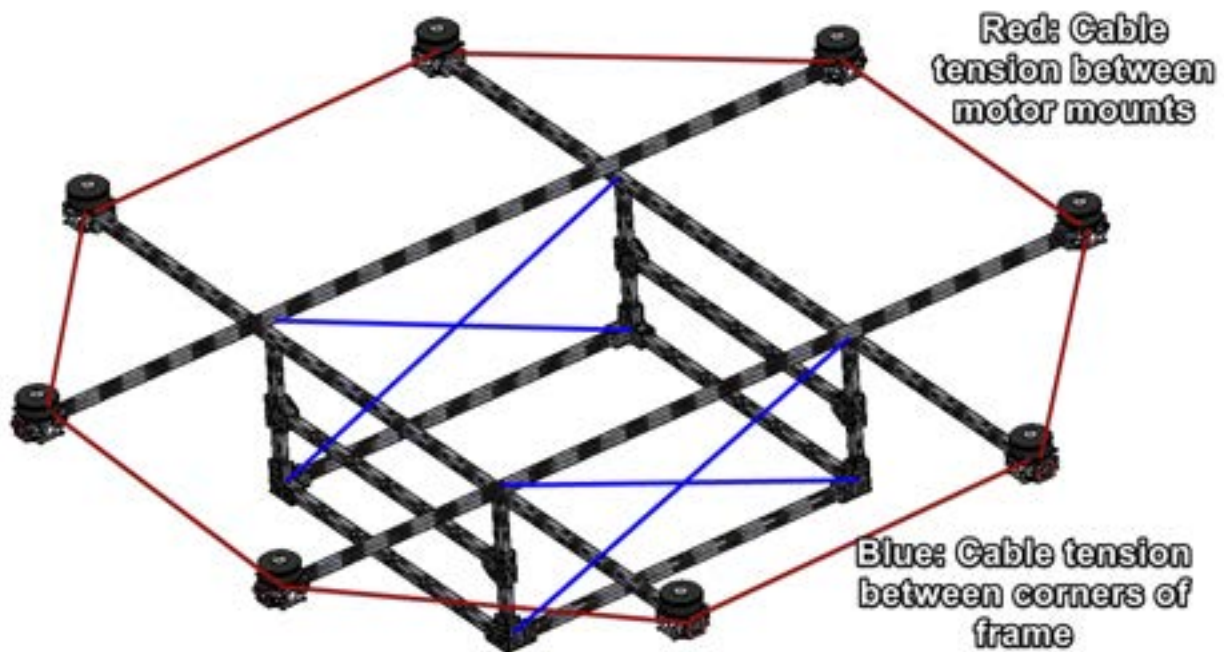
Figure 29: Carrier Drone Design Progression

### 5.3.1 Cable Tensioning

The V3 design addressed flexure of the carbon fiber members by using cable tensioning to purposely pretension the frame members to maintain rigidity. This was important for the design as it ensured that vibrations in the previously unsupported cantilever beam arms of the Carrier Drone were addressed in at least two axes. Vertical movement due to thrust, and side to side motion from motor torque were addressed by the cable tensioning schemes presented in the subsequent illustrations. Their implementation during assembly had an immediately noticeable effect on frame's rigidity, the frame acted as a rigid body when the arms were compressed together or pulled up vertically. This presented a favorable result for the cable tensioning to be the solution to previously noted frame rigidity problems. The actual flight effectiveness was evaluated during the Carrier Drone V3 air frame test section, shown later in Section 5.11.6. The connection points for the tensioning of the V3 frame is shown below in Fig. 30. Overall, 20 connections were used across the frame.



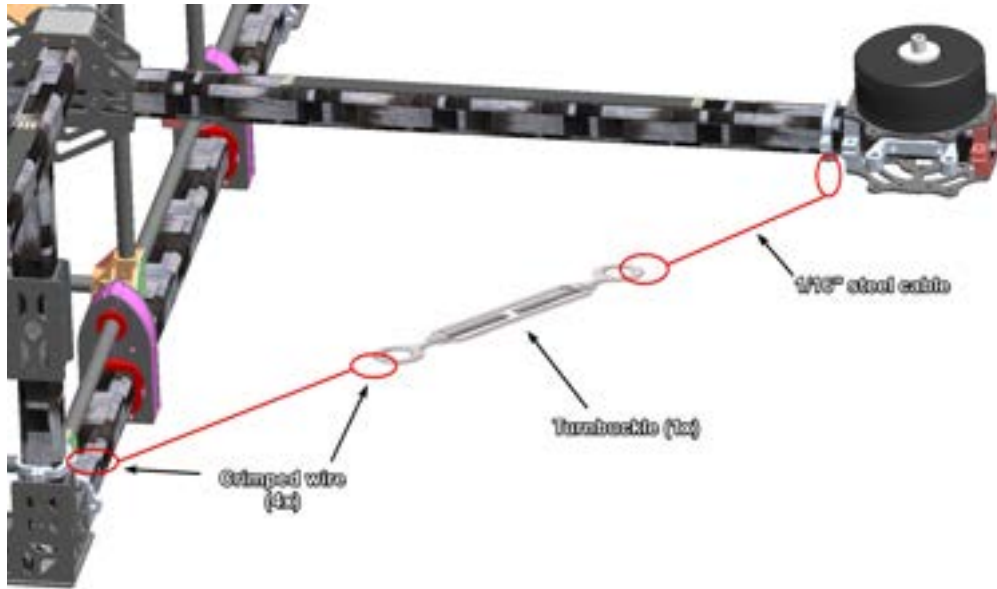
(a) Carrier Drone V3 tensioning scheme for motors to corner connectors



(b) Carrier Drone V3 tensioning scheme for individual motors and frame corner connectors

Figure 30: Carrier Drone V3 tensioning schemes

These same cable schemes were used in the assembly of the Carrier Drone V3, as shown below in Fig. 31. An additional 4 cable tensions were placed in the internal cavity of the Carrier Drone to simulate the rigidity that the Multidrop Bay would provide if it were there.



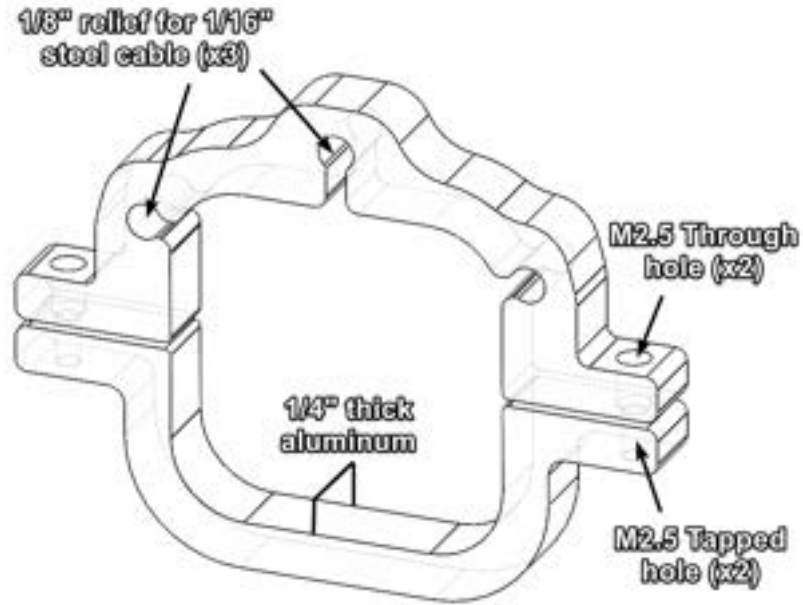
(a) Components in single cable tension



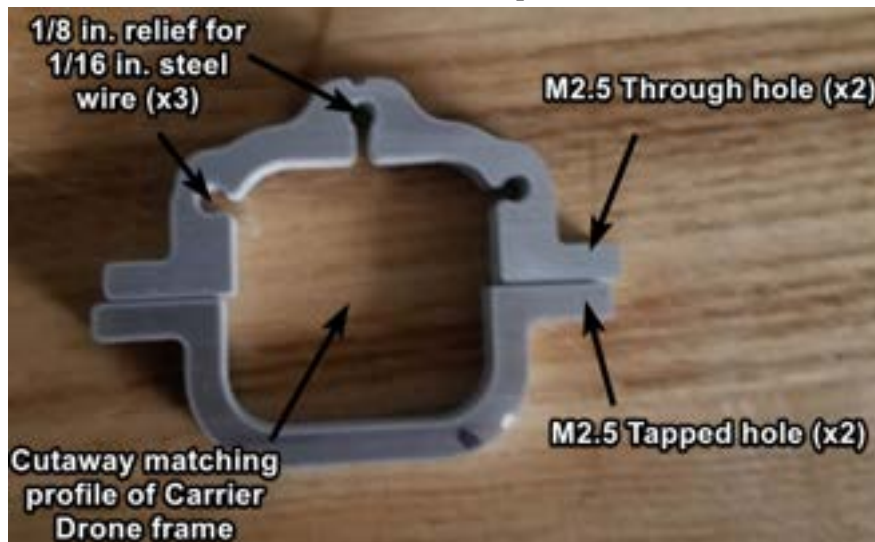
(b) Cable tensioning on built frame

Figure 31: Carrier Drone cable tensioning

To attach to the frame of the Carrier Drone, the cable tensioning used aluminum clamps designed to interface between the carbon fiber members of the frame and the 1/16 inch cables for the tensioning. The CAD, as well as the physical version of the final clamp design is shown below in Fig. 32.



(a) Aluminum clamp CAD



(b) Aluminum clamp real life

Figure 32: Cable tension clamp to Carrier Drone

The design shown above in Fig. 32 went through numerous iterations to reach the final state. The clamps were mass produced by cutting the profiles on a waterjet cutter, and performing the hole operations on a Tormac CNC machine. Optimizations were made to reduce the overall weight of the clamps to reduce the AUV such as reducing extra material and reducing the thickness of the aluminum stock to 1/4 inch. The design was also modular, meaning that it could fit anywhere on the frame and not interfere with any internal components, specifically the Multidrop Bay frame. The three slot positions go along with this, meaning that the same clamp could be used to hold three wire tension points (such as at the motor) or just one (such as on the internal frame connections). The Carrier Drone V3 is again shown below in Fig. 33 before the flight discussed later on in Section 5.11.6.



**Figure 33: Field assembly of the Carrier Drone**

### 5.3.2 Carbon Fiber Tolerance Stackup Issues

An important factor in the design of the carrier drone's lattice structure was the carbon fiber member's surface and axis straightness. The placement of flight essential hardware such as motors, batteries, payload, and FC hinged upon the members being as straight or consistently toleranced as possible. Although Rock West Composites stated no dimension control on the straightness of the material, it was assumed that it would have a surface and axis straightness within a  $\pm 2.0\text{mm}$  from end to end. During the initial inspection of the carbon fiber members for the Carrier Drone V1, it was immediately noted that there was no control of this straightness, as members deflected as far as 5.0 mm from the axis datum of the stock material. This was quantified through the use of the custom 3-axis CNC, which was able to trace the center axis of the member down its length. During machining, the group found it difficult to drill holes consistently down the center axis of the tube as the member deformed inconsistently down its length. The overarching problem that this caused was that the frame would lose its squareness or have hole placements fall outside of tolerances. This manifested itself during the assembly of the Carrier Drone V1 as many holes had to be redone. Issues with squareness of the frame due to these straightness problems only revealed themselves during the initial Carrier Drone V1 Air Frame Test in Section 5.11.5 and can be seen in Fig. 88.

In the subsequent manufacturing of the Carrier Drone V3 design, it was noted that the carbon fiber members (from a different lot) had much tighter surface and axis straightness tolerances. This made manufacturing and assembly much easier, as connectors, and components fit together with much less post machining modifications. The manufacturing and assembly time of the Carrier Drone V3 was much faster than previous versions due in part to an established manufacturing process and previous experiences of team members. Furthermore, since the majority of the components for the Carrier Drone V3 were from previous iterations, many parts could be reused. This allowed for the Carrier Drone V3 to be manufactured in two weeks, which was important to maintain the timeline of the project.

### 5.3.3 Carbon Fiber Material Evaluation

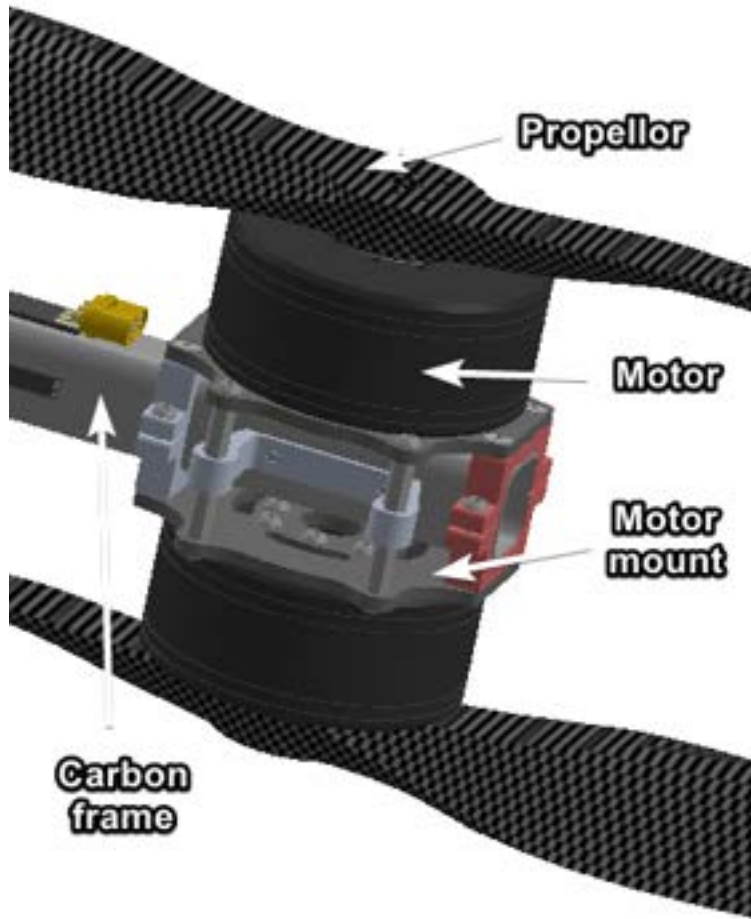
In order to mitigate deflection and torsional twisting of the Carrier Drone's carbon fiber members during operations, considerations were made to change the material to a higher stiffness material. The company Rock West Composites offers three modulus of carbon fiber square tubing in the dimensions currently used in the design. The current modulus being used is intermediate modulus, which utilizes Pyrofil MR60H 24K carbon fiber, has a modulus of elasticity of 42 msi [38]. The high modulus carbon fiber tube that was considered uses Pyrofil HR50 carbon fiber, which has a modulus of elasticity of 57 msi [39]. Although it is typically not possible to do a direct comparison between composite materials due to their orthotropic nature, due to the direct comparison of materials that use the same layup scheme, a direct comparison between laminate materials was possible. The high modulus carbon fiber had 35.7% increase in stiffness over the intermediate modulus. This came with a 52.4 % increase in cost though. The group realized that regardless of the material stiffness, that wire tensioning would have to be used to correct previously mentioned tolerancing problems with the stock material. It was therefore determined that the price to benefit of using a

higher modulus carbon fiber was unfavorable for the design, as the deformation problems of the airframe could be solved easier and cheaper using wiring tensioning schemes shown previously in Fig. 30.

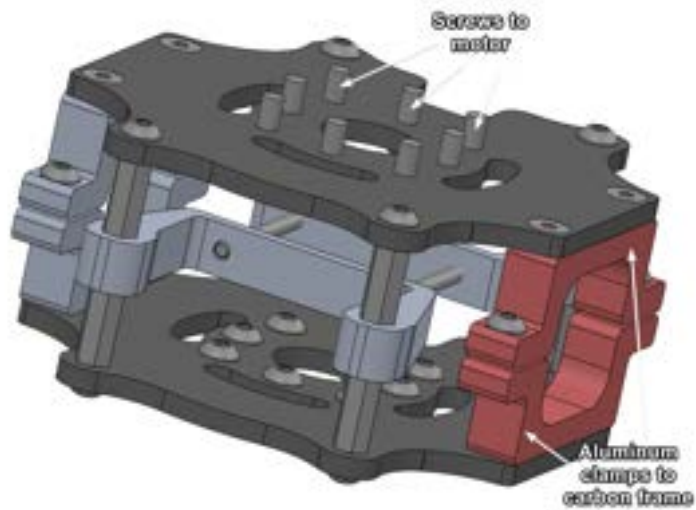
With stock in hand, square laminate from Rock West Composites was machined and used to assemble the final design of the carrier drone shown in 27. Empirical inspections were then made on the motor arms which acted as spring cantilevers due to their length. To test deformation under realistic conditions, a motor brake test was conducted. The electronic speed controllers (ESCs) used by the Carrier Drone have an 'active braking' function which abruptly stops motors following actuation commands. This formed the basis of a brake test which utilized the force generated by the inertia of the brushless motors during braking to induce elastic deformations of the frame members. The purpose of this test was merely to show the presence of flexure, not precisely quantify it. Using this method, small deformations of up to 3 mm were observed in transverse directions. These presented risk as local deformations in the frame would bias flight electronics to command false attitude corrections. To mitigate this issue, methods of improving the rigidity of the material using cable tensioning were employed. These are described in detail in Section 5.3.

#### 5.3.4 Motor Mount Design

Within the overall development of the Carrier Drone, the choice and subsequent design of a motor mounting scheme is the most critical for the overall vehicle functionality. From July to August of 2021, extensive investigations and design iterations were performed to determine the propulsion scheme required to lift the desired payload of six Swarm Drones. Early designs leveraged composite waterjet-cut carbon fiber and machined aluminum to create a fixture capable of supporting co-axial motor configurations and tensile forces of up to 30 kgf. Fig. 34 below shows the modularity of existing designs that are compatible with single and co-axial motor mounting configurations. In the future, only the single mount was used due to results regarding efficiency and all up thrust in Section 5.3.6.



(a) Co-axial Motor Mount Configuration (CAD)



(b) Motor Mount Assembly (CAD)

Figure 34: Carrier Drone Motor Mount

While capable, the motor mounts outlined above represented a vestigial design requirement which was coaxial motor placement. Given unfavorable efficiency of coaxial motors described in Section 5.3.6 below, a planar configuration was the ideal choice moving forward. In addition to improving flight performance, the removal of bottom motors reduced weight and manufacturability issues associated with 4 mm thick carbon plate. The subsequent design, shown in Fig. 35 below, utilizes a thinner, non-load bearing plate on the bottom of the mount.



(a) Planar Motor Mount Configuration (CAD)



(b) Final Motor Mount on the Carrier Drone

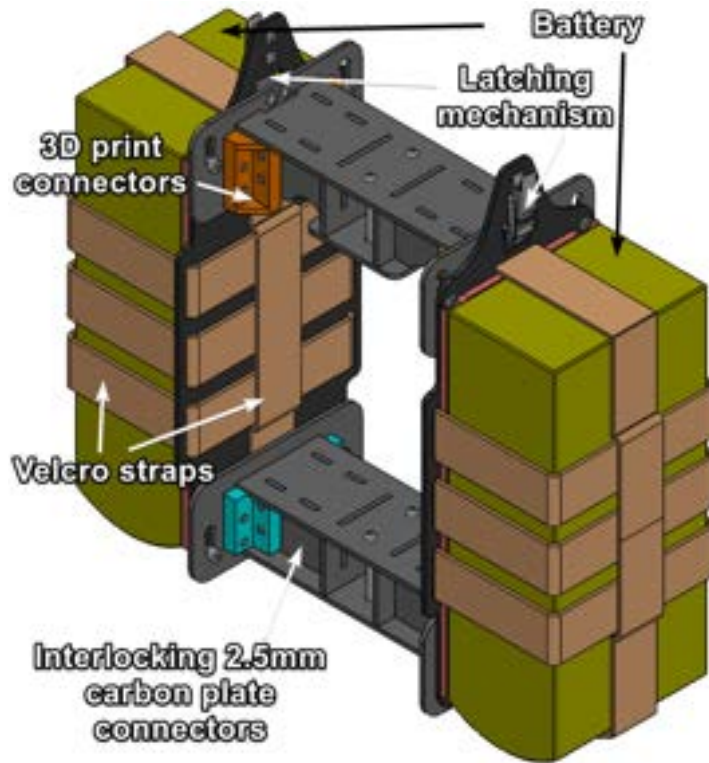
Figure 35: Final Carrier Drone Mount

Alongside performance improvements associated with the design, procedures were also developed involving field assembly and transit storage. Specifically, machined holes in the Carrier Drone's frame allowed for precise field assembly while thread lock was employed to prevent hardware from loosening. Features of the mount's design that indexed machined features and allowed for easy hardware access resulted in rapid and consistent assembly. With manufacturability improved, the final motor mount design was scaled to eight prototypes to complete the propulsion systems fixturing on the Carrier Drone.

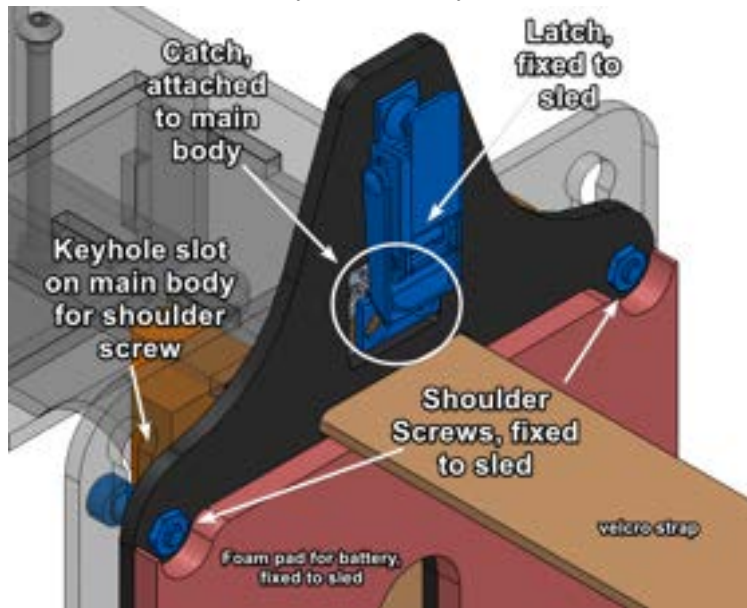
### 5.3.5 Carrier Drone Battery Mechanism

To power the Carrier Drone, four Tattu 6s 22000mAh batteries were required. These weigh 2.65 kg each, and resemble a dictionary in size. The mounting location of the batteries also must be in the center of the Carrier Drone in order to limit inertial effects and to consolidate electronics and wiring. The last constraint is that the battery mechanism must extend far enough around the Multidrop Bay to avoid interference. For efficient operation of the Carrier Drone in the field, these batteries must be quickly and securely attached to the Carrier Drone. With these constraints and criteria in mind, during July and August, solutions were brainstormed and prototyped.

The initial battery mechanism is shown below in Fig. 36. The main body of the battery mechanism is fixed to the frame, and is composed of interlocking 2.5mm carbon fiber plates. The battery is attached to a sled, shown in Fig. 36b. When assembling the mechanism in the field, the sled attaches to the main body by aligning with four shoulder screws, which also hold the weight of the sled. The entire assembly is then held together by the latching mechanism shown in Fig. 36b, which makes the entire assembly a rigid body.



(a) Assembly of the battery mechanism



(b) Close up highlighting shoulder screws and latch

Figure 36: Battery mechanism

The location of the battery mechanism in the V3 Carrier Drone is shown below in Fig. 37. Each battery weighs 2.65 kg, bringing the total weight of the battery mechanism to around 6 kg. These provide a large amount of inertia to the frame, so it is important to keep the load balanced and as close to the axis of rotation as possible. In the V3 Carrier Drone shown, the battery mechanisms are symmetric across the frame, while still leaving room for the Multidrop Bay in the center.

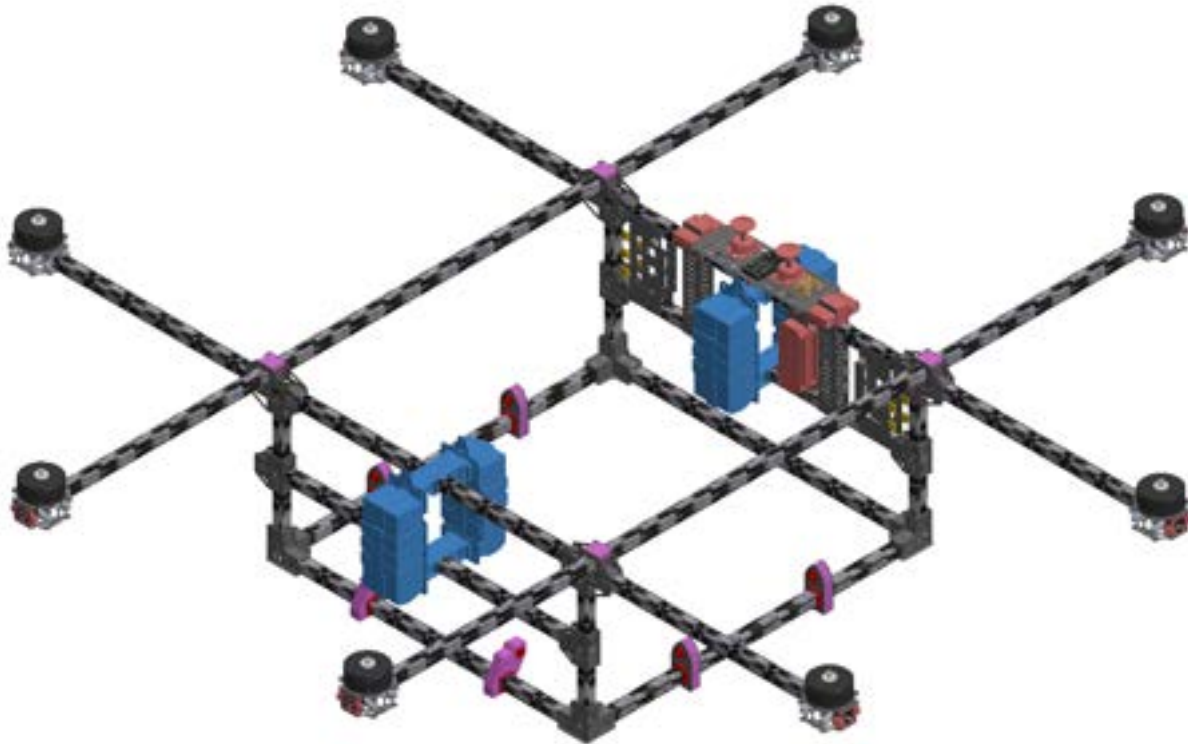


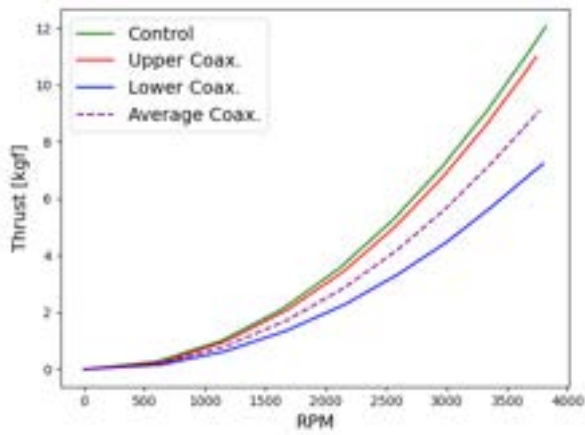
**Figure 37: Location of the battery mechanism (highlighted blue) on the Carrier Drone V3**

### 5.3.6 Motor Configuration

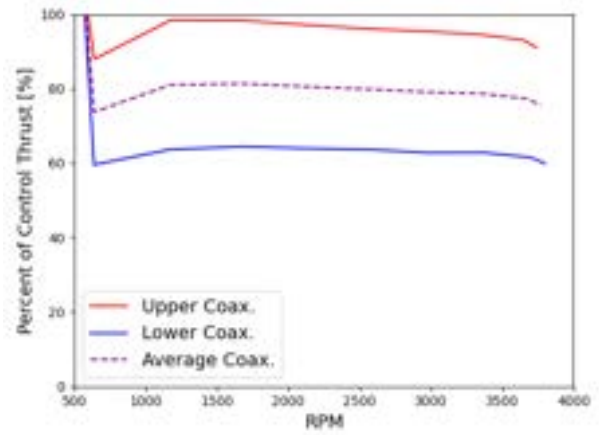
From the known Swarm Drone weight and number as well as approximations for the Multidrop Bay and carrier frame weights, the AUW was approximated to be  $48\text{lbs}$ . Using the motor and propeller calculations outlined in [14] and Eqn. 3 it was determined that the most viable Carrier Drone configurations were a dodeca-copter or a deca-copter configuration with approximately 30 inch diameter propellers. With so many large motors and the difficulty of manufacturing carbon fiber tube frames, coaxial motor configurations for the dodeca-copter and the deca-copter were considered. The coaxial configurations would reduce the overall size of the carrier UAS and be easier to manufacture.

Prior to making definitive decisions on the carrier UAS airframe designs, the percent thrust loss from coaxial configurations needed to be determined. Researched sources appear to show that the percent thrust loss is not constant between different propeller sizes, thus the need for testing arose [4, 31]. Prior to this work, four TMotor P80III 100kv motors and Foxtech 3010 Carbon Fiber Propellers had been purchased. Subsequent thrust tests utilized an RCbenchmark S1780 motor thrust test stand, the motor thrust, voltage, current, torque, and rpm were recorded. Once all the data was collected from the thrust tests, the group was able to conduct a detailed analysis for the system. The average of the upper and lower performances were averaged to display the average coaxial motor performance. The thrust vs rpm performances are displayed in Fig. 38a. It can be seen that all the motors are able to achieve the same rotational speeds. The upper coaxial motor had consistent performance with the single motor while the performance of the lower motor was significantly lower. The percentage of the single "control" motor's thrust as a function of RPM is shown in Fig. 38b. It can be seen that consistently across all RPM the lower coaxial motor had approximately 65% of the control motor's thrust output with the average coaxial motor thrust output being approximately 80% of the control. The recorded average thrust loss of 20% is consistent with [4]. From the test data, the motor electrical power vs thrust relationship  $P_m(\text{kgf})$  was determined (Fig. 38c).

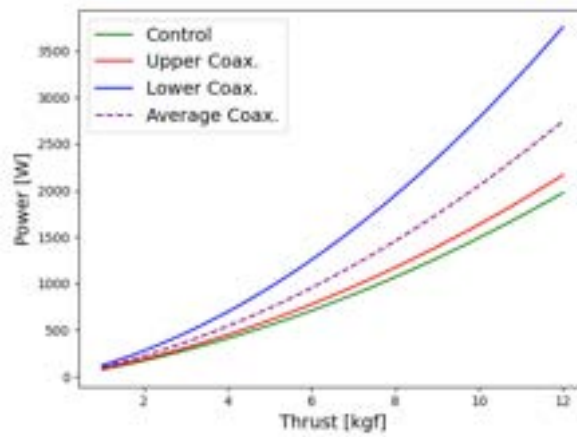
With the approximated AUW, 12 cell 46Ah lithium polymer batteries, and Eqn. 3, the predicted flight time for dodeca-copter, coaxial dodeca-copter, and deca-copter configurations were calculated for different numbers of Swarm Drones (Fig. 39a). In Fig. 39a it can be seen that the predicted flight time for the coaxial dodeca-copter falls below the defined constraint flight time of 15 minute for all 6 Swarm Drones (Section 3.4). From the thrust data, a two dimensional polynomial regression for the PWM vs thrust was determined. From the different carrier airframe configurations, the individual motor hover PWM vs number of Swarm Drones is plotted in Fig. 39b. The PWM constraint of  $1600\mu\text{s}$  (approx 60% throttle) is common in the UAS industry as a hover PWM value lower than 1600 guarantees a thrust to weight ratio of 2:1 which is required for good flight performance [14]. Both the coaxial dodeca-copter and deca-copter configurations show hover PWM values greater than  $1600\mu\text{s}$ . While the standard dodeca-copter passed the quantitative analysis for the requirements, the complexity of manufacturing for a planar dodeca-copter invalidated it. With all three of the considered Carrier Drone design configurations invalidated, different motor and propeller configurations were then considered.



(a) Thrust vs. RPM

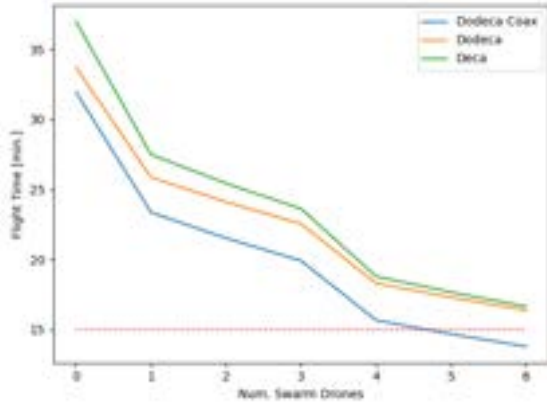


(b) Motor Power vs Thrust

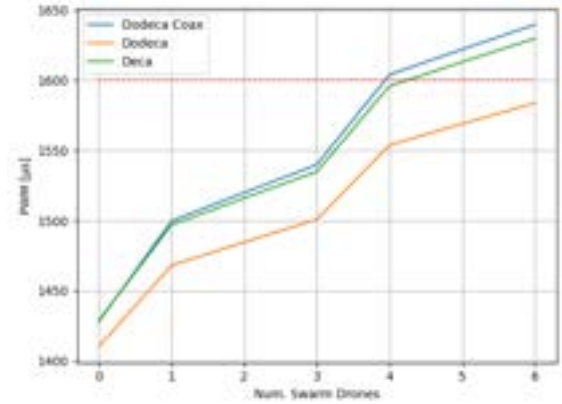


(c) Current vs. Thrust

Figure 38: Coaxial thrust test results



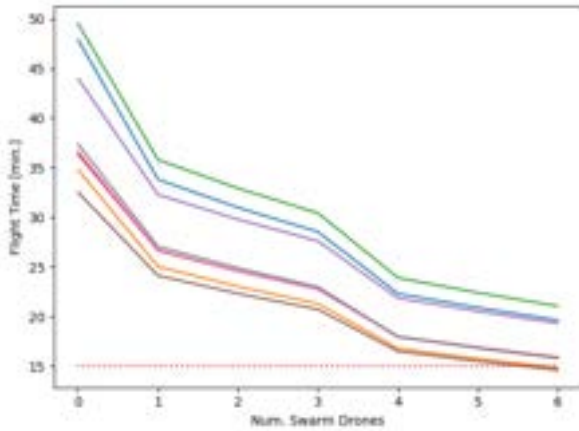
(a) Flight time vs. Num. Swarms



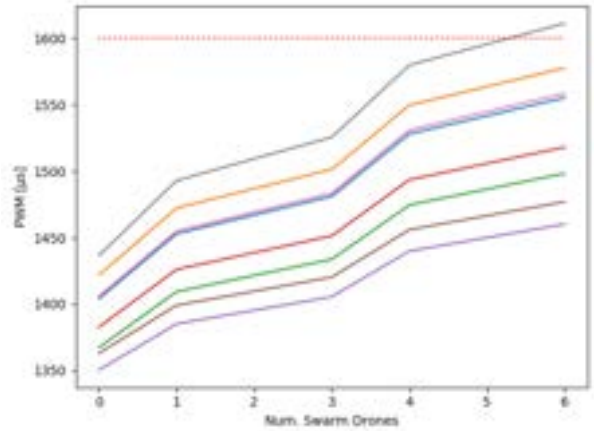
(b) PWM vs. Num. Swarms

Figure 39: Experimental results design decisions

From the manufacturers' provided specifications and the known coaxial motor thrust loss of 20%, four different motor and propeller combinations were analyzed in coaxial dodeca-copter and decaco-pter configurations for a total of 8 different configurations. Fig. 40c contains a legend of all the different configurations considered. The prefixes tell what motor configuration, different p80iii motor speeds were denoted by their kv value, 30 and 32 inch diameter propellers were denoted, and coaxial configurations were labelled as 'coax.' With similar analysis as above, the flight time as a function of number of Swarm Drones and the PWM as a function of Swarm Drones plots are displayed in Figures 40a and 40b respectively. The majority of the configurations were within the constraints as expected as they all used higher quality propellers than the experimental tests. As a result, the highest performing flight time configuration was chosen with the same TMotor P80III 100kv motors but using TMotor G32x11 propellers in a decaco-pter configuration with a predicted flight time of 21 minutes for all 6 Swarm Drones.



(a) Flight time vs. Num. Swarms



(b) PWM vs. Num. Swarms

- Deca p80iii-100kv-g30x10.5
- Dodeca Coax p80iii-100kv-g30x10.5
- Deca p80iii-100kv-g32x11
- Dodeca Coax p80iii-100kv-g32x11
- Deca p80iii-120kv-g30x10.5
- Dodeca Coax p80iii-120kv-g30x10.5
- Deca Hybrid Coax p80iii-100kv-g32x11
- Octo Hybrid Coax p80iii-100kv-g32x11

(c) Legend of motor and propeller configurations

Figure 40: Prediction design decisions

Following the Carrier Drone V1 test outlined in Section 5.11.5, the motor configuration of the Carrier Drone was reduced to an octocopter carrying only one Multidrop Bay. Flight time recalculations were performed for the new motor configuration to evaluate its capabilities. Fig. 41 displays the calculated theoretical flight time of the Carrier Drone V3 as a function of number of Swarm Drones. This plot below shows that the flight time for three Swarm Drones was approximately 32 minutes, exceeding the design requirement of greater than 15 minutes of flight time. Following this confirmation of flight capability, the team proceeded to the design and manufacturing stage of the Carrier Drone V3.

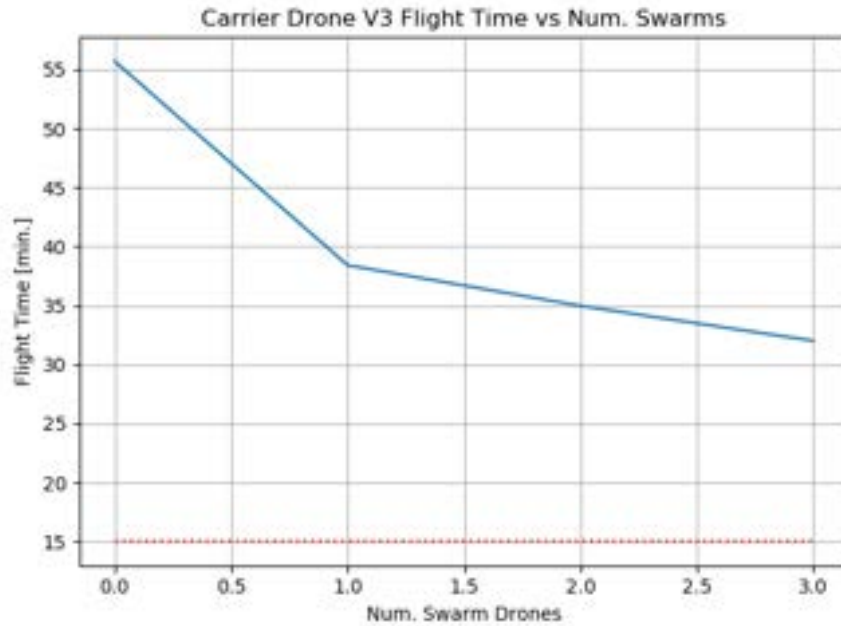


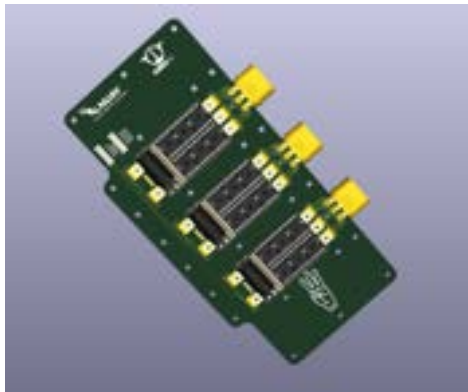
**Figure 41: Carrier Drone V3 theoretical flight time calculation**

### 5.3.7 Power Distribution

Due to the nature of the carrier UAS carbon fiber frame design, internal wire routing is not possible. It was decided that the ESCs for all of the carrier UASs motors would be centrally mounted. This reduces the overall moment of inertia of the carrier UAS as more weight is located at the center of rotation. Additionally, centrally mounting the ESCs maintains the signal integrity of the PWM signals increasing the overall safety of the carrier. Thus the three brushless motor phases need to be routed from the center of the Carrier Drone out to each motor. PCB solutions were designed for wire management and easier mounting to square carbon tube than traditional wire. While the actual circuit design for these elements is trivial, the increased organization and robustness will make assembly and maintenance easier. Fig. 42a displays the ESC mounting board which allows an APD 120 F3 12S 50V 120A ESC and corresponding MR60 connector to be soldered onto the board. Fig. 42b displays the phase wire routing PCB which was designed to be mounted on the outside of the Carrier Drone carbon frame assembly. The most difficult part of the design process for these components was the trace width calculations to ensure that the PCBs could operate at the

power demands of the motors using [40] for a two layer 2oz. copper PCB. On the Carrier drone (Fig. 25a), these boards can be seen passing power to the motors while also providing a rigid mounting point to the Multidrop Bay. Additionally they provided advertisement space to display the project's sponsors' logos as stipulated in their sponsorship agreements.

The power distribution of the LiPo batteries to the ESC exceeded the capabilities of standard PCB, thus it was more cost effective to use copper bus bars instead using [41] to meet the combine maximum continuous current draw of 12 ESC at 45A with an additional factor of safety. Due to the large number of capacitors in the ESCs there was a risk of sparking and high inrush currents when first connecting the batteries to the Carrier Drone. The inrush current had the potential to damage some of the electronics. To mitigate the inrush current, a pre-charging resistor bank was plugged in prior to the main battery connection in order to limit the inrush current.



(a) ESC routing PCB



(b) Phase routing PCB

Figure 42: Power distribution PCB

### 5.3.8 FEA of Carrier Drone

An important factor in the Carrier Drone's design is how it handles vibrations and its natural modes of vibration. This is critical to ensuring that the motor and propeller's frequency does not match with the resonant frequency of the airframe, which could prove worrisome to any flight operations. A difficult aspect of this analysis is the use of composite materials for the cross-sections of the airframe. Composite materials exhibit orthotropic elasticity that is very hard to mechanically measure and simulate without specialized equipment. In addition, the mechanical properties of carbon fiber laminates are dependent on their fiber orientations and layer arrangement, which means samples to test on have to be provided by the manufacturer to gain any reliable data. The group has been in close contact with the carbon fiber tube manufacturer, professors who specialize in composite material analysis, and other composite laminate manufacturing company specialists on simulating composites in ANSYS Workbench. These contacts have provided individual lamina layer properties and resources to properly conduct FEA simulations in ANSYS Workbench using ANSYS Composite PrepPost (ACP). This powerful ANSYS package will allow the group to recreate the carbon fiber laminate on the Carrier Drone frame to determine the modes of the system. ACP is being heavily used during Capstone II to finalize the Carrier Drone V2 design and prove the structural integrity of design. Current research is focused on the necessity of FEA ACP over empirical

tests due to the fast timeline of the project.

At the end of September 2021, the Swarm Carrier team exchanged information with the Forestry Sensor Drone team regarding workflows for testing laminates in ANSYS ACP. It was determined that vibration analysis of multiple components was not feasible within a semester deadline but quasi-static analyses were possible. The Swarm Carrier team has acknowledged this progress but has also verified the performance of cable tensioning and laminate dynamics empirically (see sections 5.3 and 5.3.3). As a result of this confidence built from real-world testing, the final development of Swarm Carrier will continue to focus on empirical testing over simulation.

#### **5.4 Behavior Trees**

Behavior trees is implemented in software by using an open source project called "BehaviorTree.CPP" [42]. This project is used in various other ROS2 projects such as "navigation2", which is a general implementation for navigation algorithms in robotics using sensors. Behavior trees are necessary to handle the control logic and recovery behavior of failed missions. For more information related to how behavior trees work see Section 4.2.5.

Custom action nodes were created for each ROS2 action, like precision land and go to coordinate actions. There are specific behavior trees being created for many purposes. The higher level precision land tree in Fig. 43 shows one of these instances.

There are plans to account for various end conditions using nodes that check sensor information, such as battery and distance from home. In cases where the voltage drops to low, behaviors that initiate a return to home for forced landing may activate. These decision nodes are vital to the safety and effectiveness of the system.

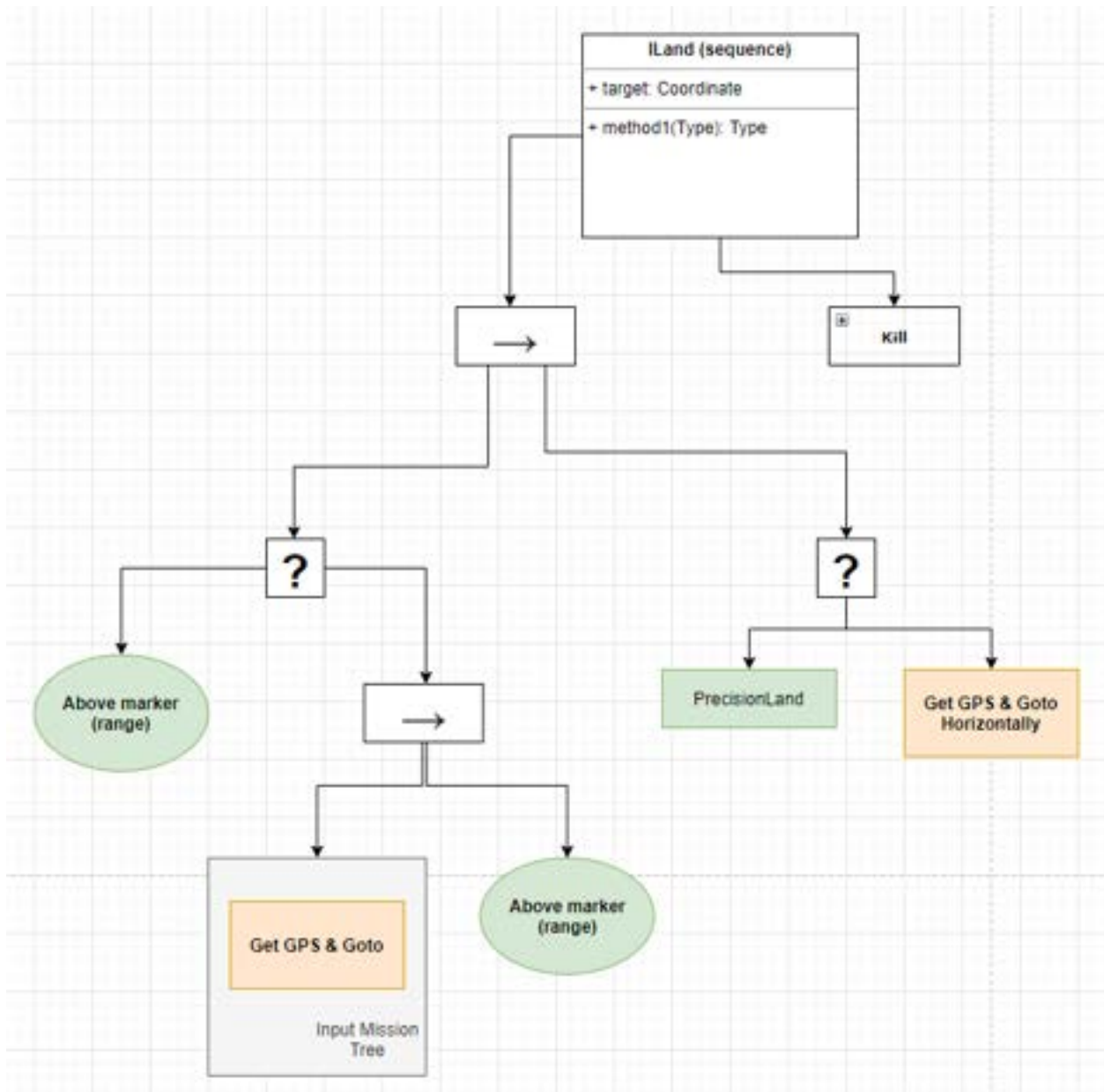


Figure 43: High-level precision land behavior tree

## 5.5 Drop Mode

Drop Mode is one of the fundamental actions being implemented for the software aspect of Swarm Carrier. Its purpose is to be an implemented mode within PX4 that catches the drone while it is falling. To implement this action, first the motors on the drone need to be blocked. This needs to be done since PX4 must spool up its internal logic assuming the motors have been activated, but for this project the motors cannot actually spin. The motors cannot spin since the Swarm Drones will be inside the Carrier Drone and would damage it. Once the motors have been blocked the vehicle must be told to move to a point higher than its current position. At this point it will try to takeoff but cannot since the motors are blocked. The Carrier Drone will then proceed to release the Swarm Drone. While the Swarm Drone is in free fall it will constantly have a loop checking if the drone reached a certain velocity and then unblock the motors. At this point in time the Swarm Drone should catch itself while it switches to a hover mode.

The current implementation of Drop Mode in the PX4 firmware is in the form of two acknowledgment (ack) message publishers. One for sending an ack message that the motors have been blocked, and one for acknowledging that they have been re-activated. The purpose of these is be able to constantly publish vehicle commands until the ack messages are seen so that no messages are lost, giving the drone the best opportunity to catch itself.

## 5.6 Precision Landing

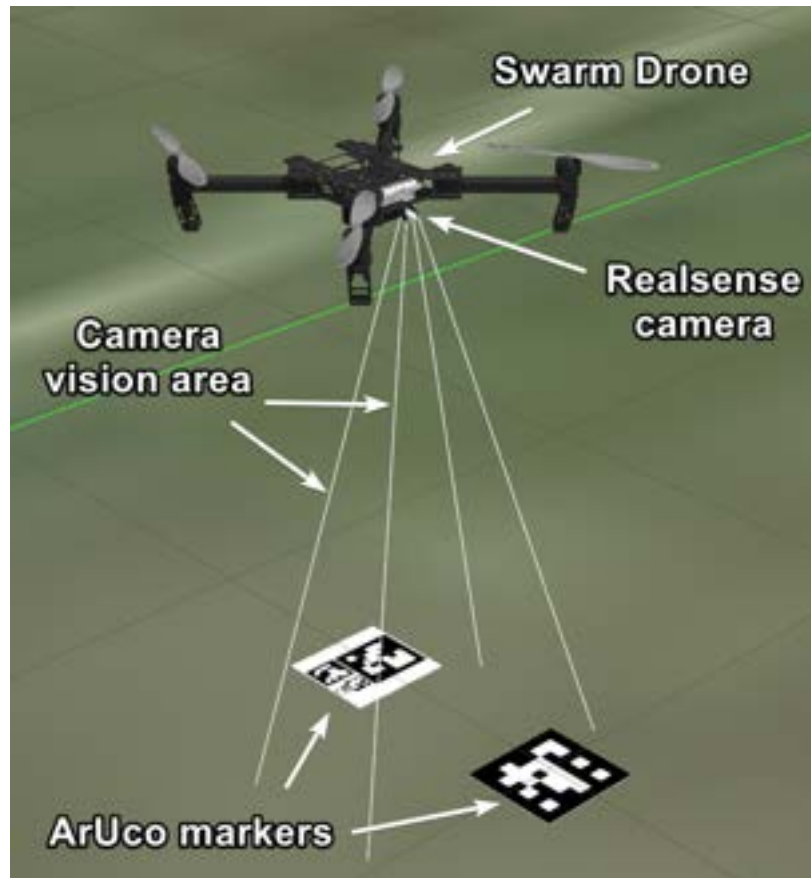
The task of precision landing is to enable fully autonomous recovery of the Swarm Drones with the Carrier Drone. To achieve this a behavior tree was designed to execute the actions required. This is shown in Fig. 43. The basic control flow begins with giving the drone an initial GPS starting point, in this case representing the location of the Carrier Drone.

The main tool utilized for this task is the computer vision required to detect ArUco markers and estimate their 3D pose relative to the Swarm Drone (see Section 4.2.4 for more information). For the task of precision landing, multiple ArUco poses are used to determine the landing pose at any given height. Each marker is a different size in order to guarantee consistent detections. The ArUco landing array, below in Figure 45, was updated to place progressively smaller markers towards the center to improve detections at lower altitudes. An offset is applied to each marker to return the actual landing pose, which is then smoothed using a moving average. In the case that a marker detection is drastically off a filter is also applied to the final result. Using the Carrier Drone's position, detections that are not close to it can be ignored in the algorithm.

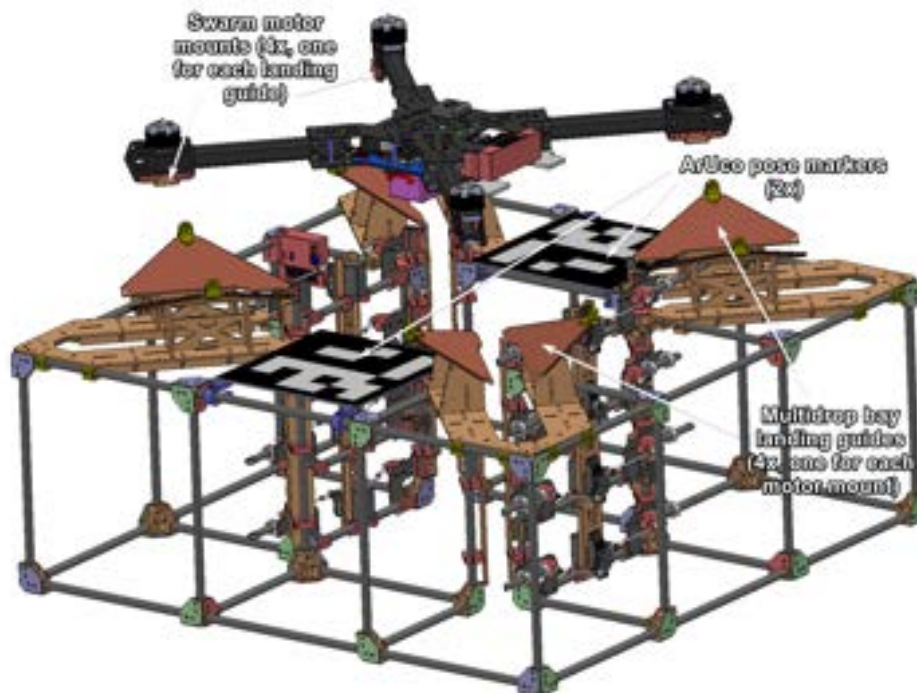
Once the landing pose is calculated, proportional-integral-derivative (PID) controllers are used to correct for errors and adjust velocity commands appropriately. This control phase is separated into four phases: quick adjustment, horizontal alignment, yaw alignment, and vertical descent. First, the Swarm Drone will quickly move towards the marker until it reaches an arbitrary altitude determined through experimental results. Once at this altitude, it will adjust its positioning so that it centers itself above the landing pose. After centering, it will align its yaw so that the Swarm Drone is aligned with its camera facing the smallest ArUco markers. After it is centered and looking in the correct direction, it initiates a descent phase to land directly on the marker. If it ever falls outside the horizontal tolerance or yaw tolerance it will revert to the corresponding stage and follow the same procedure again. The behavior tree (see Section 4.2.5) is also structured so that

if the ArUco marker is lost, a recovery action will be performed to regain visual detection of the markers. Fig. 44a demonstrates the simulated precision land process. Instead of the ground, the markers would actually be placed on the Multidrop Bay, shown in Fig. 44b.

The end condition for the task of precision landing is reintegration with the Multidrop Bay. The Swarm drone detects reaching the Multidrop Bay using contact sensing (see Section 5.8). The current implementation constantly polls a general-purpose input/output (GPIO) port, when it is true a motor kill command is sent. Initial testing has been done and has shown the delay from contact to full motor kill to be approximately 40ms which is useable for the system going forward.



(a) Gazebo view of precision land



(b) Swarm Drone example landing position in the Multidrop Bay

Figure 44: Precision landing in simulation

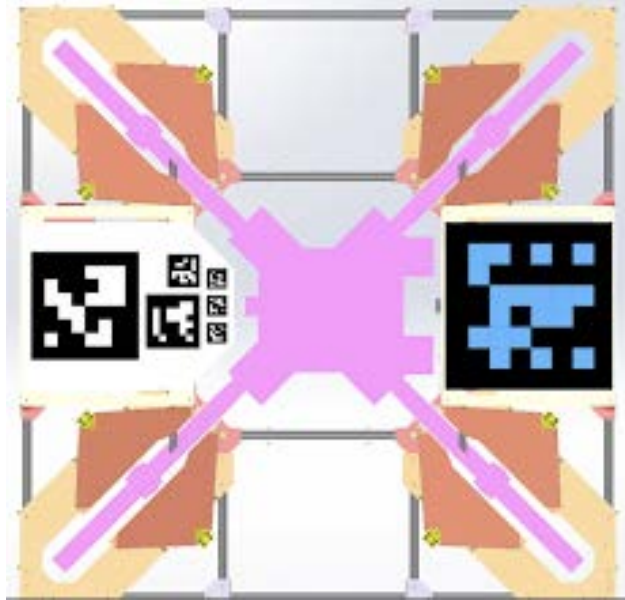
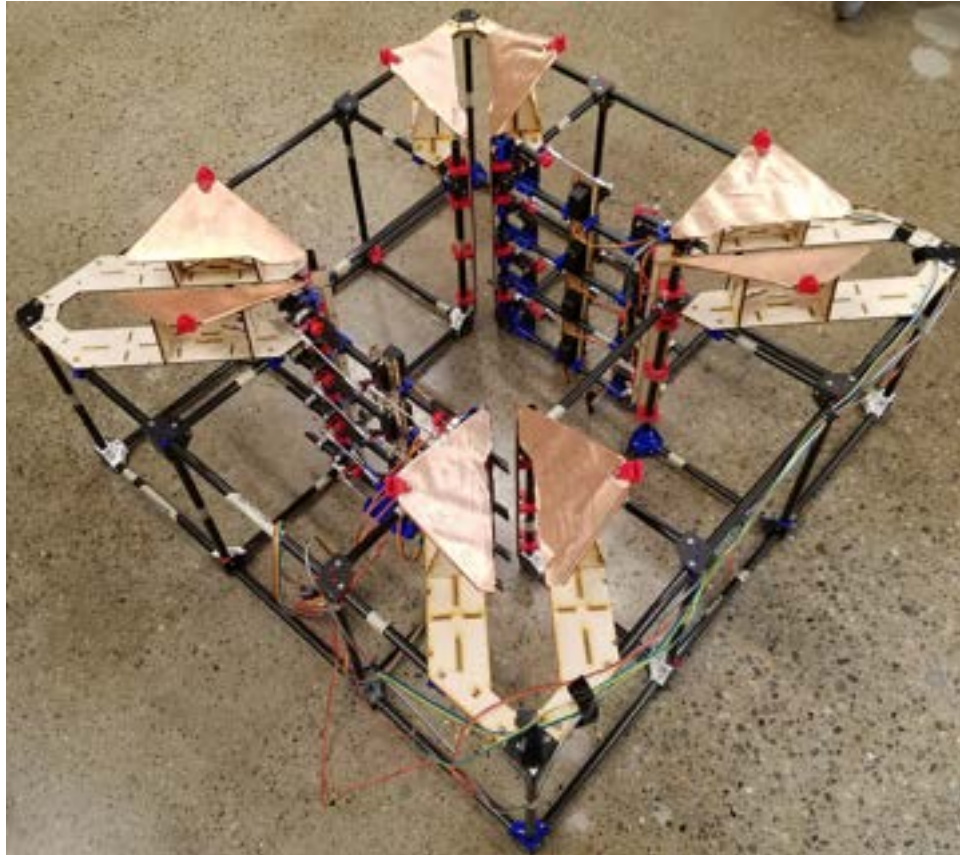


**Figure 45: ArUco landing array V2**

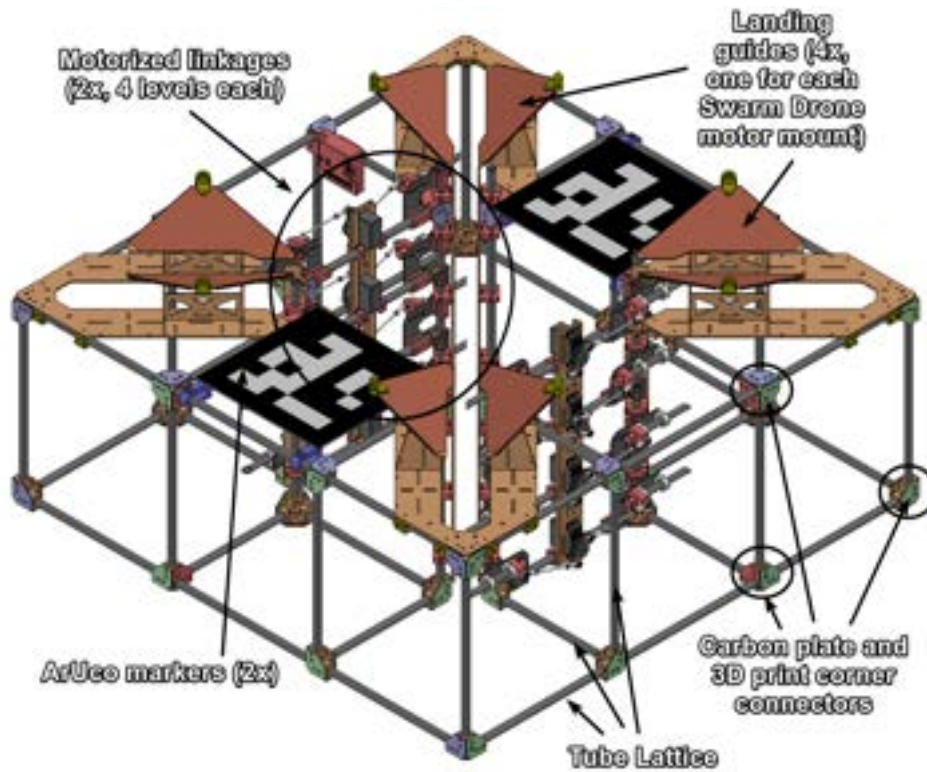
## **5.7 Multidrop Bay**

Development of the Multidrop Bay V3 began in July 2021 based on lessons learned from the previous iterations mentioned in Section 4.3.3. Notably, the unreliability of pulley-based linear actuators prompted research into rigid linkages. These applied uniform force in tension and compression. Furthermore, given the high unique part count and assembly difficulty of the V2 design, the V3 required optimized frame dimensions and connectors to reduce the probability of tolerance stackup. Lastly, landing geometries and their associated fixtures were optimized to reduce weight and improve ease of assembly.

Functionally, the V3 iteration had the same constraints as the V2. It utilized gravity to reintegrate landed drones and then servo linkages to pass them through the carrier drone frame. Fig. 46 below shows the V3 CAD assembly and prototype of the lattice structure and mechanisms completed in summer 2021.



(a) Initial prototype



(b) CAD model

Figure 46: Multidrop Bay V3

The Multidrop Bay V3 was designed to sit inside square openings of any of the Carrier Drone designs, with empty space both above and below allowing for recovery and deployment of the Swarm Drones. Due to heavy usage of lightweight components like wood and carbon fiber, the overall weight of the Multidrop V3 frame was only 2kg. Most of the remaining weight came from the motorized linkages and hardware, which brought the overall weight to 5.5kg. Specific developments relating to landing guide geometries and linkage mechanisms are discussed in detail in the following sections (5.7.1, 5.7.3, and 5.7.4).

### 5.7.1 Multidrop Bay Lattice and Connector Optimization

The development of simple, light weight joinery for the Multidrop Bay designs was a critical constraint in order to produce a rigid design. Payload rigidity was prioritized to reduce internal sources of vibrational noise within the carrier drone as well as to prevent jamming of vehicles during passage through the mechanism. Adhesives were invalidated due to concerns with jiggling, lack of control of tolerance stack up, and overall difficulty of assembly for round, hollow tubes. In order to produce a modular, rigid, and easily assembled design, bolted connectors were developed to join members of the lattice frame.

Initial connector designs for the Multidrop Bay V2 involved multiple configurations depending on the number of members at a given joint. Composite design was also leveraged with 3D printed clamps to comply to round tubes that were surrounded by carbon fiber plates to absorb the majority of loads on the frame. Prototypes for the V2 and V3 bay design can be seen below for fixturing joints with up to 4 members.

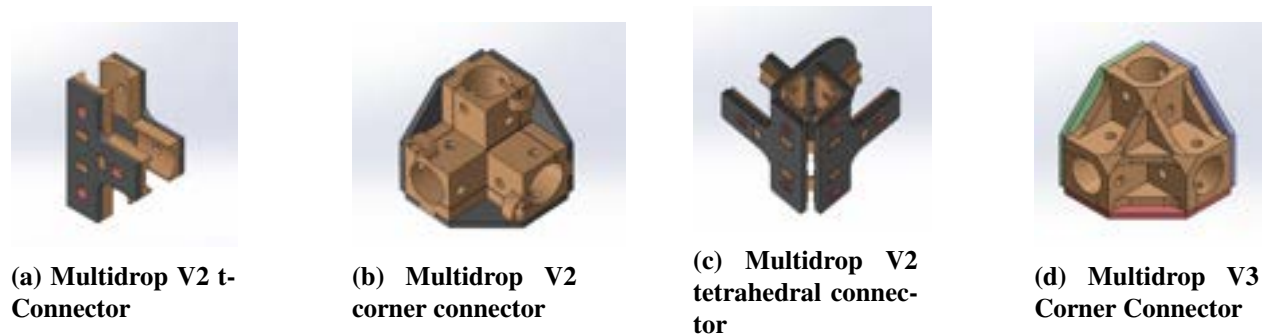
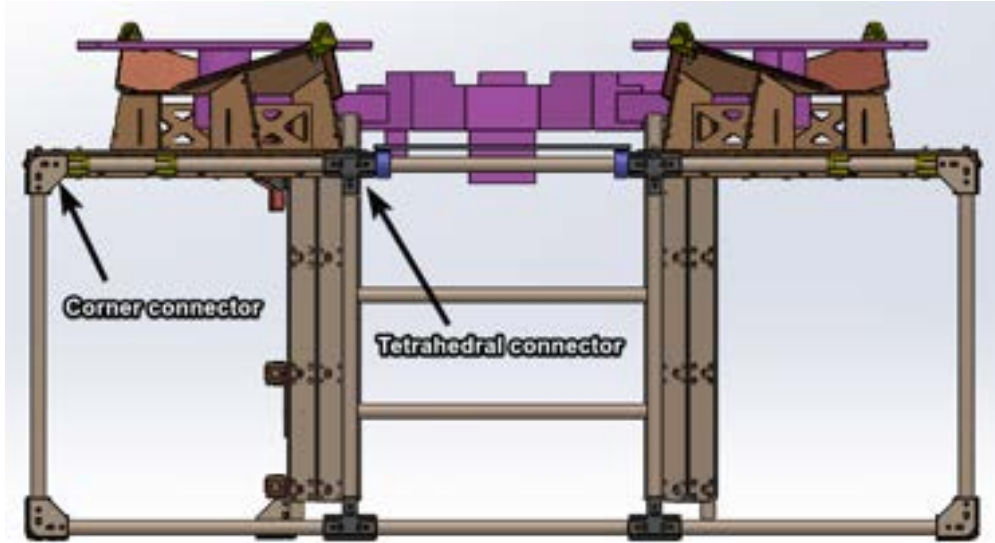
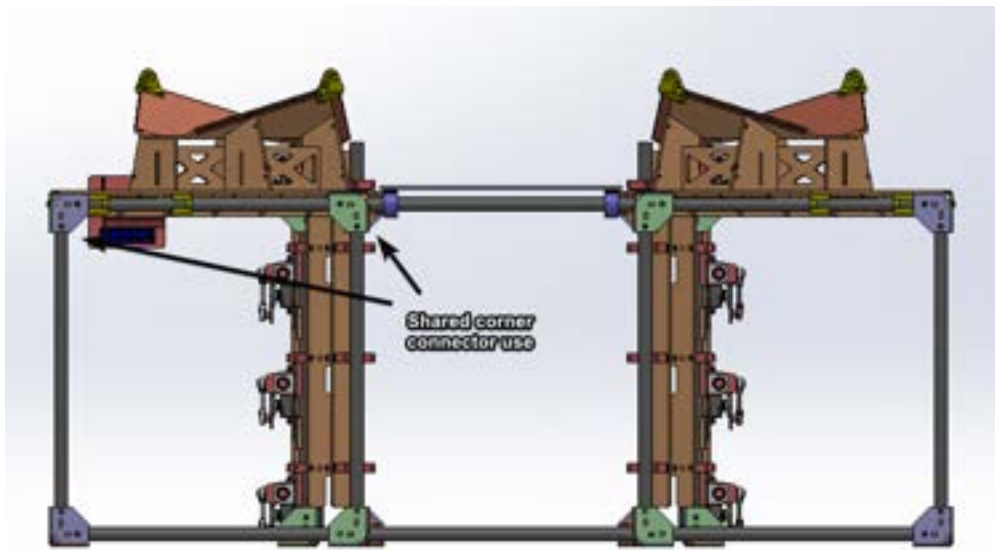


**Figure 47: Multidrop Bay V2-V3 connector iterations**

The t-connector, tetrahedral connector, and corner connector iterations all leveraged the clamping force of 3D printed elements to comply to round frame members. External carbon plates also provided constant compression of 3D printed components to prevent tensile failure modes. While capable, the t- and tetrahedral connectors resulted in large part counts and reduced manufacturability of the V2 bay design. The V3 corner connector shown above was designed to act as a corner or tetrahedral joint to reduce unique part count. Fig. 48 below shows the V2 and V3 bays with their respective connector configurations. It can be seen that the more versatile corner connectors of the V3 iteration can accomplish the same fixturing as the V2 tetrahedral joints with fewer unique parts.



(a) Multidrop Bay V2 connector configuration



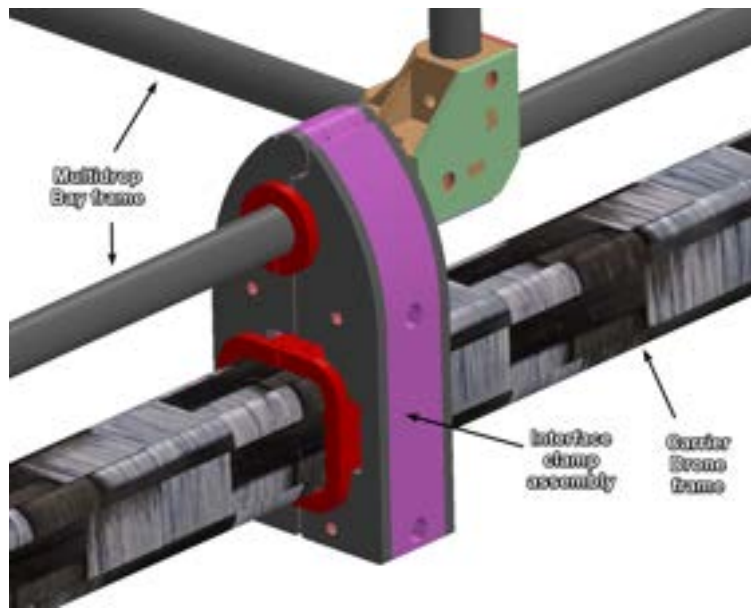
(b) CAD model

Figure 48: Multidrop Bay V3 connector configuration

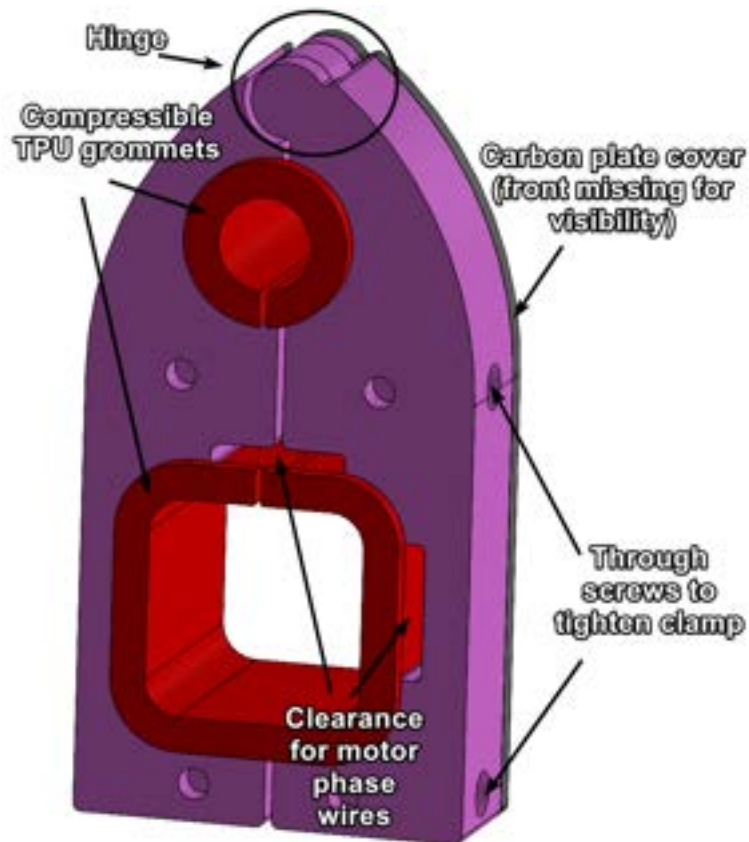
### 5.7.2 Multidrop Bay Connections to Carrier Drone

The final area of development in the Multidrop Bay's frame is its attachment into the Carrier Drone. Fixture points and designs will have to be iterated in order to maintain guide rigidity. An example for the interface clamp between the Multidrop Bay and the Carrier Drone is shown below in Fig. 49. The purpose of these fixtures is to rigidly support the Multidrop Bay within the Carrier Drone. Due to the fact that the Carrier Drone is pre-assembled, fixture points cannot be slid onto its square frame members. Furthermore, given the flexibility of the Multidrop's lattice frame in multiple areas, fixture points had to be adaptable in order to determine the best mounting positions during tests. Therefore, the goal of the subsequent designs is to constrain the motion and flexure of the Multidrop while being adaptable to different placements based on need.

To accomplish this goal while maintaining strength, the developed fixtures used a 3D print-in-place hinge with TPU grommets to comply to varied frame cross sections. Similar to the Multidrop's frame connectors shown in Fig. 47, the clamp used external carbon fiber plates to absorb the bulk of tensile and compressive loads. With the design shown in Fig. 49b below, the clamp was easily opened, inserted around the frames of the Multidrop and Carrier drone, and subsequently tightened using two bolts.



(a) Location of interface clamp



(b) Detail of clamp assembly

Figure 49: Aligned interface clamp between Carrier Drone and Multidrop Bay

Crucially, Fig. 50 below shows the anatomy of the print-in-place hinge which has a hyperbolic cross section. This was specifically designed to mitigate shear stresses and maximize compressive strength.

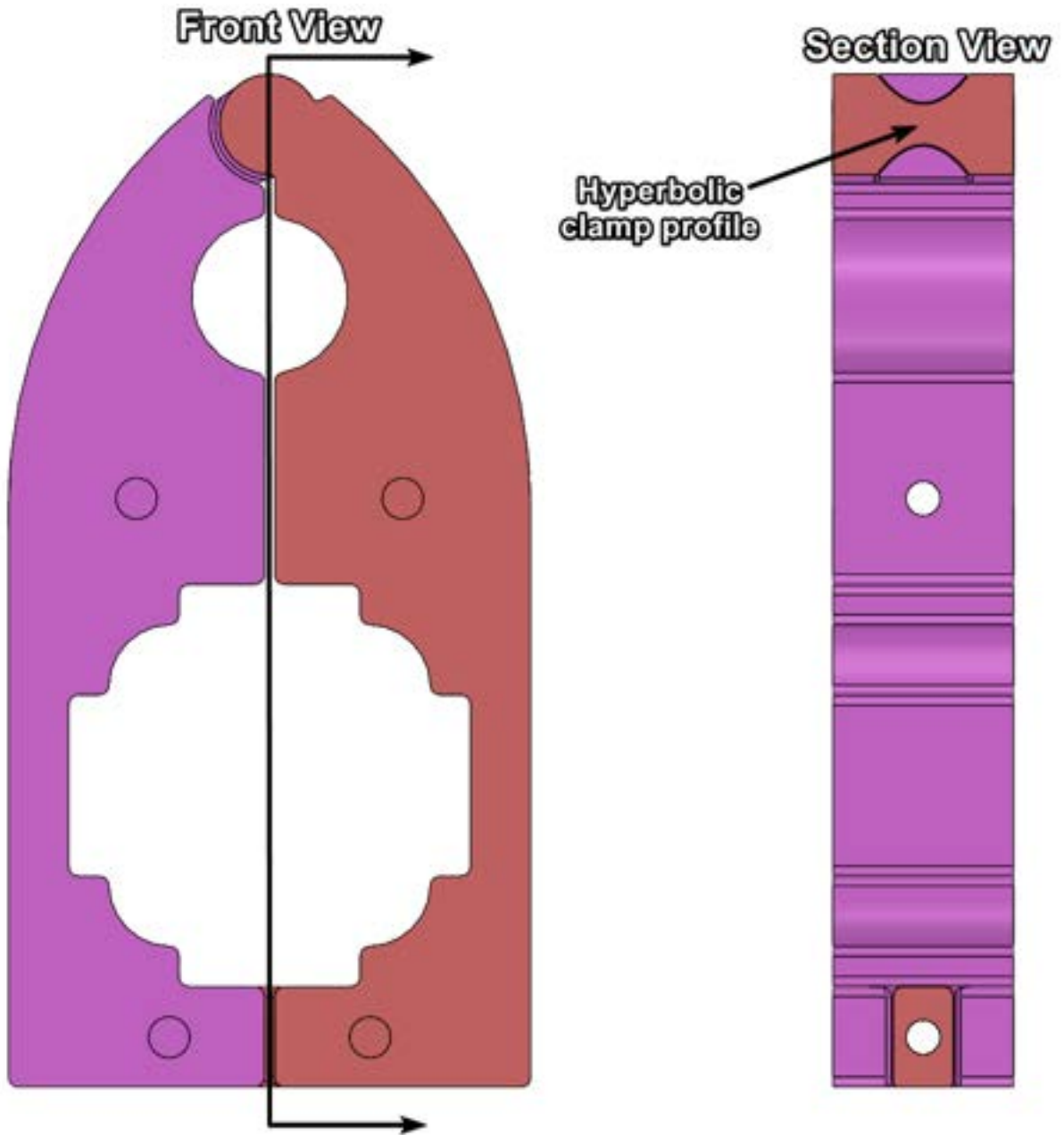


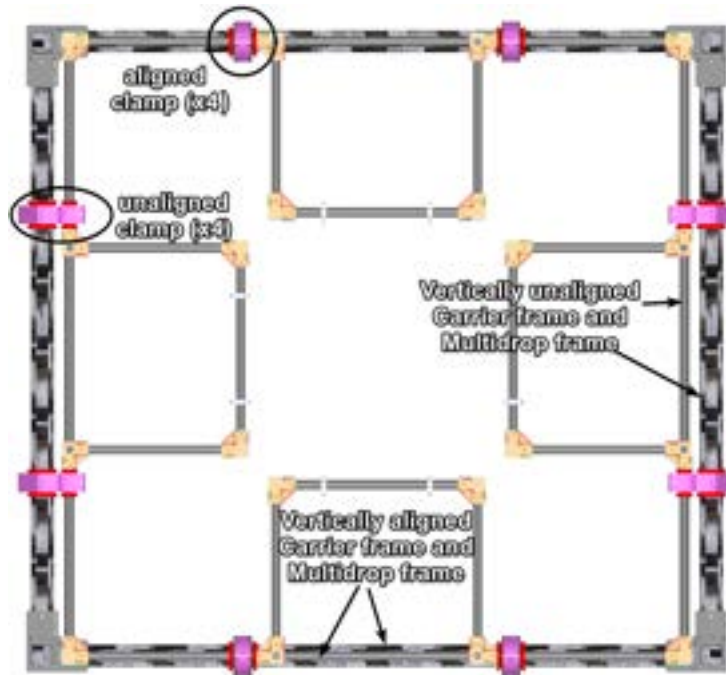
Figure 50: Hyperbolic profile of clamp

The physical implementation of the clamps shown above in Fig. 49 and Fig. 50 performed as designed, allowing for strong and easy to assemble contacts. The real implementation is shown below in Fig. 51.

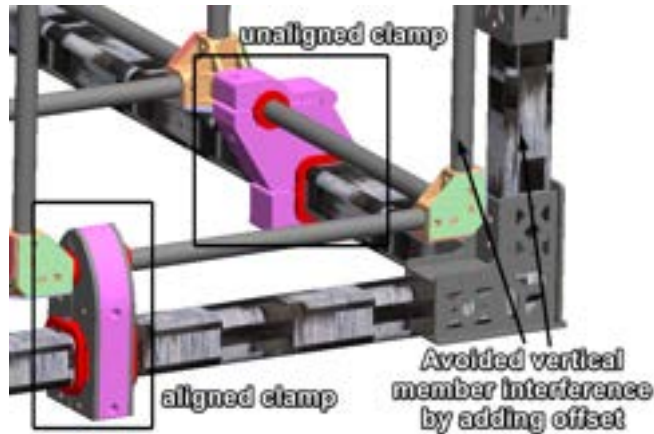


**Figure 51: Real life application of clamp to frame**

The Multidrop Bay to Carrier Drone connectors shown above in Fig. 49, Fig. 50 and Fig. 51 only work in 4 out of 8 desired clamping positions on the bottom of the Multidrop Bay. This is due to geometric constraints of fitting the Multidrop Bay inside of the Carrier Drone. In order to fit, one side of the Multidrop Bay can not be vertically in line with the Carrier Drone, otherwise the two assemblies would intercept at the corner. This is shown below in Fig. 52. The aligned connectors shown above in Fig. 49 and Fig. 50 are shown, as well as the unaligned connectors shown below in Fig. 53.



(a) Top down section view showing offset



(b) Position of both bottom clamp types and avoided interference zone

Figure 52: Offset between Multidrop and Carrier frames

The unaligned Multidrop Bay to Carrier Drone connector is shown in detail below in Fig. 53. The design for this connector was largely the same as the one shown in Fig. 49 and Fig. 50 above, using TPU grommets to give strong contact between clamping surfaces, the same hyperbolic hinge profile, and tightened using bolts. The main difference is the added offset to accommodate for the geometry of the relative position of the Carrier frame to the Multidrop frame, as well as adding an additional part that is screwed on separately from the hinge.

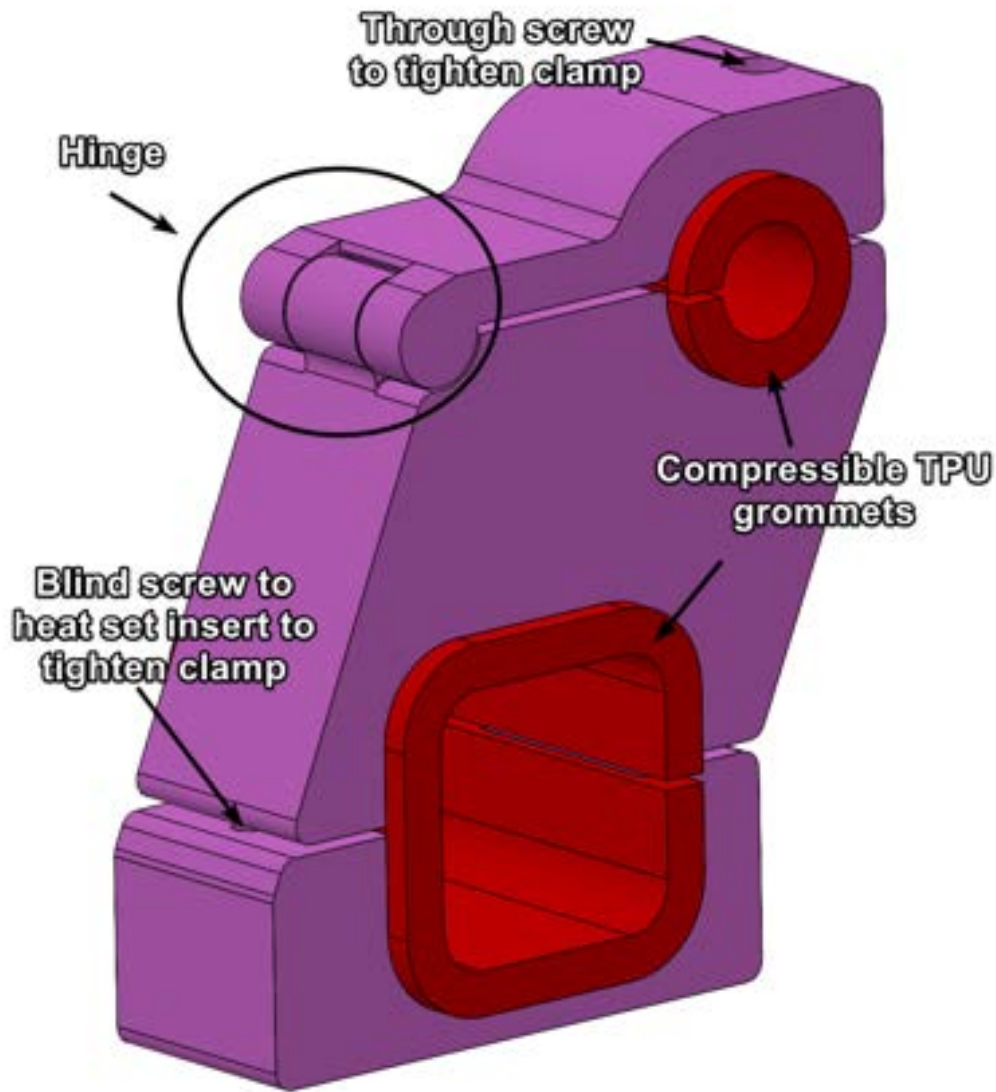


**Figure 53: Unaligned interface clamp**

Similar to the physical implementation of the clamp shown in Fig. 51 above, the unaligned interface clamp also performed well. A real life picture is shown below in Fig. 54.



**Figure 54: Real life application of clamp to frame**

The designs for the 8 connection points to the bottom of the Multidrop Bay discussed above were not transferable to the 8 desired connection points to the top of the Multidrop Bay. Fundamentally, the purpose of the bottom connectors is to keep the Multidrop Bay secured within the Carrier Drone. These accomplished this task well, though after prototyping with only the bottom 8 connectors attached, the Multidrop Frame lacked overall rigidity and sagged within the Carrier Drone. This is an area of concern, as any flexing of the internal guides and linear actuators can potentially cause jamming during the movement of the Swarm Drones inside of the Multidrop Bay. The issue of the rigidity is shown below in Fig. 55.

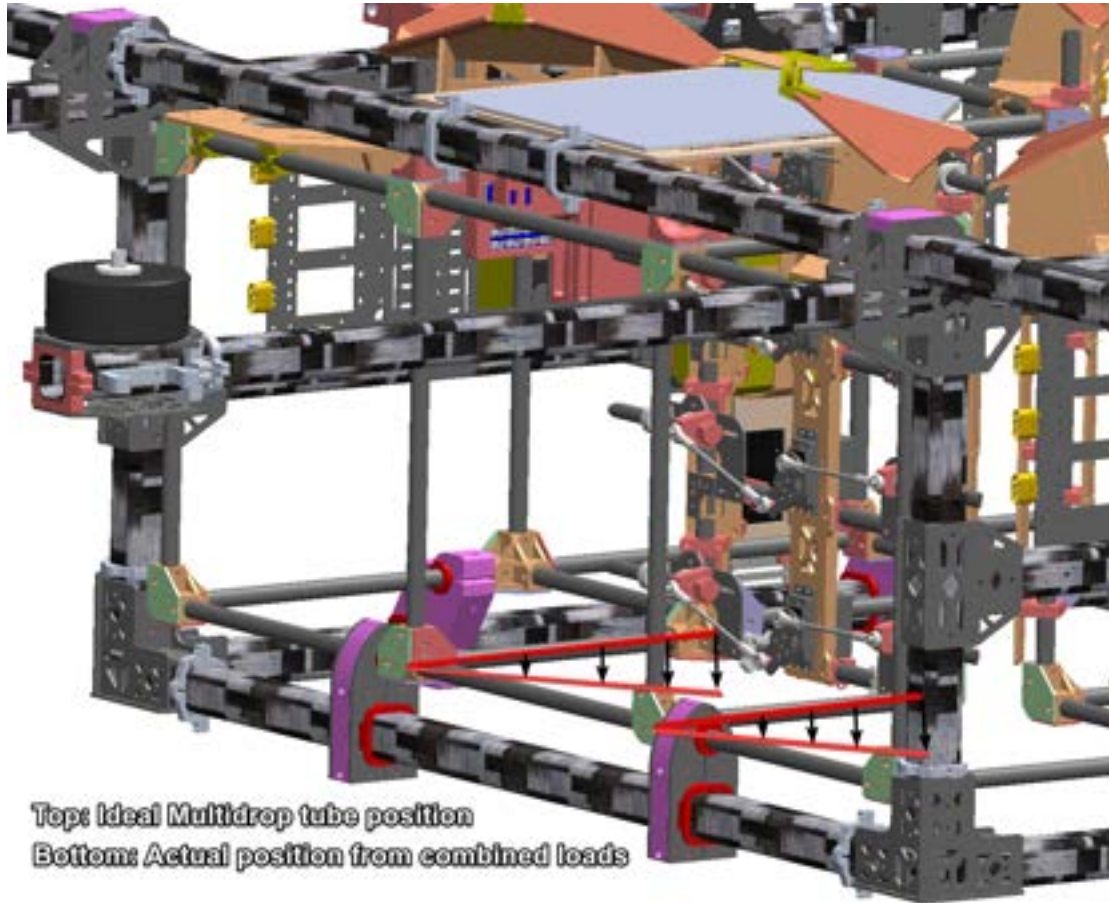
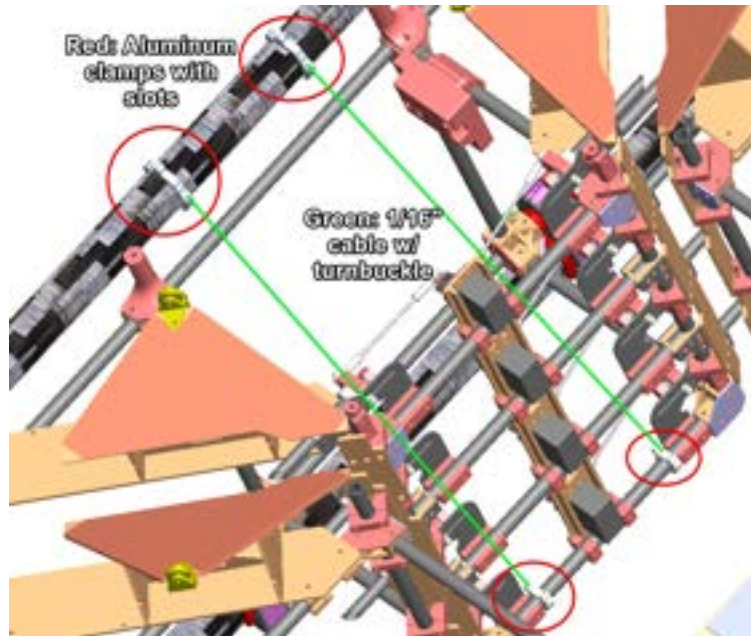


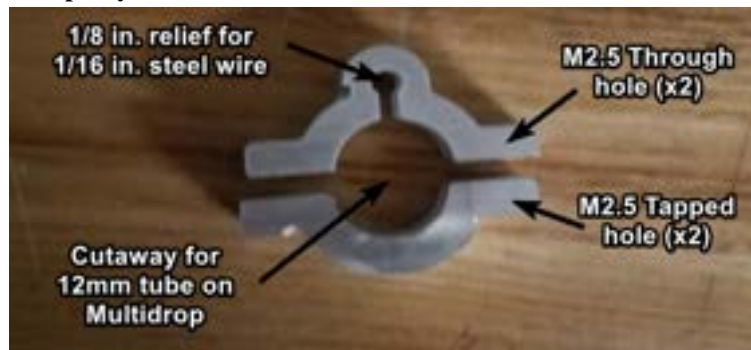
Figure 55: Deflection of bottom of Multidrop Bay

Through testing, it was determined that the cause of the Multidrop Bay sagging was due to the weight of the motorized linkages and three swarm drones inside. The initial plan to fix this was to reuse the bottom clamp connections between the Multidrop Bay and the Carrier Drone on the top of the Multidrop Bay, though initial prototypes did not solve the issue. This was because the source of the sagging was actually due to the loading of the weight being on cantilevers as shown above in Fig. 55, so a direct attachment was needed to fix the flexing.

To fix this issue, a similar approach to the cable tensioning discussed in Section 5.3 above was used. The proposed scheme is shown below in Fig. 56.



(a) Cable tensioning between Carrier Drone and bottom of Multidrop Bay



(b) Physical aluminum clamp

Figure 56: Fix to Multidrop Bay rigidity using cable tensioning

The proposed scheme turns the loading situation from a pure cantilever on the Multidrop Bay frame, to a cantilever supported by a cable in tension. Using a turnbuckle, the length of the wire can be shortened to apply tension, similar to the wire tensioning scheme outlined in Section 5.3. The aluminum clamp to the Multidrop Bay follows the same design process as the aluminum clamp to the Carrier Drone. It uses 1/4" aluminum water jetted profiles, with the M2.5 through holes and taps performed using a Tormach CNC. The physical implementation of these new clamps and the cable tensioning scheme shown above in Fig. 56 are shown below in Fig. 57.

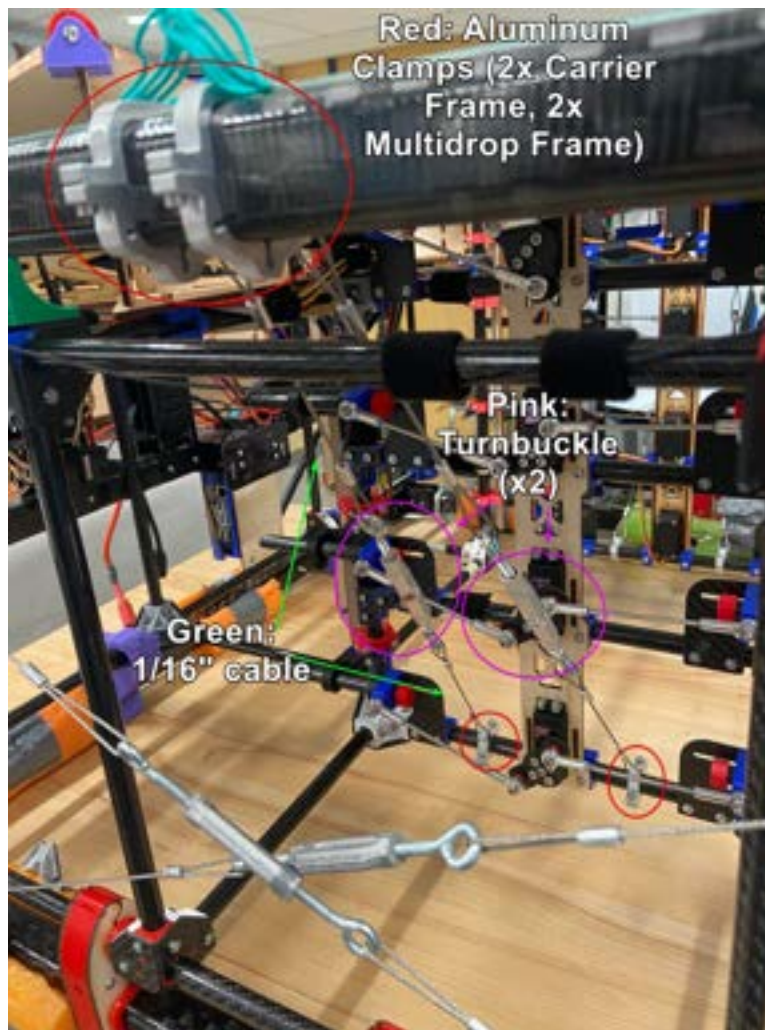
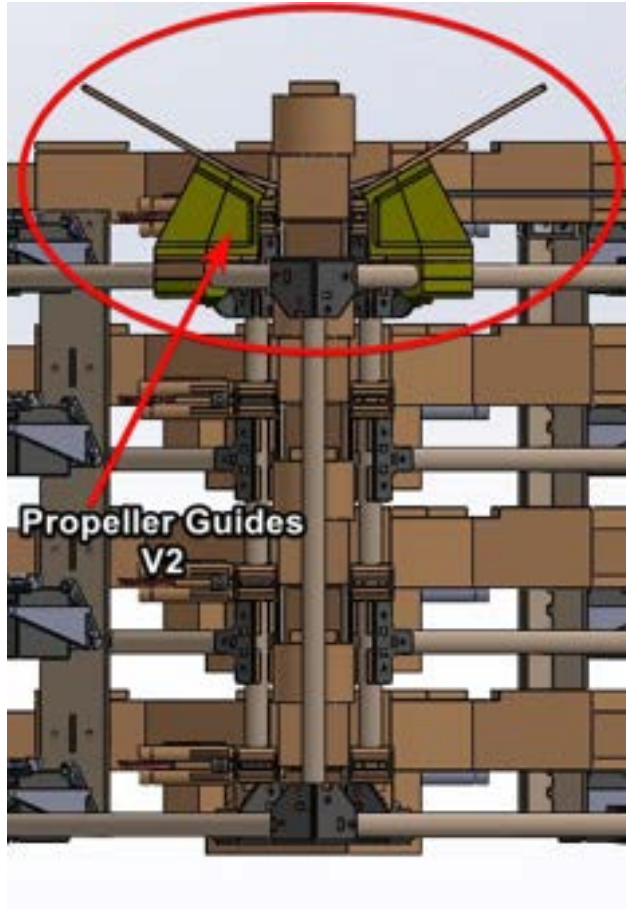


**Figure 57: Cable tensioning to fix Multidrop Bay sagging**

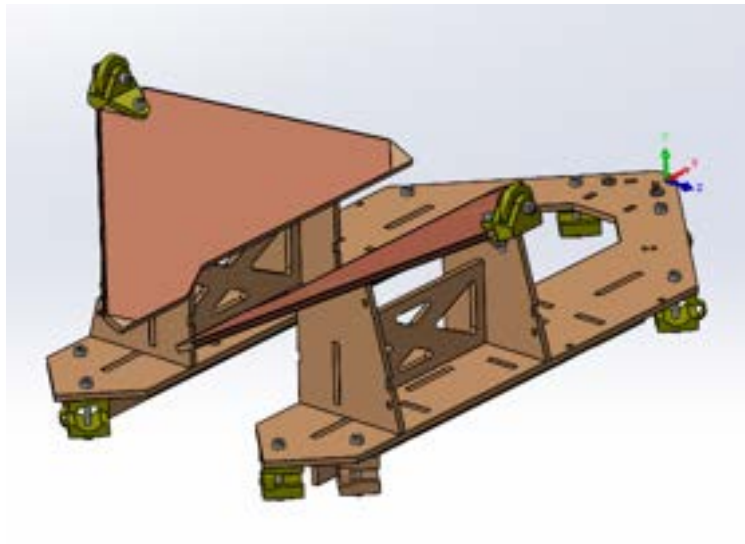
By using the cable tensioning, the sagging of the inner Section of the Multidrop Bay was fixed. By adjusting the tension in the turnbuckle, the location of the Multidrop Bay frame was precisely adjusted to the desired location.

### 5.7.3 Landing Guides

In addition to actuating the Swarm Drones, a constraint of the Multidrop bay V3 was passive alignment of propellers during reintegration. To accomplish these, designs employed triangular geometries to maximize the area in which the Swarm Drone land and be successfully rebounded into the mechanism. Preventing propeller damage was also a key consideration of the guides which influenced their shape. Figure 58 below shows the differences between the guides of the V2 and the initial guides for the V3 Multidrop Bay. The initial V3 design improved upon the 3D printed supports of the V2 guide (shown in yellow) and reduced weight using a glued wood structure instead of bolted subcomponents.



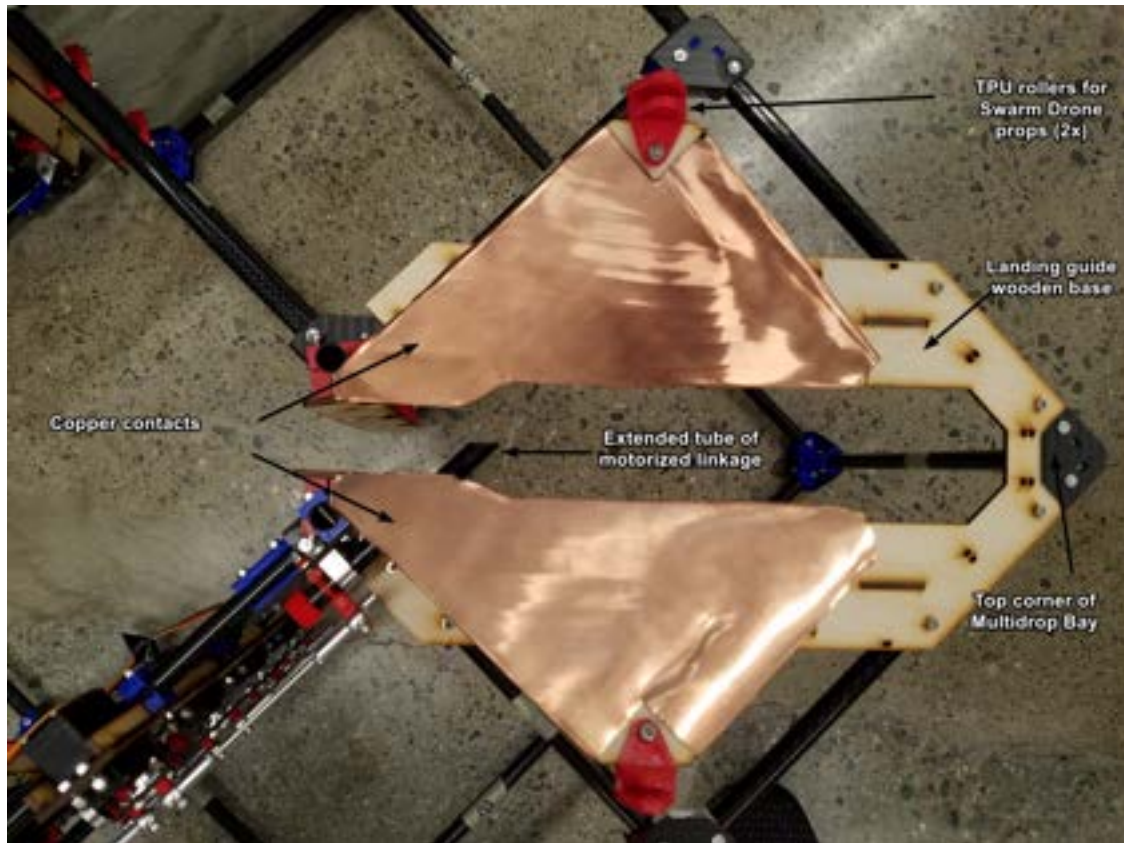
(a) Multidrop V1 propeller guides prototype



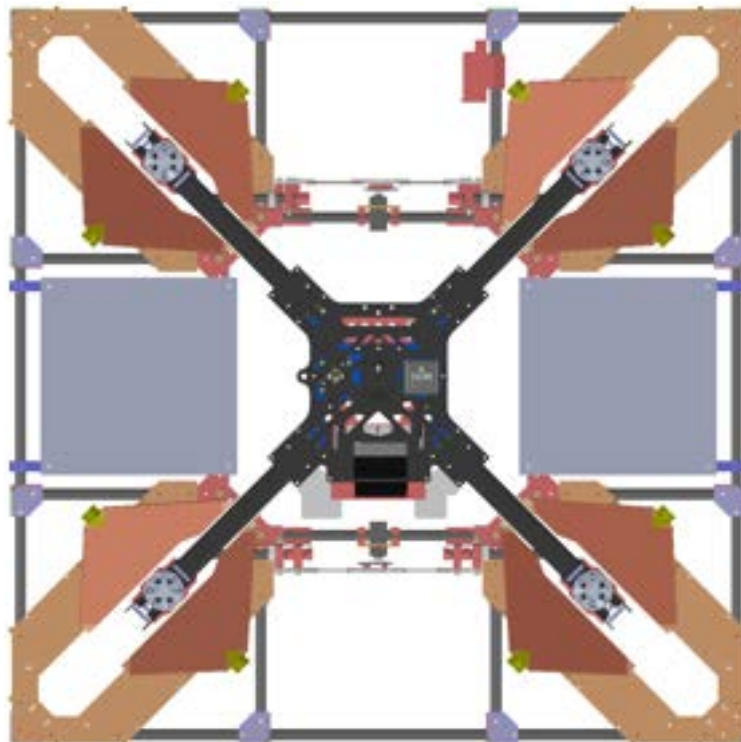
(b) Multidrop V3 propeller guides prototype

Figure 58: Landing guide designs for Swarm Drone reintegration

During summer 2021, the additional functionality of contact sensing was added to the Swarm Drones and Multidrop Bay V3. For the latter, this involved the addition of copper sheets to the V3 landing guides in order to interact with the contact sensors on the Swarm Drones described in Section 5.8. The functional scenario for the use of the copper contacts is as follows: during a precision land, the Swarm Drone guides itself over the Multidrop Bay using the ArUco markers and descends to the landing guides. To have a physical motor kill, there are copper contacts on both the bottom of the Swarm Drone and the top of the Landing Guides. When at least two of these connections are detected, a motor kill is initiated on the Swarm Drone, and it drops into the top level of the Multidrop Bay. Fig. 59a below shows the copper contacts on the initial Multidrop V3 prototype as well as their overall position in the CAD model in Fig. 59b. Fig. 59a below also shows TPU rollers on the tips of the triangles which are intended to induct the Swarm Drones during worst case alignments where their propellers are perpendicular to the slot between the guides.



(a) Top down view of landing guide for one Swarm Drone arm (copper contacts shown)



(b) Top down view of Swarm Drone aligned in four Landing Guides

Figure 59: Landing Guides

The landing guides shown above in Fig. 59 were prototyped and tested during the precision landing tests outlined below in Section 5.11.2. Difficulties occurred during those tests due to the accuracy that the computer vision and autonomous landing was capable of achieving was lower than the landing guides allowed for. There were also issues noticed with the angle and interference areas with the propellers of the Swarm Drone, which were seen during the motor kill tests outlined below in Section 5.11.3. From these observations from testing, a new design was required.

The new landing guides had many variables and constraints to create the best new geometry while maintaining the overall core concept. These requirements are outlined in detail below, with a side by side comparison to the previous version shown in Fig. 60.

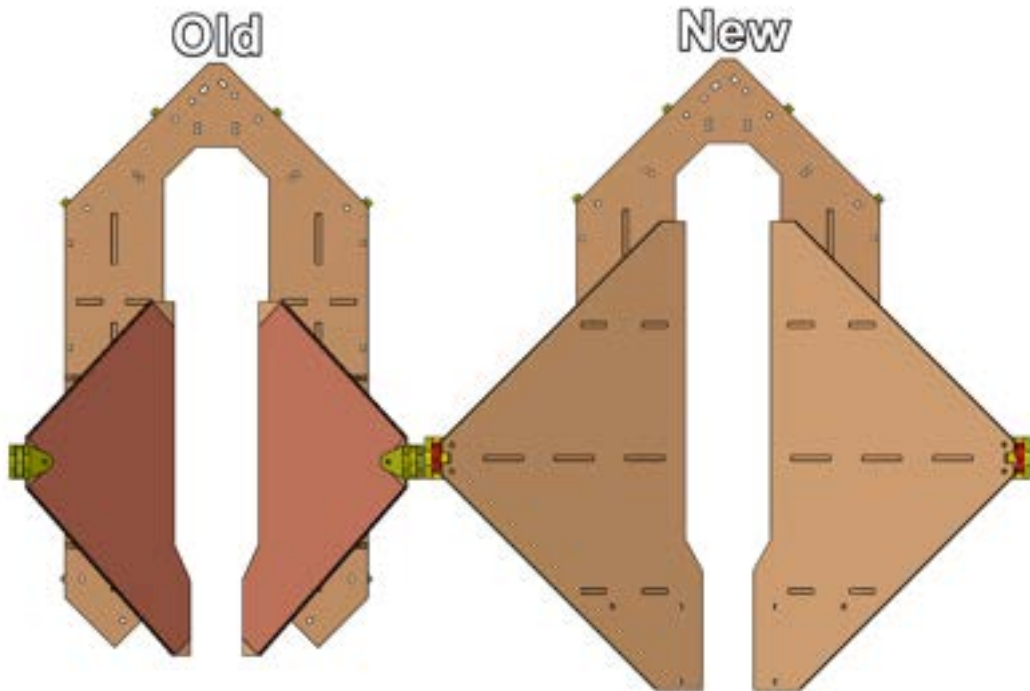


**Figure 60: Top down view of old and new guides**

These guides have a larger surface area as viewed from the top, fulfilling the requirement to make a larger landing area for the Swarm Drones. To perform an autonomous landing, the software requires allowable tolerances that it can consider acceptable to initiate landings inside of. These measurements are how far off the yaw of the vehicle can be, as well as how far off it can be in x and y. These measurements were performed analytically in Solidworks as shown below in Fig. 61.

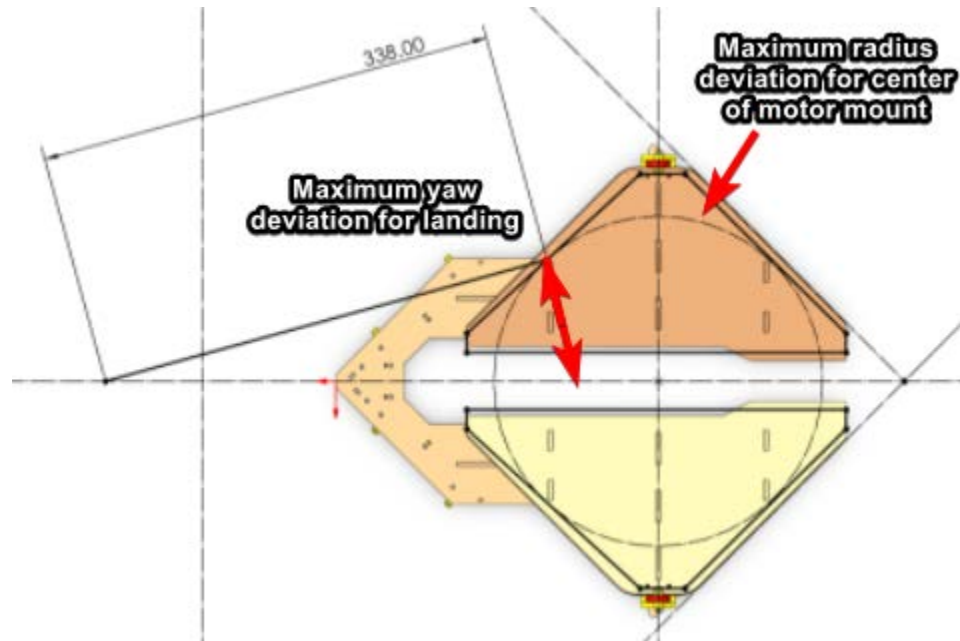


**Figure 61: Accuracy calculations for autonomous landing**

The previous guides, shown above in Fig. 60 as the old version had a yaw tolerance of  $\pm 10$  degrees and a radial accuracy of 9 cm. The new version had a yaw tolerance of  $\pm$  and a radial accuracy of 13 cm.

Another requirement while maximizing the size of the guides was to not occlude vision of the ArUco markers, as shown below in Fig. 62.

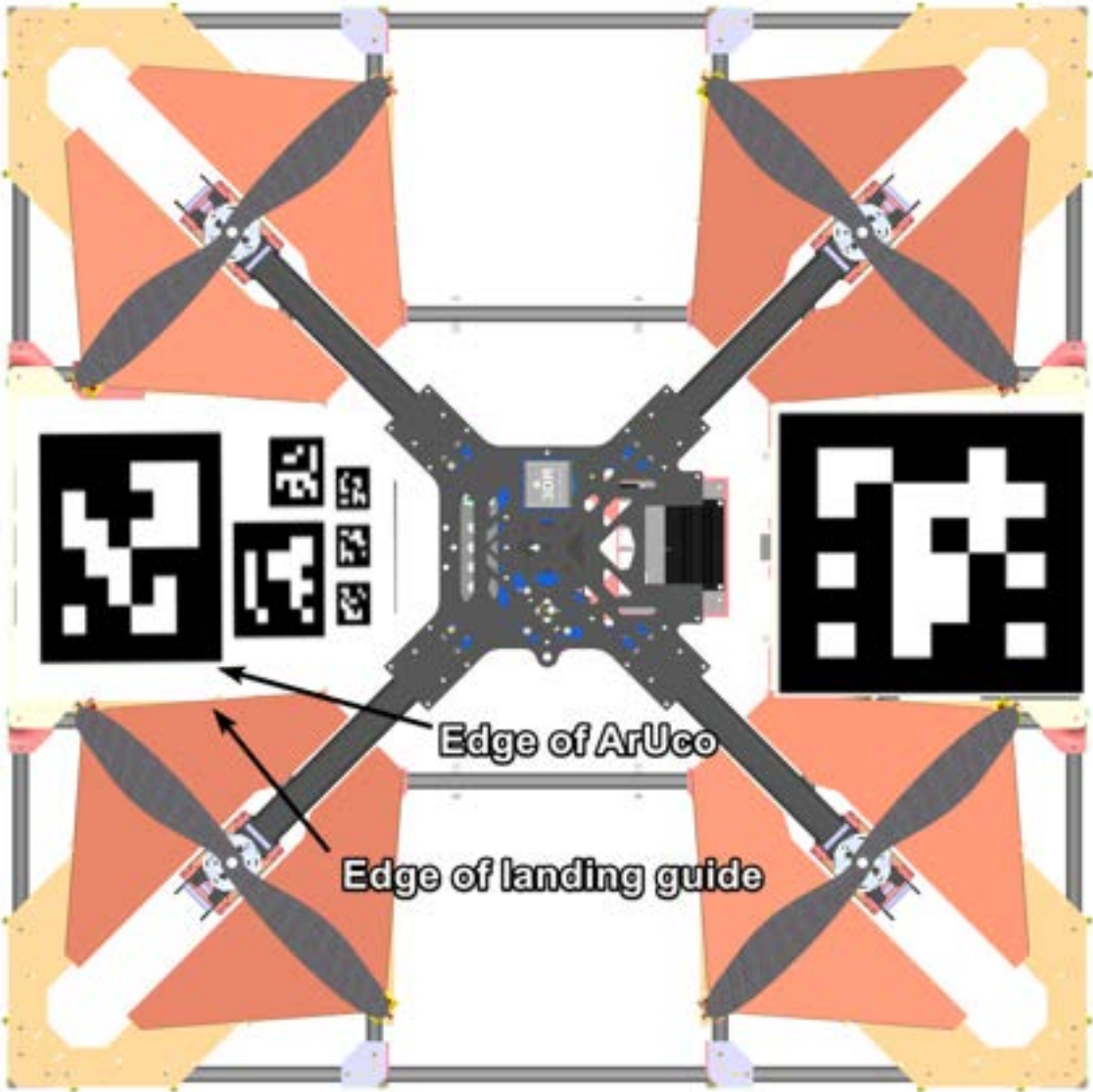
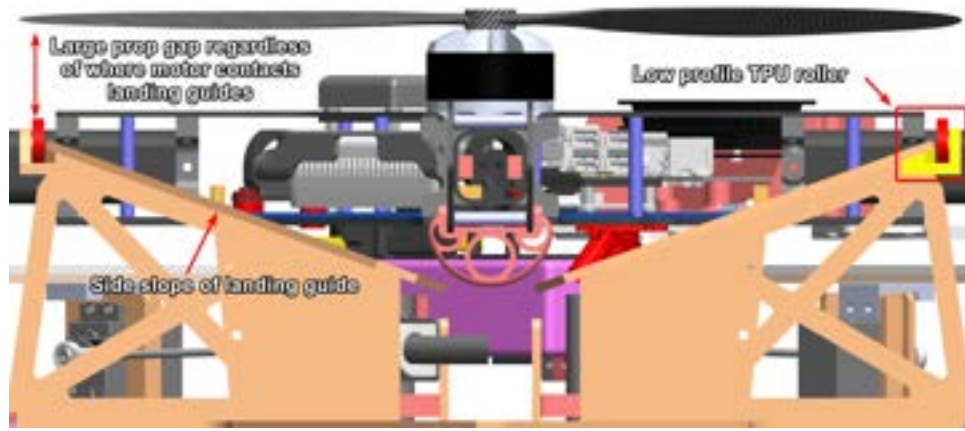


Figure 62: Top down view of Multidrop Bay with new guides

The last requirement while maximizing the size of the guides was to not allow the propeller of the Swarm Drone to intersect with any area of the landing guides before the motor mounts made contact, initiating a motor kill. This is shown below in a side view in Fig.



**Figure 63: Side view showing interference gap between propellers and top of guides**

This non-interference zone was achieved by lowering the angle of the guides from 25 degrees to 20 degrees, which was tested as the lowest angle of the landing guide that still allowed for the Swarm Drone motor arm to slide into the Multidrop Bay. This allowed for an increased distance even at the lowest area of the landing guide, eliminating potential for collisions.

In addition to revisions of the integrating guides themselves, improvements were also made on the design and placement of the ArUco markers. Notably, while previous Multidrop Bay designs oriented the markers above empty sections of the payload bay, the new orientation placed them over the actuator assembly (detailed in Section 5.7.4 below). This stemmed from a higher level design requirement to maintain marker orientation on the left and right hand side of the Carrier Drone. Mounts employed light weight wood and foam mounting plates to rigidly fix the markers. These designs are shown below in Fig. 64.

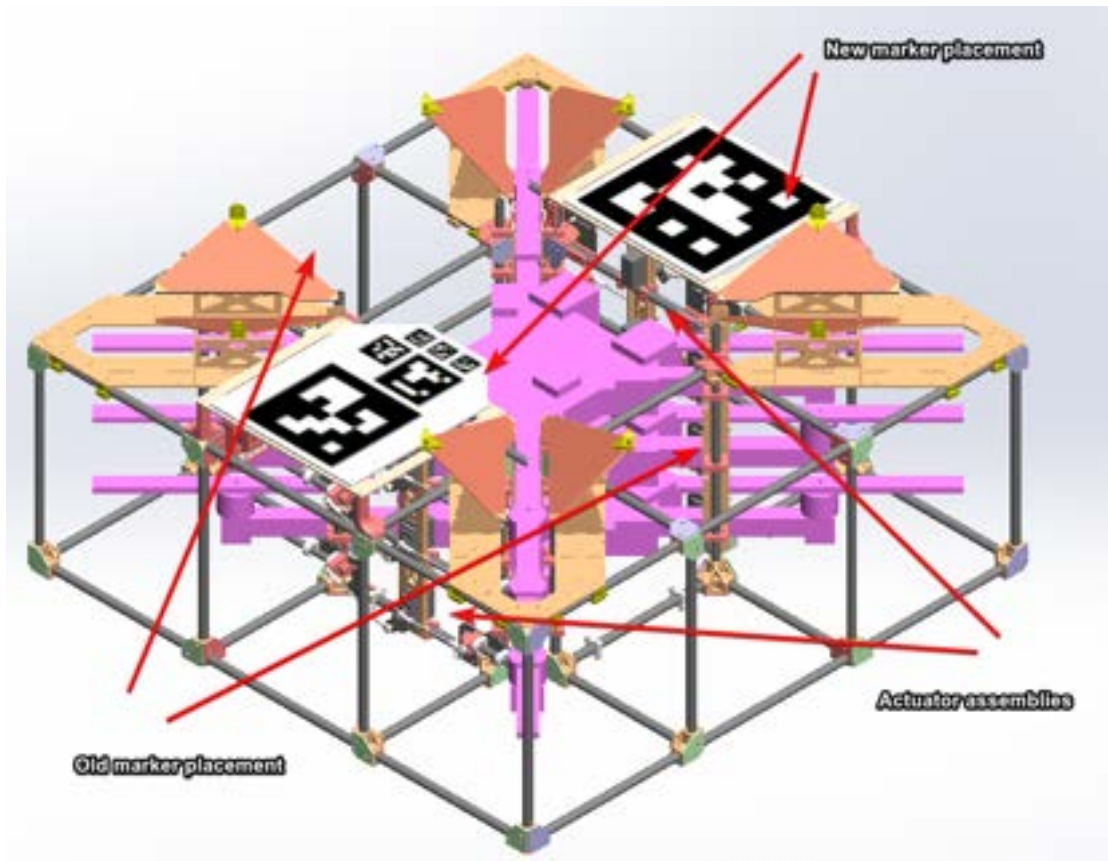
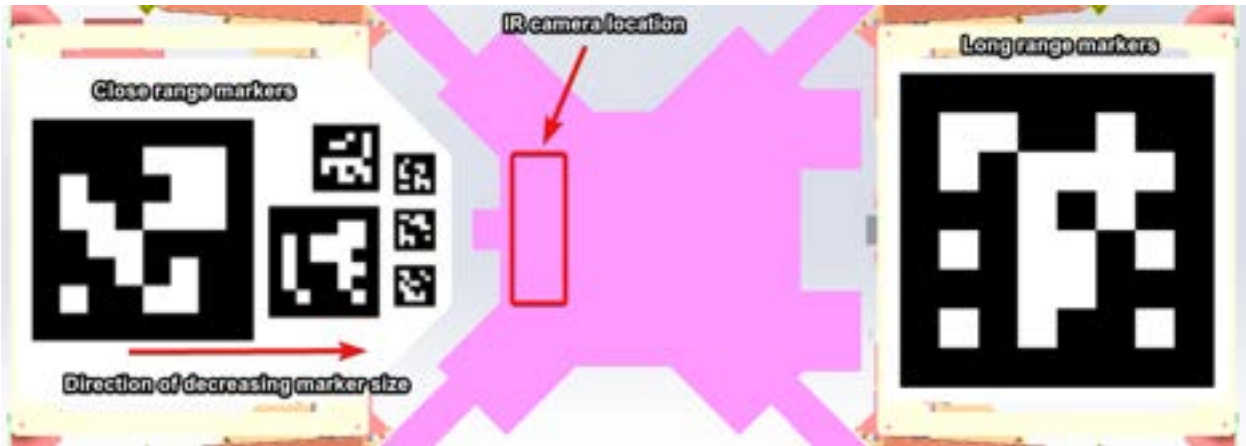


**Figure 64: Revised ArUco target placement: Multidrop Bay**

Fixturing was also motivated by the new markers themselves. Previous marker designs had used identically-sized ArUcos which made no attempt to increase the probability of detections at greater ranges. This flaw resulted in the detecting camera's field of view not being able to fully encompass the markers at close range. To solve this, the marker closer to the detecting camera in the Swarm Drone was modified to contain a series of markers aligned in decreasing size. This allowed the camera's field of view to fully encompass targets, even at close range. Acquiring full images of the markers at close range was critical for the achievement of final attitude corrections right before impact with the propeller guides. Fig. 65 below shows the new and old marker designs as well as the camera placement within the Swarm Drones.



(a) Old ArUco marker design and placement



(b) ArUco marker design and placement

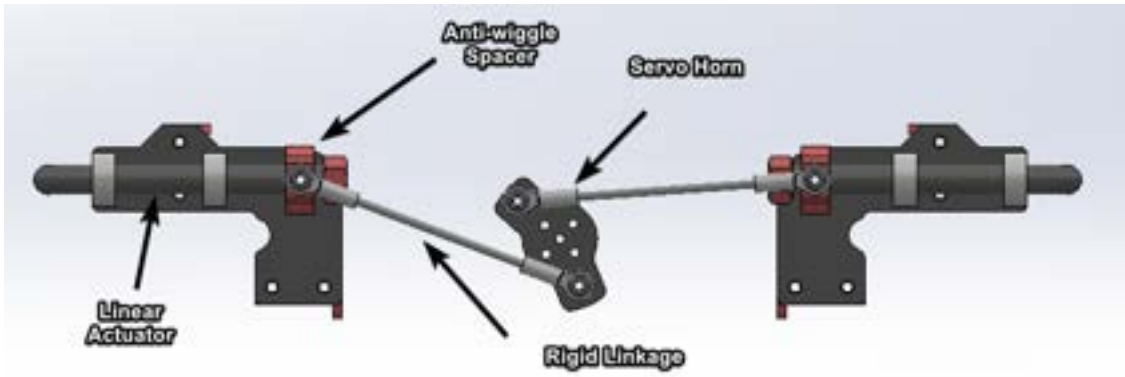
Figure 65: ArUco design iterations

#### 5.7.4 Actuators

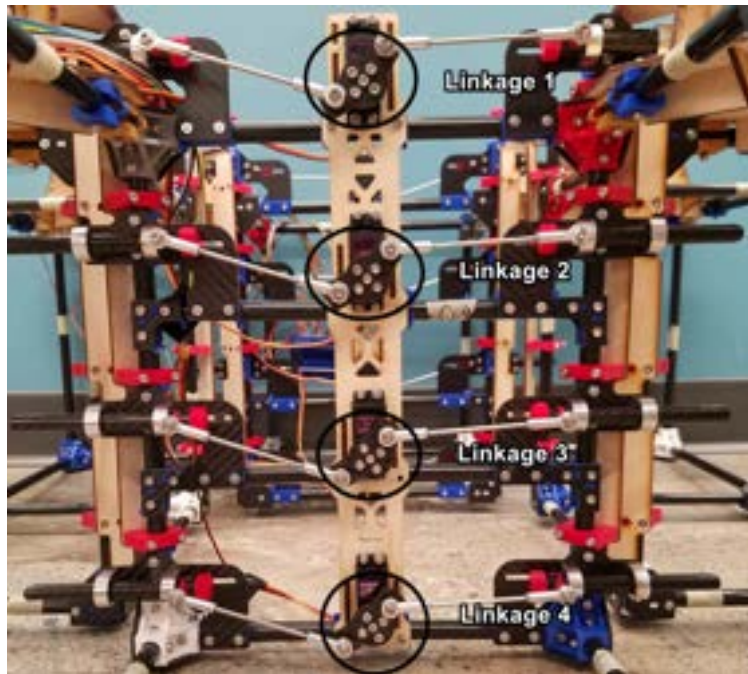
To progress away from the unreliable, pulley-based actuators mentioned in Section 4.3.3, subsequent iterations focused on simplifying the mechanisms. These were developed to allow Swarm Drones to selectively pass through the 4 levels of the Multidrop Bay. The top level is used as an initial location to first catch the Swarm Drone after it reintegrates. The first level of linear actuators was designed to prevent reintegrated drones from damaging their propellers by preemptively falling to lower levels of the mechanism. The remaining levels were intended to store up to three Swarm Drones during flights of the Carrier Drone. When a drop of a Swarm Drone is desired, the bottom level of the linkages can actuate, dropping only the bottom drone. The bottom linkage then closes, and the remaining Swarm Drones inside the Multidrop Bay can shift down.

The next iteration after pulley-based linear actuators used rigid linkages actuated by a servo to translate a linear pins. These pins extended extended into the path of Swarm Drones within the bay, therefore preventing their movement to lower levels. The linear pins consisted of carbon fiber tubes that were free to slide inside of tightly toleranced guide brackets, making for a reliable and compact method of actuation. Figs. 66 below shows the design of the linkage mechanisms and linear pin actuators, their assembly in the Multidrop frame, and an example placement of a Swarm Drone among the mechanisms.

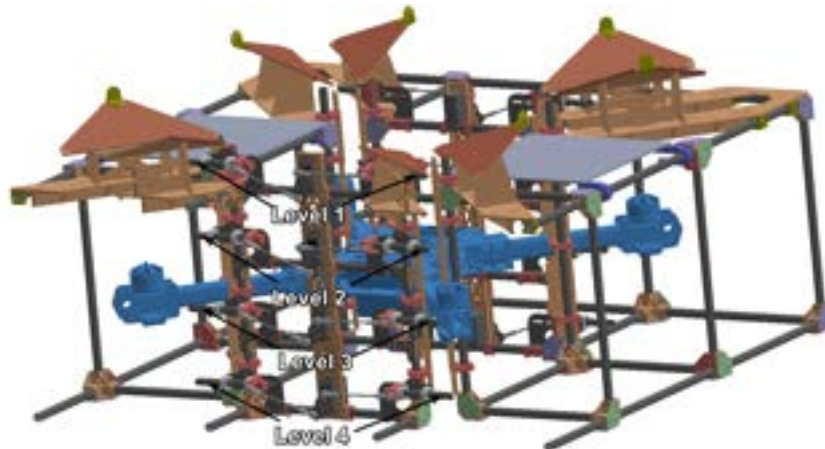
Each servo actuator is able to be indexed and controlled by the Carrier Drone's onboard Jetson Nano through I2C communication. Through a ROS2 service, an operator is able to open and close each level allowing the Swarm Drones to be shifted down and eventually dropped from the bottom level. A daughter Arduino is used for the lower level actuation commands. A simple four-bit message is sent from the Jetson Nano to the Arduino to set the state of all four of the servo levels. This allows all of the levels to be controlled essentially simultaneously.



(a) Linkage mechanism CAD



(b) Assembled view of linkage mechanisms



(c) Example Swarm Drone position within the Multidrop Bay

Figure 66: Motorized Linkages

While more reliable than the early, pulley-based actuators, the rigid linkages still suffered from jams due to loose tolerances in machined parts and wear during multiple cycles. These variances resulted in wiggle of the mechanisms and linear actuators, resulting in jams once the weight of Swarm Drones was applied to them. Misalignments were removed by adding 3D printed spacers within the mechanisms that prevented wiggle during actuation. These parts, shown in Fig. 67 below, were a simple phase-in solution that resulted in the completion of the Multidrop Bay V3's mechanisms to the required reliability for Swarm Carrier.

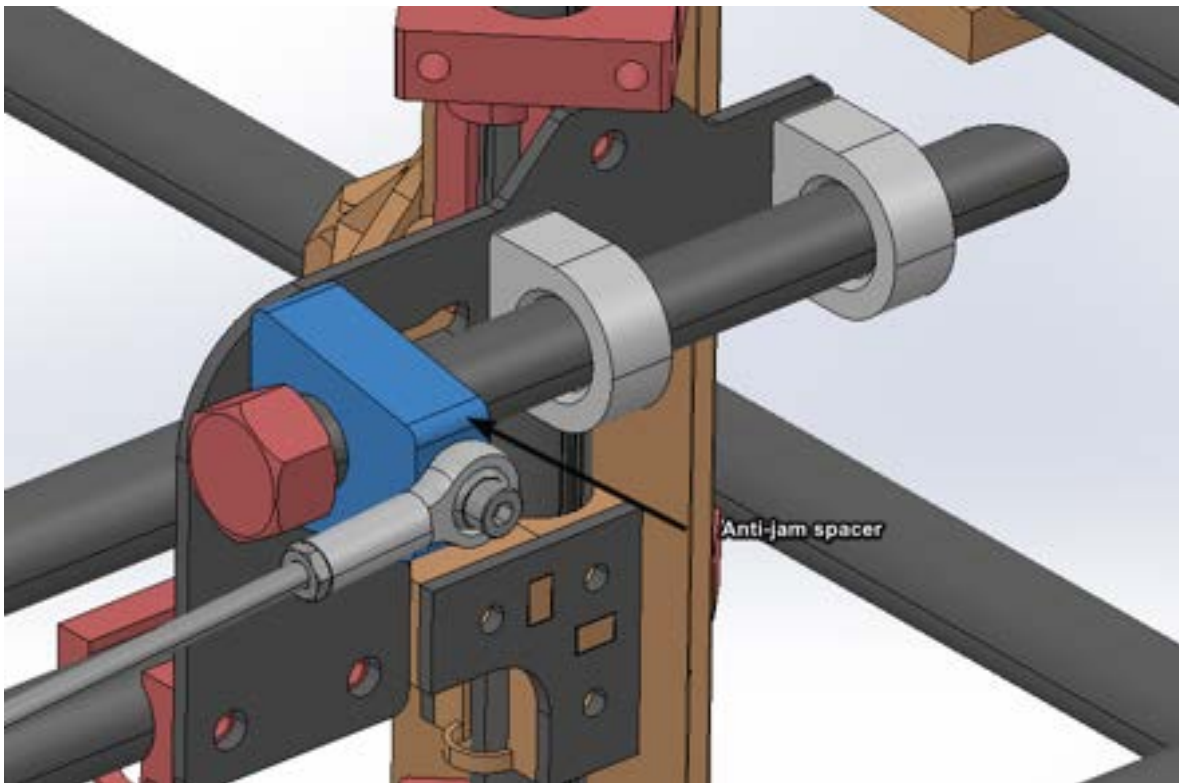


**Figure 67: Anti-jam spacer on the Multidrop bay's actuators**

A new failure mode that was noted was the propellers of the Swarm Drones getting caught on top of the linear actuators. The propellers in CAD were idealized in such a way that they were perfect rectangles, but in reality have a unique contours that extend beyond the modeled surface area. This meant that there were certain propeller configuration that resulted in the propellers striking and getting stuck on the linear actuators. Although this would not typically be a problem if the linear actuators are completely clear of the alignment channel, the interaction of the alignment channel and the propellers geometry allowed it enough degree of rotation to get itself jammed on top of the fully retracted linear actuators. In future iterations, the vertical wood guide plates should be extended to fully cover the linear actuator and avoid this failure mode.

## **5.8 Swarm Drone V3 Design**

Building off of Section 4.3.1, the next design under iteration was the V3 Swarm Drone. The V3 design was a series of phase-in improvements with the goal of modifying older components of the vehicles with current payloads and software in development. Required features included the replacement of older ArduCopter-preferred Flight Management Unit (FMU)-V3 flight controllers with PX4 FMU-V5 boards, vibration damped stereo camera mounts, new fixtures for mounting the flight computer, and new carbon fiber motor mounts with built-in collision sensing abilities. The latter sensors underwent two design iterations.

Figures 68, 69b, and 69a below display these features as well as initial designs collision sensors. Designated as contact sensors, these were passive (un-powered) conductive contacts that delivered a logic input to the drone's flight computer. This feedback allowed the autonomy to sense the contact point between the Swarm Drone and Multidrop Bay during landing, power off the vehicles motors, and integrate into the bay without absorbing damage to propellers.

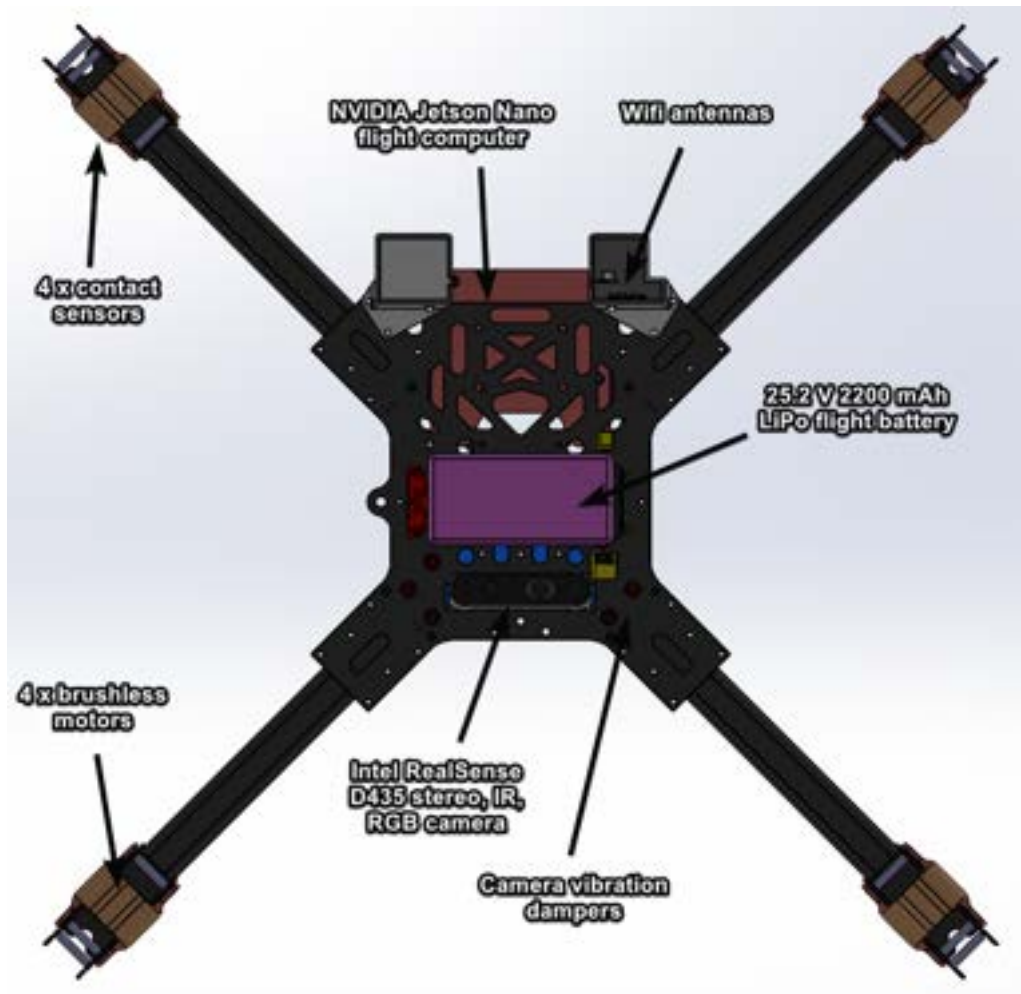
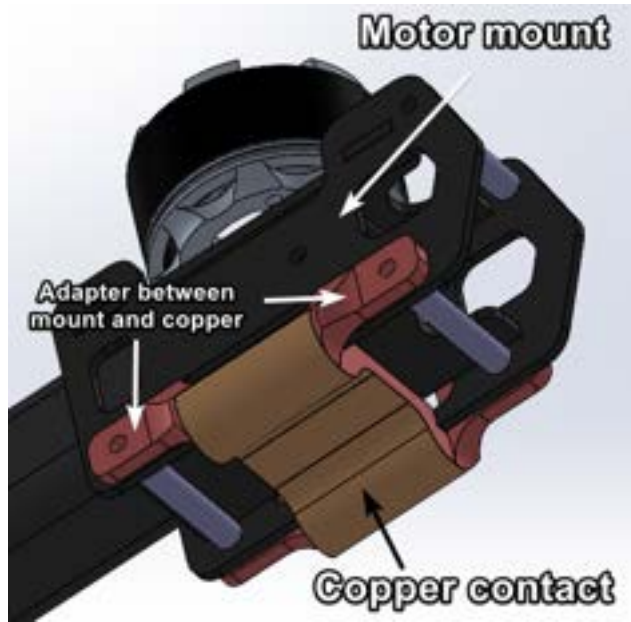
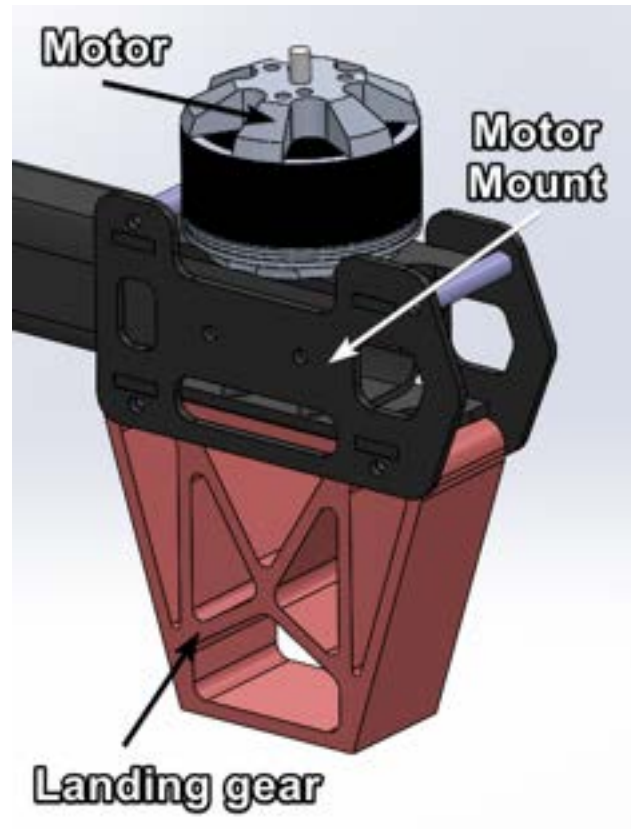


Figure 68: Swarm Drone V3 CAD



(a) Swarm Drone V3 motor mount with contact sensing



(b) Swarm Drone V3 motor mount with landing gear

Figure 69: Swarm Drone V3 motor mount with collision sensing

Functionally, the designs of the contact sensors were specifically-contoured, 3D-printed geometries wrapped with copper tape. Within the airframe, the copper-wrapped contours were separated in two pairs which were wired in parallel to two GPIO pins on the flight computer. Fig. 70 below outlines this wiring schematic as well as its interface with the Multidrop Bay.

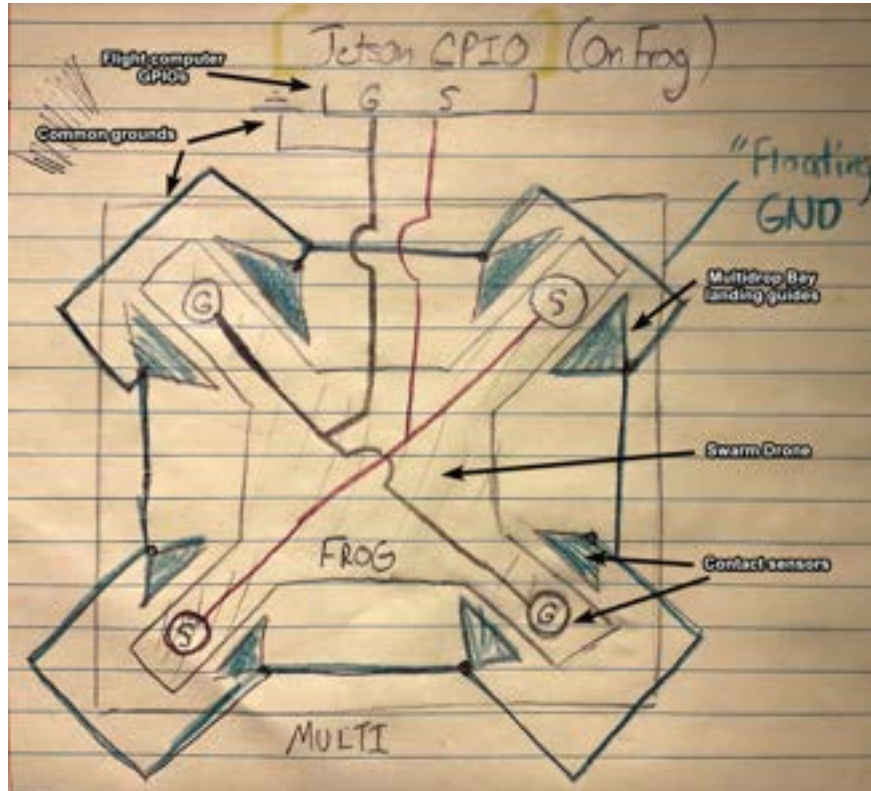
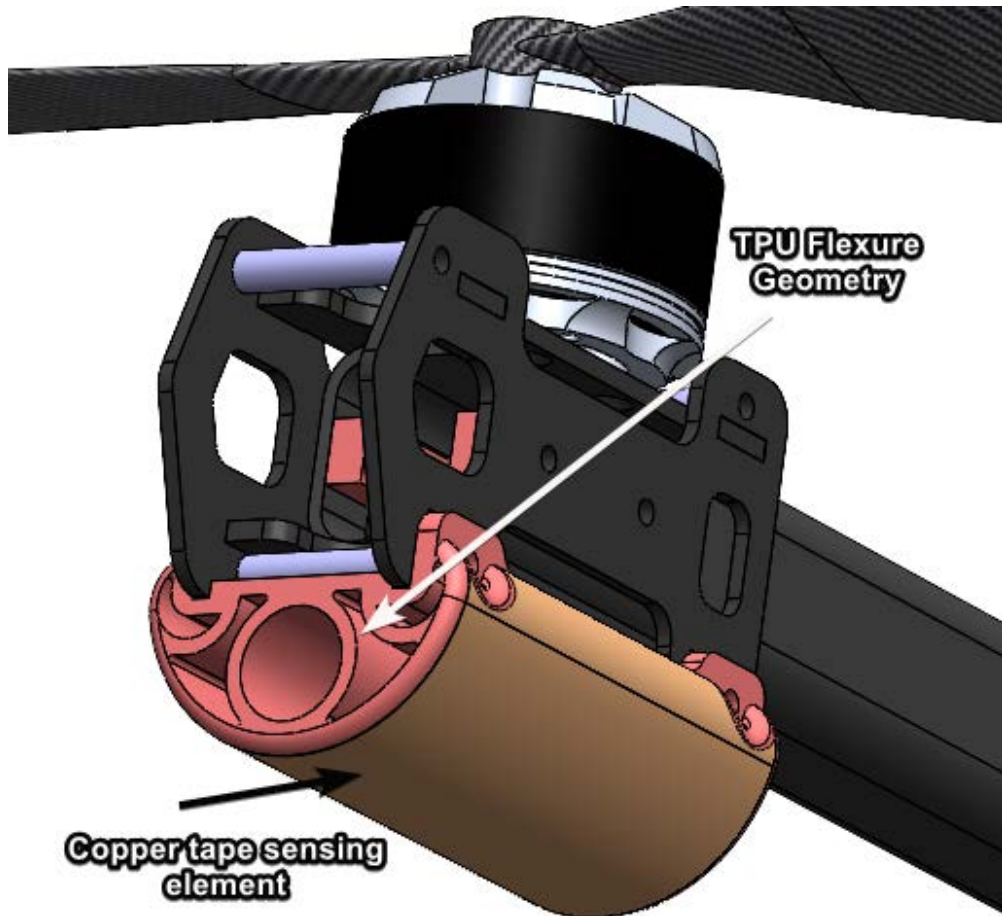


**Figure 70: Swarm Drone contact sensing schematic**

From Fig. 70, it can be seen that if any of the two adjacent arms of a given Swarm Drone make contact with the landing guides of the Multidrop Bay, at least two of the GPIO pins will be shorted. This allows for the mentioned motor shutoff to be initiated. With this feedback, the Swarm Drones have a hardware failsafe during autonomous landings that increases their reliability and safety.

While functional architecturally, the first iteration of the contact sensors did not perform favorably in testing due to their high coefficient of restitution during impacts. Specifically, when 3D-printed out of PETG or nylon, the rigidity of the mounts protected the copper tape but caused the sensors to rebound rapidly during collisions. Further explanations of these limitations are outlined in Section 5.11.3 which sufficiently justified a second iteration of the contact sensors.

The second iteration of the Swarm Drone's arm-mounted collisions sensors sought to mitigate the large time constant of detections associated with the previous scheme. To accomplish this, it employed a compliant, damping design which prolonged contact time with surfaces. This allowed for a greater probability of collision detection within a minimized sensing window and equivalent sampling rate of ROS topics. The design employed a 3D-printed, TPU geometry with purpose built features to enable flexure during collision. This enabled the mentioned damping and compliance that allowed the final version of the Swarm Drones to shut of their motors in as quickly as 20 ms. The design and prototype of this subsequent sensor iteration are shown below in Fig 71.



(a) Compliant sensor CAD



(b) Exaggerated example: compliant sensor compression

Figure 71: Second contact sensor iteration: compliant, damping geometry

In addition to new sensing solutions, the new carbon fiber motor mounts replaced dated nylon parts. These prevented fractures of 3D printed components during landings and finalized the Swarm Drone V3 as a robust and versatile test vehicle for Swarm Carrier. Since their implementation in September of 2021, they have substantially improved the serviceability of the Swarm Drones during autonomous landing tests (detailed in Section 5.11.2). The design has also been adopted by the Forest Drone Sensor team for its simplicity, ease of manufacturability, and durability.

## 5.9 Simulation

Custom models are being developed for the Swarm Drone and Carrier Drone in the Gazebo simulation environment. To get the vehicles in simulation they are first exported using SolidWorks Unified Robot Description Format (URDF) Exporter [43]. After exporting they are modified to contain common sensors such as GPS and IMU. Motor models are then added for each propeller and the dynamics of each motor are captured using various coefficients. For the Swarm Drone and Carrier Drone various other additions were necessary to capture the vehicle's systems in their entirety.

The Swarm Drone had an extra sensor for the RealSense added. This was modeled using a multi-camera with Red Green Blue Depth (RGB-D) capabilities. Custom software had to be written to extract image information from the simulation and output it to ROS2. Besides sensors, the swarm drone also had to have a custom collision model created. To avoid unnecessary computations during the physics simulation this collision model contained the fewest possible geometric faces possible. By modeling its collision fairly accurate tests can be performed by reintegrating the vehicle in simulation. An example of the Swarm Drone can be seen in Fig. 72.

The Carrier Drone did not require any additional sensors, however, custom implementations of the motors and their relevant mixers had to be created. Mixers are the foundation to PX4 flight controllers: they define where the propellers are located, how they should spin, and what electronics control them. Initially, a model was added for the Carrier Drone V2. This required a completely new version of a motor mixer as PX4 does not support a decacopter configuration natively. To create the mixer, various files had to be added to the PX4 firmware. Using the propeller locations from Solidworks and rotations derived from other configurations, the motor mixer was created and tested. Figure 73 below shows the Carrier Drone V2 in simulation. Flight capabilities were verified, but never tested on the field due to a design alteration and the switch to a V3 model for the Carrier Drone.

The Carrier Drone V3 used a native configuration supported by PX4, the octocopter. Using their motor mixers a simulation model was created in a similar fashion to the V2. To fully utilize the custom collision model for the Swarm Drone, a custom collision model was also designed for the carrier drone. This collision model focused on the reintegration aspect and contains a hole that fits the Swarm Drone inside it. With this geometry the Swarm Drone can be fully reintegrated. The Carrier Drone V3 can be seen in simulation in Fig. 74.

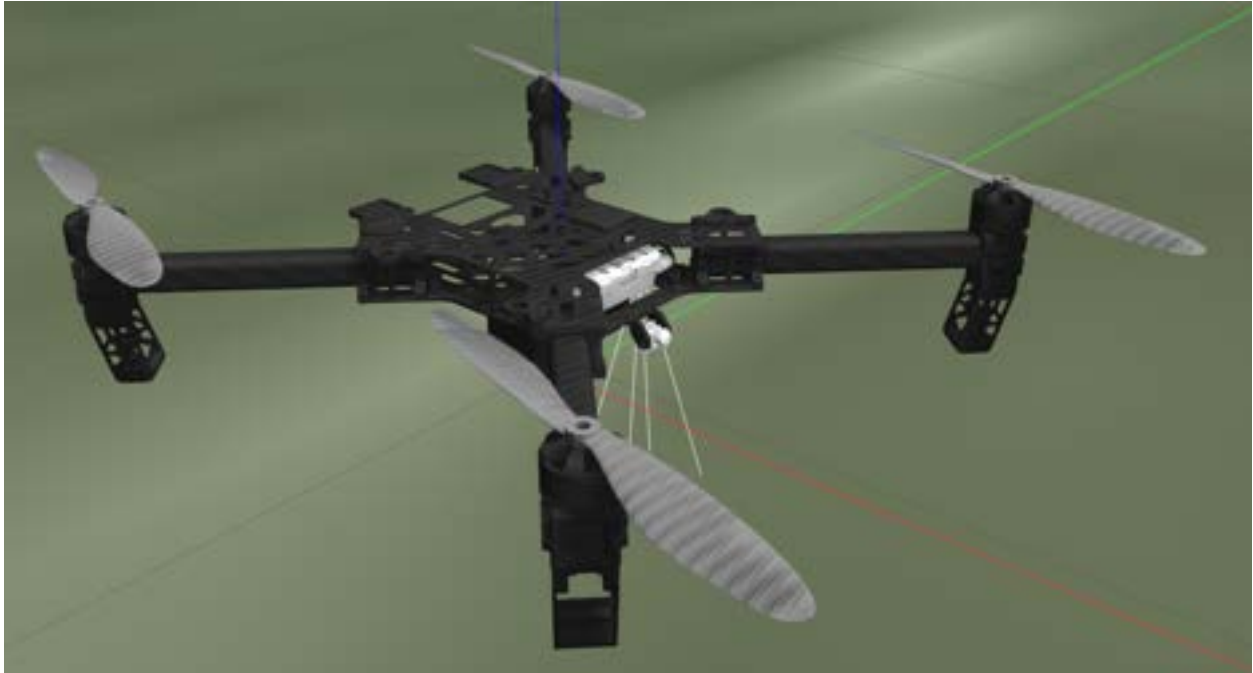


**Figure 72: Custom Swarm Drone in simulation**

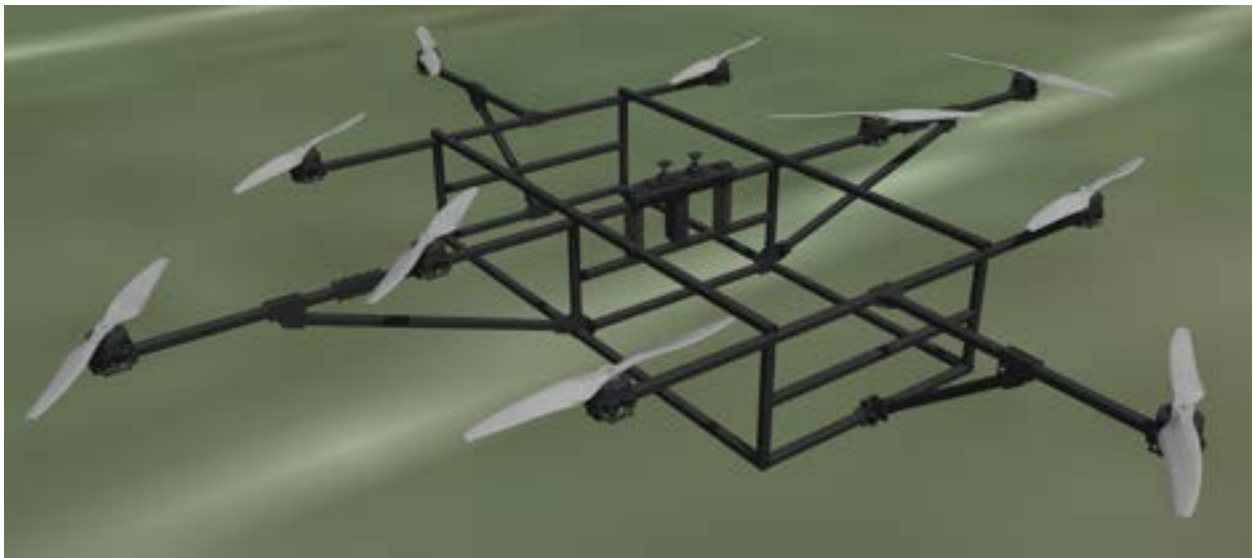


**Figure 73: Custom Carrier Drone V2 in simulation**

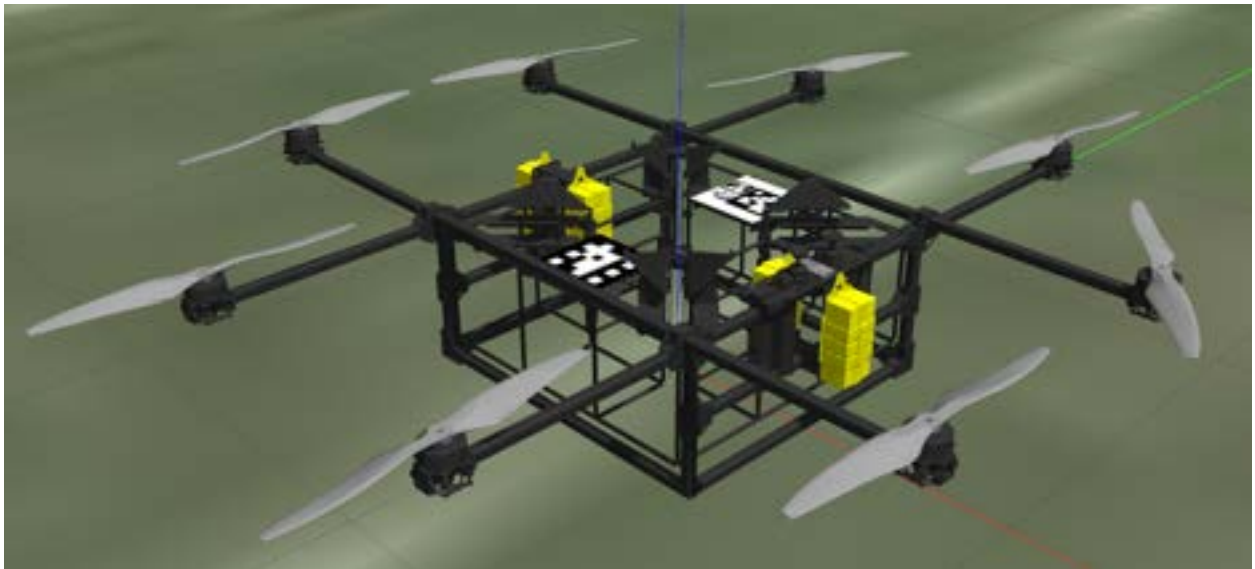


**Figure 74: Custom Carrier Drone V3 in simulation**

## 5.10 Visualization

ROSboard is an open source, web based application for visualizing ROS2 topics. An example of this GUI running in the simulation is shown in Fig. 75. This feature allows for the viewing of any sensor (i.e GPS, camera, battery, IMU) or high level flight/mission log. The alternative to this was to simply read data values off of the terminal of the ground station. This was what the team previously used for monitoring the system. ROSboard has been invaluable for field testing and allows for greater insight into what the drones are doing for safety and debugging purposes. One of the main reasons the ROSboard library was chosen was because it is lightweight and extensible. It was simple to extend the base viewer and add support for specific visuals the team wanted. For example, the battery and attitude viewers were both added by request of the team's pilots. Additionally support for the visualization of swarm missions with multiple GPS points was implemented.

Another platform that is being used is Foxglove which is also an open source platform for ROS2 topic visualization. Currently, Foxglove is being used for post-processing precision land field tests (see Section 5.11.2). Its main advantage over ROSboard is that it has a great ROSbag playback feature that is not available in ROSboard. Through the use of Foxglove, the team is able to go through each landing test to find the source of error, visualize the 3D position of the drone and camera feed, and view the velocity commands that the vehicle is sending compared to the actual velocities achieved by the vehicle. An example of this information is shown below in Figure 76. This post-processing workflow has been extremely valuable in informing the improvements to the precision landing algorithm and the landing pose calculation. The ultimate goal is to phase out ROSBoard and to only use Foxglove as the main GUI while operating the drones.



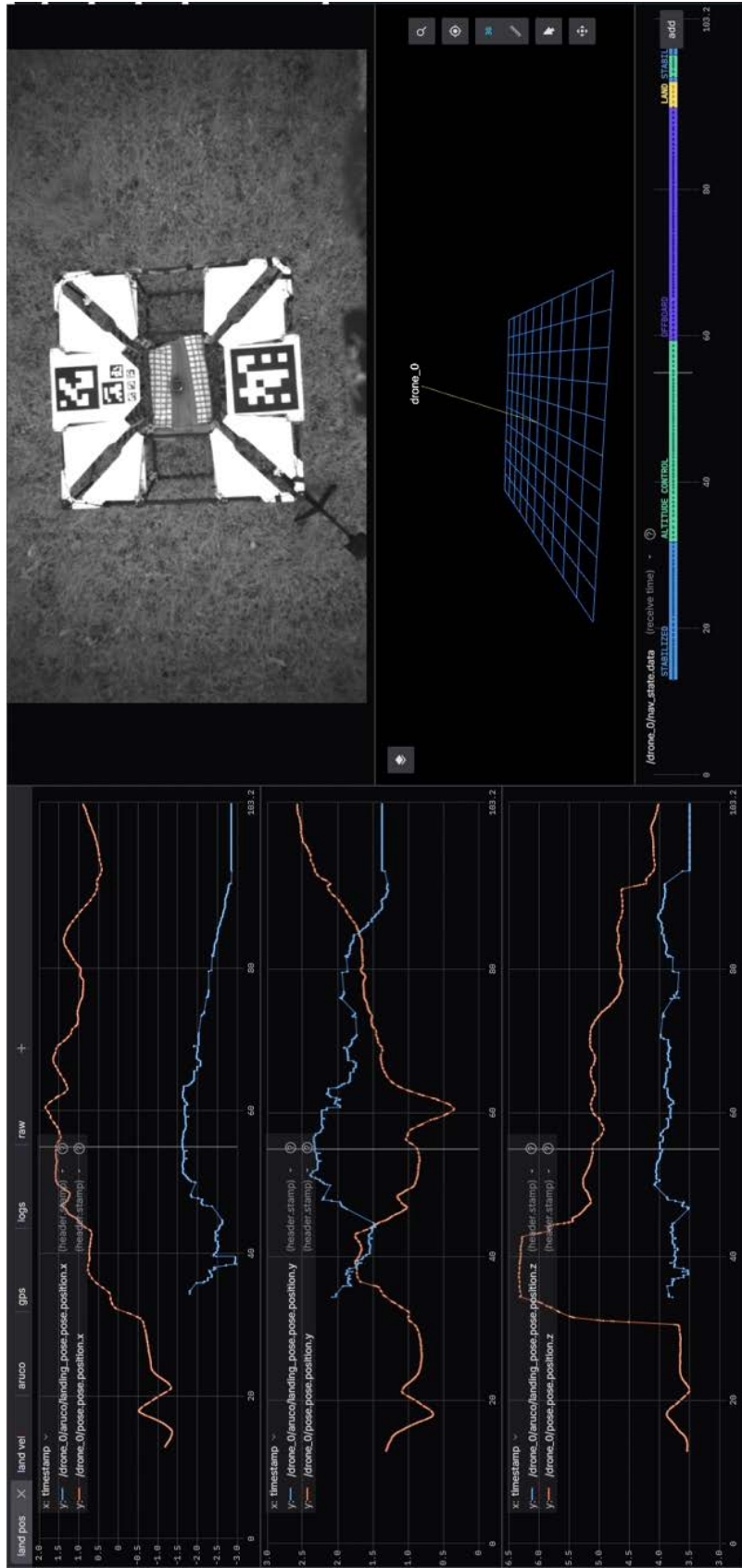


Figure 76: Foxglove running in simulation

## 5.11 Design Validation

An important aspect of the Swarm Carrier project is the design validation of subsystems to ensure safety and reliability. This entailed preparing plans for carefully choreographed tests to evaluate key functions of the system. During July to the end of December of 2021, tests were conducted in accordance with SOPs. These were submitted for static thrust tests, maiden hover of the Carrier Drone, and precision landings using ArUco markers. The following sections outline the history of performed tests alongside tests.

### 5.11.1 Thrust Tests

A series of thrust tests was performed in August 2021 on the Carrier Drone's propulsion system. These served to tabulate the operational characteristics for coaxial motors using T-Motor P80III 100kv motors and Foxtech 3010 Carbon Fiber Propellers. Using an RCbenchmark S1780 motor thrust test stand, the motor thrust, voltage, current, torque, and rpm were recorded. First, a control test was recorded where the performance of a single motor was monitored. Then the performance of both the upper and lower motors in a coaxial configuration were measured. An additional test of offsetting the axial distance between the motors was also conducted at 9 inch and 4.5 inch distances. To ensure consistent power calculations, single motor and coaxial tests were performed consecutively to avoid different voltage levels of the LiPo battery. Analysis of this data was done in Section 5.3.6. Fig. 77 below shows the S1780 thrust stand with motors and propellers mounted in a coaxial configuration.



**Figure 77: RCbenchmark S1780 Motor Thrust Test Stand with Coaxial Configuration**

The outcome of the thrust test was a library of data, discussed in Fig. 38, which heavily in-

formed the Carrier Drone's frame design and propulsion systems selection based on data-driven decisions (DDD). For example, the Foxtech 3010 propellers were determined to provide inadequate thrust output given the constraints of the system outlined in Section 3.4. In addition to the mentioned results from the thrust data, this fact motivated the team to shift to T-Motor GL32X11 32 inch carbon fiber propellers as a replacement.

#### 5.11.2 Precision Land

The precision land test was conducted to view the fidelity and precision of the Swarm Drones. It was tested to the full extent of the standard operating procedure (SOP) submitted with landings occurring on top of the Multidrop Bay. Figure 78 shows the procedure that followed for all tests.

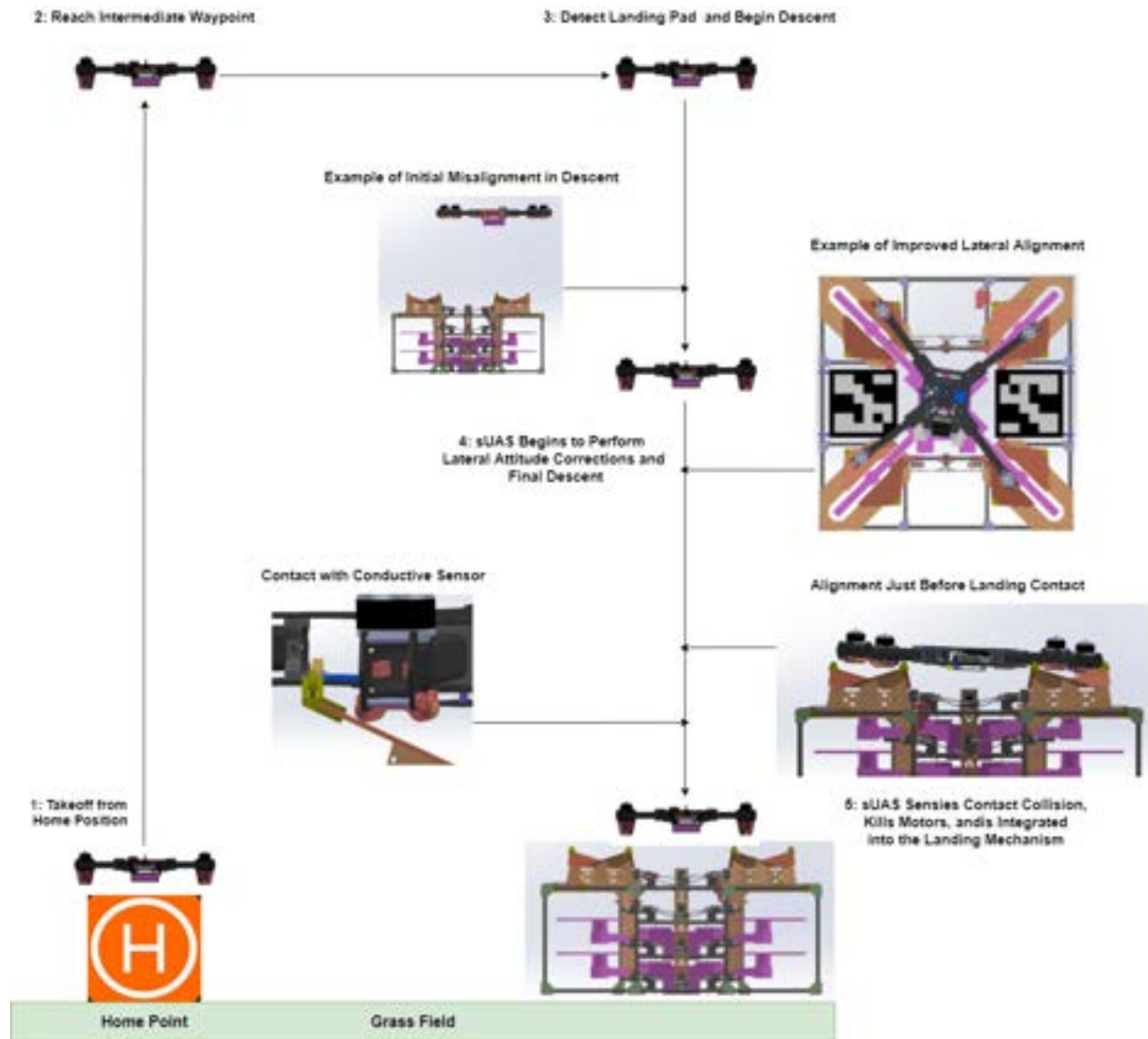


Figure 78: Flowchart: Precision landing test in a Multidrop Bay

During precision land tests, issues arose when integrating the test into the Multidrop Bay. This required two added procedures on top of the autonomous landings: the motor kill as outlined in Section 5.11.3 above and the reintegration into the Multidrop Bay using the passive landing guides in Section 5.7.3. The motor kill performed well, with the copper contacts successfully making contact and stopping the motors in less than 40 ms, preventing collision between spinning props and the guides as outlined in Section 5.11.3. Issues arose with the landing guides passively guiding the Swarm Drone into the Multidrop Bay, as during some successful landings the drone adhere to the guides instead of being integrated into the lower mechanisms. While this procedure was fully vetted and confirmed in the laboratory section, due to the outside weather measuring around 30 °F, the robustness of reintegrations.

While performing these tests various problems were faced. It was discovered that the control stack was inconsistent at connecting with the Swarm Drone, precision lands did not land within the desired tolerance, GPS positioning had high variance, and the latency of computer vision detections were high (about 400ms). For the first problem, infinite loops and stalls were occurring at points during Swarm Drone initialization and processing. These problems were the result of invalid access to various objects at runtime and multi-threading issues. To overcome these problems, more memory management logic and threading control logic was added. The second problem was resolved by adding the additional stages for precision landing. By separating control for horizontal movement and vertical descent, the velocity commands tended to overshoot less often and more accurately align with the ArUco markers. Various techniques for generating the pose were analyzed such as specifically weighted averaging, raw measurements, and processing with a kalman filter. It was determined that raw estimates were ideal since the other methods over-filtered the system without noticeable benefits. For the third problem, a solution was found by protecting the GPS from electromagnetic interference (EMI). After talking to individuals in industry, it was decided that copper shielding needed to be added around the GPS and the USB cable from the RealSense camera. Adding a shield and distancing the GPS from interference sources significantly diminished the interference affecting positional setpoints. The final issue was improved by examining the runtime of various processes within the ArUco detection generation. A process for outputting a debug image was discovered to be doubling the latency of detections. By removing this, the latency significantly improved which achieved detection speeds of around 150ms. The test, seen in Fig. 79, validated these changes and proved that the swarm drone could precision land.

Precision land was iteratively improved and tested with the Multidrop Bay. First, the vehicle was tested by manually flying into the Multidrop Bay and validating that the motors were killed prior to entry using the contact sensing system discussed in Section 5.8. Once that was performed several times with confidence, the test proceeded with the Swarm Drone autonomously navigating into the Multidrop Bay. Finally, the Multidrop Bay was placed into the Carrier Drone and a full system test was completed. Fig. 80 shows this test being performed at Northeastern University's Dedham campus.



**Figure 79: Swarm Drone performing a precision landing during testing**



**Figure 80: Swarm Drone performing a precision landing on Carrier Drone**

### 5.11.3 Motor Kill Test

In order to motivate design requirements outlined in sections 5.8 and 5.7.3, a series of tests was conducted to validate collision sensing abilities of the Swarm Drones as an early integration test of Swarm Carrier's subsystems. The significance of a successful test would prove that the Swarm Drones could respond to collisions, using active feedback, by shutting of their motors before propeller damage could occur.

Collision detection is processed onboard each of the Swarm Drones. The copper contact circuit was wired to the GPIO ports of the Jetson Nano. Here, a ROS2 node is implemented to continuously publish the state of the GPIO port at a rate of 100 Hz. Subsequently, when a detection was made, a motor kill command is sent. The latency of detection to motor kill was measured by how many motor kill commands were logged. For example, if two commands were sent it therefore took two positive detections until the eventual kill. At a detection rate of 100 Hz, this results in 20 ms response time.

Tests began on the first iteration of contact sensors which utilized rigid, non-compliant contact sensors mentioned in Section 5.8. Trials began by arming the motors to an idle speed via terminal commands and manually dropping the Swarm Drone into the Multidrop Bay's landing guides. These contained the corresponding ground loop that allowed for the collision sensors to switch states during impacts. Results from the rigid contact sensors immediately showed a high coefficient of restitution which lead to large rebounds and complete detection failures. Crucially, the system was only capable of detecting collisions during 20% of trials within a response time of over 40 ms. An image of a rebound followed by a failed collision detection can be seen below in Fig. 81 below shows an example of a large rebound followed by a detection failure.



Figure 81: Contact sensing test: failed motor kill

Rebounds were unfavorable for the obvious risk of damage to the Swarm Drone. However, high coefficient of restitution impacts were a non-trivial issue. Due to the rigidity of the initial contact sensing design, any collision occurred over such a small window that the sampling rate of the monitoring ROS2 topic would not detect events. Similar to a bouncing bearing on a steel plate, the collisions were repeated over sufficiently small windows as to prevent reliable and timely detection. The best performance that they provided was  $\sim 40$  ms which proved insufficient from analysis of slow-motion test footage.

After incorporating these lessons into a new design iteration of the collision sensors, tests resumed with a similar procedure. Unlike the previous design, the new, compliant sensors did not rebound significantly or show a small window of collision detection. Due to the compressibility of their geometries, the sensors were able to maintain a contact point over a greater number of time-steps within an equivalent sampling interval. This allowed for reliable and fast detections while damping the magnitude of rebounds. The result was a reduction of motor kill time to under 20 ms which was reliably fast enough to prevent propeller damage. Fig. 82 below shows a successful motor kill of a Swarm Drone within the MultiDrop Bay.



Figure 82: Contact sensing test: successful motor kill

#### 5.11.4 Drop Mode Test

The Drop Mode test evaluated the Drop Mode functionality of the Swarm Drones, which use this flight mode when deployed out of the Multidrop Bay. The test involved dropping a single Swarm Drone from the edge of a 15m tall wall, allowing the Swarm Drone to catch itself and then land itself on the ground autonomously. An 80/20 constructed frame held the Swarm Drone and the payload deployment mechanism taken off the original octocopter UAS. This ensured that the Swarm Drone deployed away from the wall to reduced the chance of any collision during deployment and during the recovery. The Swarm Drone deployment mechanism was a previously utilized system to deploy compact payloads. It utilized a bumper latch system with an affixable mate mechanism to the center of the Swarm Drone airframe. The drop mechanism alone, and with the Swarm Drone interfacing with it are shown in Fig. 83 and Fig. 84, respectively. This ensured controlled, repeated deployments of the Swarm Drones for the Drop Mode test. If the Swarm Drone failed to activate its Drop Mode in time, a 50 ft x 50 ft net system on the ground will catch the Swarm Drone. Testing is slated to start at the end of October 2021. Fig. 85 shows the intended test procedure.

During the wall drop test the Swarm Drone was initiated and placed into the software Drop Mode. The Swarm Drone attached to the dropping apparatus was extended over the edge of the wall and a software message was sent to the drone allowing it to arm motors when it sensed a drop event. The apparatus dropped the Swarm Drone, within approximately 5 meters it autonomously detected the drop event, activated its motors, and achieved stabilized flight. Fig. 86 displays a visualization of the wall drop test. What is different between this wall drop test and the prior in Section 4.3.2 is the firmware detecting the drop event. The previous work involved using an off-the-shelf feature of the flight controller used. In order to send faster messaging with the RTPS protocol, the team needed to program its own drop detection algorithm which was validated in this wall drop test.

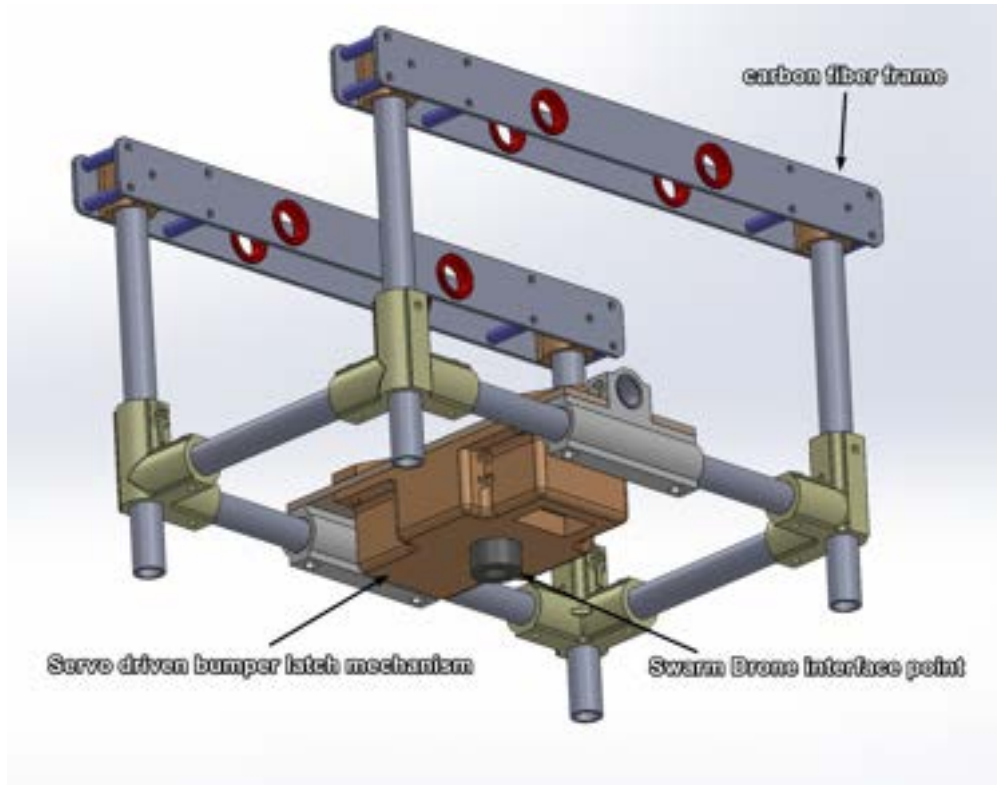


Figure 83: Drop mechanism utilized for the Drop Mode test

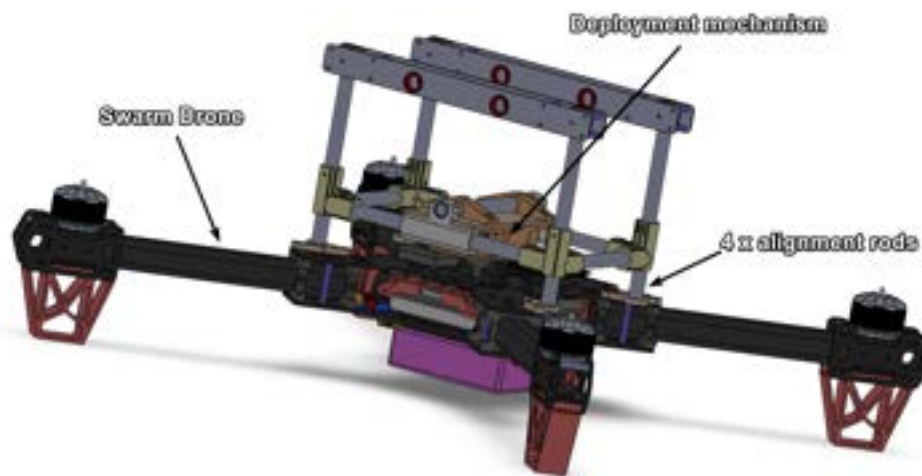


Figure 84: Drop mechanism interfaced with the Swarm Drone

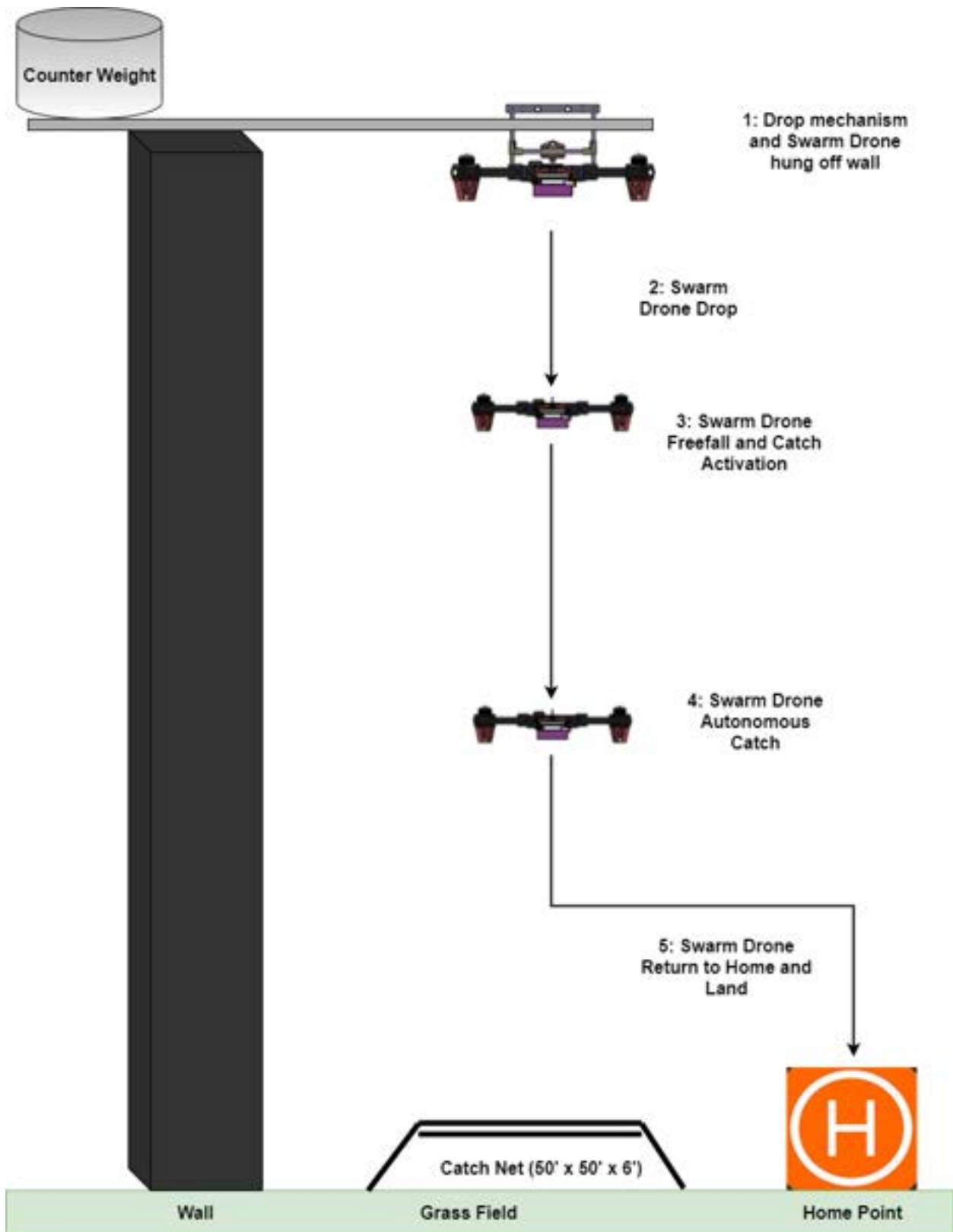


Figure 85: Drop Mode test overview



**Figure 86: Wall Drop Mode test long exposure**

#### 5.11.5 Carrier Drone V1 Air Frame Test

Given the scale of Carrier Drone designs and their experimental nature, iterative validation of the frame versions was critical. In September 2021, the Carrier Drone V1 was completed and first subject to these evaluations. Tests were a series of ground and air trials of the air frame in a quadcopter configuration. An abbreviated motor configuration, instead of the full 12 motor setup, was employed to remove any potential confounding factors that might influence the team's assessment of the frame only. Tests of the V1 frame specifically involved inspecting the rigidity and tolerance stack-up of the constructed assembly and confirmation of the functionality of power distribution components. In a laboratory environment, the electrical functionality and frame structure was confirmed at the beginning of September 2021.

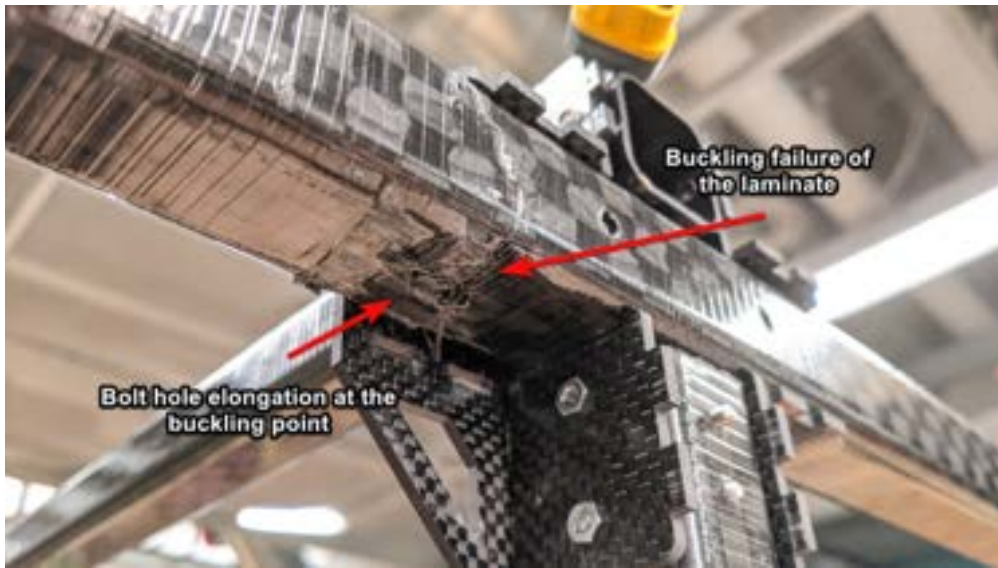
Subsequent tests of the Carrier Drone V1 involved powered flight trials. The goal of these was to confirm motor configuration, propeller orientation, and the attitude control of the vehicle. In addition to ground confirmations, the main goal of flight tests was to get the vehicle flying reliably enough to tune its on-board controllers [44]. These consist of multi-leveled attitude, rate, velocity, and position PID controllers that must be manually tuned for experimental vehicles. A manual hover test was planned to assess the performance of the vehicle and begin tuning parameters for these controllers to achieve stable flight.

In addition to plans to tune the Carrier Drone's flight controller, multiple cameras and viewing locations were established to inspect the dynamics of the frame in flight. Flexibility, aggressiveness of attitude correction, and the extent of positional drift were critical for performing such assessments. In addition to visual observation, the PX4 flight controller stored data for all of the vehicles sensors after each flight for detailed analysis. This is expanded upon in subsequent paragraphs.

In the middle of September 2021, the Swarm Carrier team conducted a flight test of the Carrier Drone V1 in accordance with the above test criteria. The vehicle passed all pre-flight checks and successfully hovered with no positional drift. Handling was noted to be slightly unresponsive which was indicative of the large size and weight of the vehicle. During the second hover test however, the vehicle experienced a rapid and unexpected throttle increase that led to an increase in vehicle altitude. This was interpreted as a vehicle runaway by the team members who executed a motor stop of the vehicle after it reached a height 10 ft above its expected hover altitude. This resulted in an unpowered freefall from 15 ft and ground impact. The result was medium damage to the frame, light damage to several fixtures, and no damage to electronics or sensors. Fig.87 below shows examples of the frame damage which include buckling failure of the cantilever members holding the motors. Fig.88 below also shows the first successful hover test of Carrier Drone V1. Critically, it shows static frame deformation whose impact on the flight controller is discussed subsequently.



(a) Carrier Drone V1 failure of motor cantilever arm



(b) Buckling failure mode of carbon laminate (Carrier Drone frame)  
Figure 87: Examples of damage to the Carrier Drone V1 (Post Crash)



**Figure 88: Carrier Drone V1 successful hover**

The critical takeaway from observation of frame damage was that the motor cantilever arms were the weak point of the Carrier Drone V1 design. During the free fall, the front corners of the frame made impact with the ground first. This resulted in the formation of an instant center of rotation about the front of the frame that accelerated the impact of the rear corners. The resulting impulse caused the momentum of the motors to buckle the cantilever arms they were mounted on. Critical failures occurred at the stress concentrations generated by the bolt holes with the frame's connectors. In addition to subsequent analysis of the flight logs, these visual conclusions motivated the improvements to the Carrier Drone's design outlined in Section 5.3.

The crash of the Carrier Drone V1 during the second hover resulted in an investigation of log files in order to understand the reasons and causes behind the uncommanded ascent of the vehicle. To assess flight data, Pixhawk 4 FC logs were analyzed that contained information on every operation, process, and parameter that was set on the vehicle for each flight. This allowed the group to have an extremely in depth look into the control loop, perceived pilot input commands, and parameters set during the final crash.

The analysis determined that during the final seconds of the vehicle's flight before it suddenly ascended, a manual yaw input by the pilot was received by the flight controller. At the 6:05:67 timestamp the pilot gave a slow ramp input to the vehicle, which resulted in the vehicle slowly trying to yaw. The pilot continued to give yaw input but at a higher magnitude now in an effort to get the vehicle to yaw faster, finishing at approximately 30% yaw input at 6:05:852 timestamp. At this point the vehicle control loop started to ramp exponentially in an effort to achieve the desired yaw rate and deflection desired by the pilot. By 6:06:245, the motors tried to ramp to 100% power in order achieve the yaw angular rate setpoint of 145 degrees per second. This had an unintended effect of causing the vehicle to rise in altitude drastically, without pilot input, as the vehicle tried to yaw to the desired setpoint. By 6:06:468, the pilot cut throttle completely, but the vehicle still maintained high individual motor outputs and continued its ascent. The control loop was then commanding an uncontrolled ascent sequence. The pilot then initiated an emergency motor kill to stop the vehicle from ascending. Fig. 89 shows the Pixhawk 4 logs for the timestamps previously mentioned.

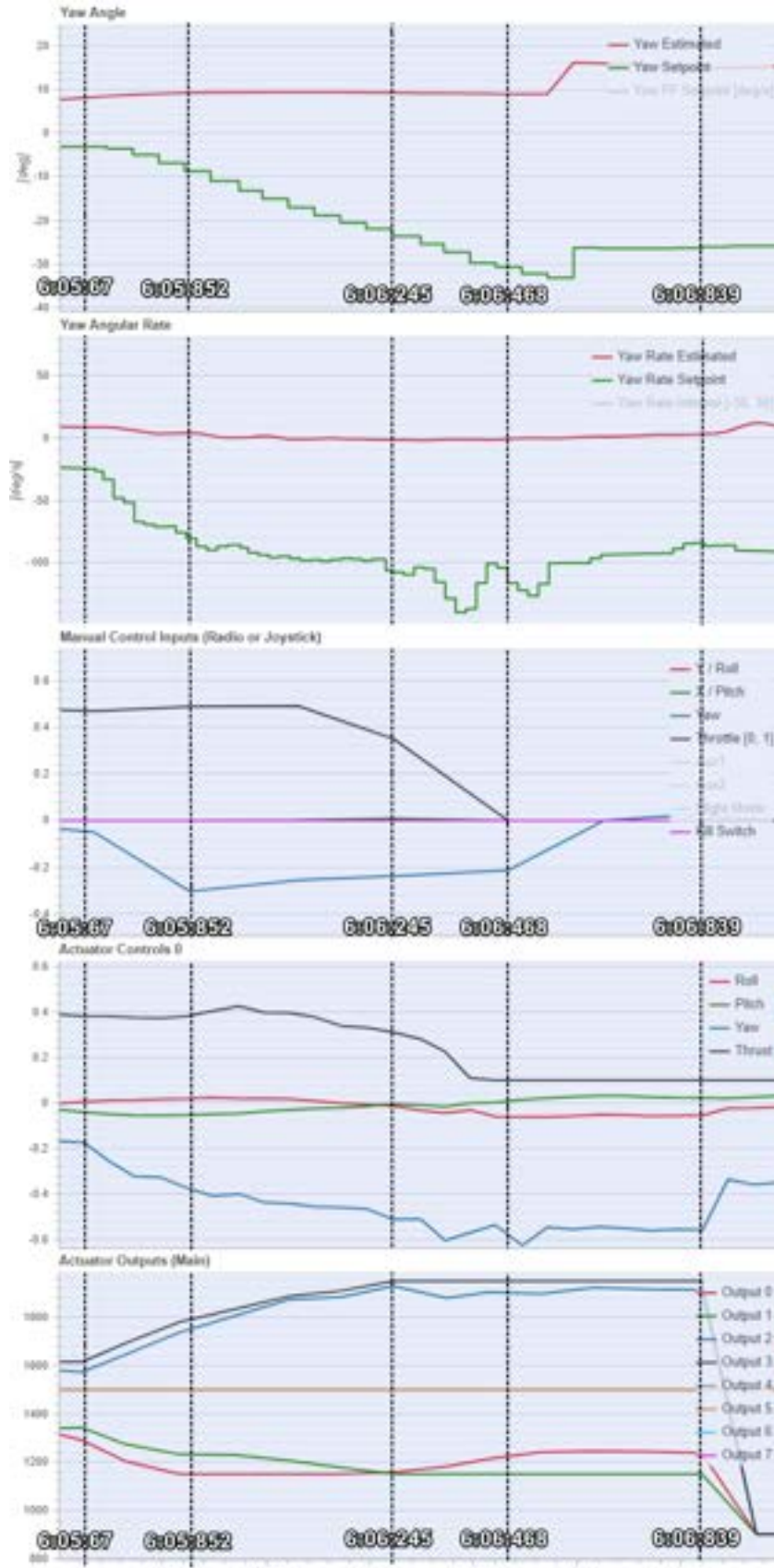


Figure 89: Pixhawk 4 flight logs for Carrier Drone V1 quadcopter hover test

One key factor that caused the ascent was the limits for the yaw rate, pitch rate, and roll rate programmed into the vehicles flight controller. These gains were set for vehicles of much smaller size, meaning that they were incompatible with the scale of the Carrier Drone. This allowed the control loop to try to achieve rates of rotations as high as 220 degrees per second, which would only be possible on smaller vehicles. Another factor was the parameter called Air Mode which exponentially adds rate and magnitude to control loop setpoints to improve vehicle maneuverability. This caused the control loop's yaw response to ramp rapidly which was an unexpected behavior according to the test's procedure.

Moving forward the group will carefully consider flight specific parameters such as rate limits, flight modes, and PID controls. With this new found knowledge on the limited applicability of small sUAS to the larger UAS vehicles, the group will start with a clean slate on tuning the vehicle. In addition further safety measure will be taken for subsequent tests, as chances of such an event are low but not fully erased. The Carrier Drone V3 hover tests will have the vehicle tethered to the ground to create a mechanical hardstop for flight runaways. Safety measures such as tethers will be used until the vehicle has had its flight dynamics fully checked. Despite the failure event, this quadcopter test proved incredible valuable for the team and has defined a faster route to completing the Carrier Drone.

#### 5.11.6 Carrier Drone V3 Air Frame Test

The Carrier Drone V3 was developed and manufactured within the one month period following the Carrier Drone V1 test. It was essential that the group validate the flight performance, dynamics, and wire tensioning mechanisms as soon as possible to allow for work to continue on other subsystems of the project. The tests consisted of a series in air trials in a similar vein to the Carrier Drone V1 tests. Due to the rapid timeline of the capstone project, the Carrier Drone V3 was configured with its full octocopter motor configuration to avoid the need for a separate test for the quadcopter and octocopter motor configuration. Electronics, wiring, and flight critical subsystems were validated in a laboratory setting before flight operations.

A critical objective of the test was to monitor the frame's rigidity during testing. It was previously noted during the V1 tests that the frame dynamically deflected based on the loads imparted on it from the motors. The previously mentioned wire tensioning would be scrutinized during the test in order to prove its ability to correct static flexure and prevent dynamic vibration.

Another of the concerns prior to the flight test was the use of a non-centrally-mounted flight controller. Typical UASs have onboard accelerometers and gyroscopes mounted as close to the center of rotation and center of mass as possible. While parameters were adjusted in the flight controller of the Carrier Drone, it was unclear if there would be adverse flight dynamics.

The subsequent tests of the Carrier Drone V3 involved powered flight trials. The main goal of these was to confirm motor configuration, propeller orientation, and the attitude control of the vehicle. The secondary goal was to validate the design decisions for the V3. A manual hover test was planned to assess the performance of the vehicle and make any tuning alterations to parameters in order to achieve stable flight. Similarly to the previous test, multiple cameras at different viewing angles and internal flight logs were used to record the tests.

On October 24th the Swarm Carrier team conducted a flight test of the Carrier Drone V3 in accordance with the above test criteria. The initial hover occurred while tethered to the ground on

all four corners approximately 10 feet diagonally from the Carrier. Fig. 90 displays the tethered hovering Carrier Drone. During the initial hover, only roll, pitch, and throttle manual inputs were given. The vehicle presented stable flight dynamics and responded aptly to control inputs. The vehicle was landed and the second hover test was started. In the second hover test roll, pitch, yaw, and throttle manual inputs were given. The vehicle maintained stable flight dynamics and responded well to control inputs. Unlike the previous V1 test, there was no altitude increase caused by yaw inputs. Additionally the pilot deemed that no PID tuning was required for the yaw, pitch, or roll axes. The third flight test continued similarly with the pilot setting the Carrier into "position hold" mode where the flight controller made autonomous adjustments to maintain the same 3D position. The Carrier successfully entered position hold and was exceptionally stable. At this point the pilot felt comfortable enough with the airframe to remove the tethers and to attempt simple autonomous missions. The fourth and fifth flight tests involved the Carrier drone autonomously taking off and holding position at a waypoint. In the fourth test the pilot took manual control when the Carrier pitched to traverse to the waypoint. This proved the functionality of the software's manual override capability. The fifth test saw the Carrier successfully take-off and traverse to a waypoint and hold position. The sixth and final test performed involved a fully autonomous test where the Carrier took-off, traversed to three waypoints, returned to the start position, and autonomously landed itself. Fig. 91 shows multiple angles of the Carrier Drone V3 in untethered autonomous flight. The Carrier was able to successfully complete a fully autonomous mission. Fig. 92 shows the Swarm Carrier team behind the Carrier Drone V3.

The result from the Carrier Drone V3 flight tests was to confirm that the Carrier was capable of sustained stable flight. The wire tensioning and the reduced frame size drastically increase frame rigidity thus improving flight dynamics.



**Figure 90: Tethered Carrier Drone flight test**



**(a) Distant view: Carrier Drone flight test**



**(b) Bottom view: Carrier Drone flight test**



**Figure 92: Team picture: Carrier Drone V3 maiden flight**

### 5.11.7 Multi-system Integration Tests

On December 4th, the team conducted the full multi-system integration test at Northeastern University's Dedham campus. The goal for this test was to demonstrate the system's capability to deploy and reintegrate a Swarm Drone in a single mission. Up until this point Swarm Carrier's subsystems had only been tested independently. There were two safety pilots for both the Swarm Carrier and the Swarm Drone who said "signal is good" before flight. The Swarm Carrier was flown manually to an altitude of 20 meters. Then the manual flag to enable Drop Mode was enabled. The bottom row of the Multidrop Bay was opened and the Swarm Drone fell. It detected the drop and autonomously corrected itself. Then, the Swarm Carrier was manually landed and the Swarm Drone was reintegrated into the Multidrop Bay while it was on the ground.

The test was a success as the team was able to successfully drop a single Swarm drone and subsequently land and reintegrate back into the Multidrop Bay. Additionally, the team validated that the Carrier Drone could fly with all three Swarm Drones in the Multidrop Bay.

Although the test was considered a success, the project was unable to fulfill all mission objectives due to weather limitations. Although the team was able demonstrate system functionality with a single Swarm Drone, it was unable to utilize the full capabilities of the system with multiple Swarm Drones. The cold weather proved to be a major detrimental factor in system operations as electronics and operators alike struggled in the almost freezing temperatures. During ground checks of the Multidrop Bay, the linear servo mechanisms between levels demonstrated uncontrolled behaviors. These errors included uncommanded actuations, inconsistent servo opening speeds, and different servo endpoints. These errors detrimentally impacted the reliability of the Multidrop Bay and hindered the success probability of multi-vehicle tests.

In the field, the team performed detailed troubleshooting in an effort to increase system reliability. The connections between the servos and the micro controller had already been calibrated previously which ruled out theories of mechanical error. The servo's endpoints and actuation speed were also tuned in the days leading up to the test with satisfactory results. This led to the conclusion that the driving factor for the errors was the cold temperature which negatively impacted the servo's position and speed control. Despite efforts to address the symptoms of the cold, the group deemed the test unfeasible with more than a single Swarm Drone.

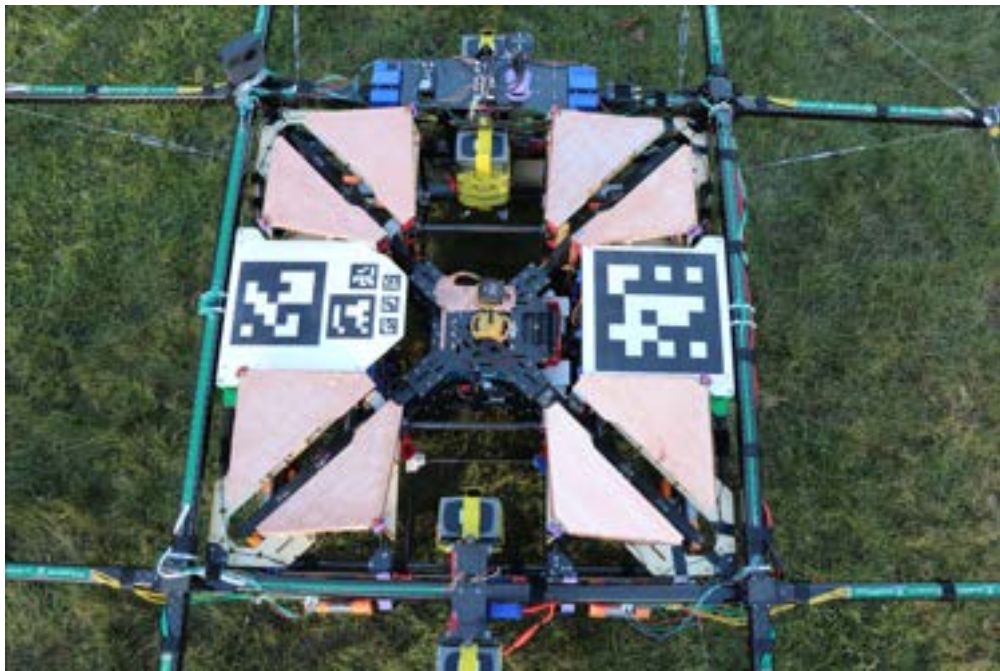
The crucial takeaway from this test was that the Swarm Carrier system could function given the proper temperature and weather. The team had previously demonstrated individual subsystem functionality and was able to utilize a single Swarm Drone for the multi-system integration test. The system's use of OTS components limited its operational temperature to 50-60 °F. Below these temperatures battery performance deteriorates and network connectivity between vehicles becomes less reliable. These factors made failure of the Multidrop Bay understandable as the team had never considered testing the system this late in the Capstone II cycle. Pictures of the system in operation and in the field are shown below.



**Figure 93: Carrier Drone hovering with two Swarm Drones**



**(a) Side view: Carrier Drone loaded with 3 Swarm Drones on the ground**



**(b) Top view: Carrier Drone loaded with three Swarm Drones on the ground**

**Figure 94: Carrier Drone loaded before flight tests**



Figure 95: Drop deployment of a single Swarm Drone from the Carrier Drone



**Figure 96: Long exposure of the Swarm Drone deploying from the Carrier Drone**

## 5.12 Design Review: MassDOT

The Swarm Carrier team invited Noel Zamot, as a connection to the MassDOT's UAV review team, to review the system in development. Noel Zamot is a retired Air Force test pilot turned entrepreneur with decades of experience in the aerospace industry and military systems testing. The team originally reached out to Rob Knochenhauer through the FAASTeam Online Directory which provides the public access to drone experts for system evaluation and safety assessment. Alongside Rob K, Andrew Mihaley, Robin Grace, and Terrence McKenna (the other members of the MassDOT), Noel was involved in the establishment of many core FAA regulations for drones in use today. Due to this, the team was highly interested in performing a system review with Noel and his team to evaluate the feasibility, legality, and test plans for the Swarm Carrier System.

The Swarm Carrier team's original plan was to apply for a special exemption (Section 44807) for experimental vehicle approval under the FAA. For this process, an FAA representative must physically inspect designs, codebases, and test procedures which was a huge logistics concern for the team. It was this issue that prompted the team to reach out to Noel as an individual with many connections in the drone industry and knowledge of laws.

After getting an understanding of the system, a series of meetings was set up with Noel spanning from the beginning of September to now. Delays between review meetings were required for Noel and his team to reach out to other FAA and industry representatives for information on the testing of the Swarm Carrier. These difficulties were attributed to the legal uniqueness of the Swarm Carrier system in that it violates FAA but is non-commercial and non-DOT sponsored. Therefore, many avenues had to be addressed to find a test plan that suited the Fall semester deadline.

To summarize key legal points, Noel first proposed that the team filed for 44807 to fly at Joint Base Cape Cod which is an officially designated site for experimental vehicle testing under the FAA. However, because the project has no DOD affiliations, the team would have to either go through the entire 4480 review or find a DOD affiliation through Northeastern to expedite testing. Neither of these outcomes were favorable for the team or MassDOT so other options were pursued.

Next, Noel reached out to FAA representatives regarding advice for student groups testing experimental unmanned aerial systems. The team was then connected to the educational director of the AMA (Academy of Model Aeronautics), Kyle Jaracz, for advice on operating experimental vehicles as an independent student research group. The AMA is a coalition of organized RC hobbyist fliers with FAA approved flying fields all over the US. He recommended that the team test under an amateur flight status, therefore skirting the commercial requirements of the FAA. Noel presented this information to the team and connected members with AMA chapters in the Boston area for final flight approval.

In addition to discussion of regulations, Noel also critiqued the team's test plans and provided valuable feedback to structure the project more efficiently. He provided extensive reviews and feedback on the team's SOP writing strategies, ORM generation for external entities, and system plans. As an external entity, he was able to identify ambiguities that the team could not internally see. Following these reviews, the Swarm Carrier team was able to efficiently draft SOPs and ORMs for external entities, Capstone, Northeastern's Risk Services, and Northeastern's UAV review board (UASRB).

From a test perspective, Noel provided valuable organization of the team's plans to achieve

a full system test by the end of the term. Specifically, he promoted compartmentalized tests of subsystems to gain confidence before the final integration of the carrier drone, payload, and swarm drones. This allowed the team to efficiently structure its tests which have been largely successful thus far.

### 5.13 Final Design

Before the completion of the final multi-system integration tests 5.11.7, the designs of the three subsystems of the Carrier Drone, Swarm Drones, and the Multidrop Bay completed. The comparison between the CAD of the design and the final constructed subsystems are shown below in Fig. 97 and Fig. 98



Figure 97: CAD of completed system



**Figure 98: Completed system**

#### **5.14 Regulations**

The Swarm Carrier capstone has pivoted away from registering the system as a commercial UAS and instead as a recreational system. This will allow the project to avoid the legal headache of Part 107 regulations and operate a UAS without weight regulations and the 1:1 ratio of pilots to drones [45]. After talking with MassDOT representatives, they highlighted a pathway to operating a UAS under the recreational banner. A stipulation though of the recreational operation of a UAS is that it must be conducted under a community-based organization's approval at a fixed site [46]. To meet this requirement, the MassDOT connected the group with the AMA, a large hobby organization that has fixed flight sites throughout the state of Massachusetts. The AMA informed the capstone group that they must register as AMA members in order to use any AMA field, but seemed very receptive of the idea of using one of their fixed sites for the final system-level demonstration. The group is currently working to reestablish the Northeastern University AMA charter, which the members of the group had previously established during their time in Aerospace NU. As of this point, the project has a clear legal direction that has been used to conduct testing and final demonstration for the end of Capstone II.

## **6 Conclusions**

The Swarm Carrier System has been substantially developed from previous research with the goal of conducting a full-circle test. Hardware developments have been dedicated to revising the Swarm

Drones to their V3 configuration, validating the Carrier Drone's design, and improving the Multidrop Bay. During Capstone I, the group completed assembly of the Carrier Drone V1, and performed an initial hover test. The group has designed, manufactured, and tested the final version of the Carrier Drone. The team has also finished development of the Multidrop Bay in preparation for an autonomous landing test. A portion of the Swarm Drone fleet has been upgraded to the V3 configuration, with small changes needed to bring all 3 versions to completion.

Software development has been focused on building the architecture for controlling the drones. Throughout Capstone II, various improvements have been added to the existing system; consistency in Drop Mode and GPS initialization, as well as updated precision landing logic. With these improvements, simulation tests have moved to field tests for features such as precision landing. There has also been significant work on the GUI for field tests and these systems are being tested actively.

The team successfully tested precision landings and drop deployment both using targeted subsystem tests and full-system integration evaluation. The latter validated the proposed method of Swarm Drone transportation, deployment, and recovery. Future projects may entail using more robust wireless communication than WiFi such as Software Defined Radios, usage of active alignment techniques of the landing geometries, or implementation of the system into specific Swarm Drone applications.

The Swarm Carrier team has passed off all advancements, resources, vehicles, and innovations of the system to the students of Northeastern's aerospace engineering club: AerospaceNU. From this path, the research of the project will continue to educate and drive future students towards novel engineering challenges.

## 7 Intellectual Property

### 7.1 Description of Problem

The problem statement for this capstone project is to design, manufacture, and test a system capable of deploying and recovering a swarm of multirotor UAS.

### 7.2 Proof of Concept

The capstone has developed extensive systems and tests in order to complete the problem statement. This project is multidisciplinary, as all subsystems of the system heavily use mechanical, electrical, and software intensive concepts. The members of the project have extensive experience in numerous fields of unmanned aerial vehicle (UAV) development and usage, which is extensively used in the development of this capstone

At the subsystem level, the Carrier Drone is responsible for carrying in flight the combined payload of the Multidrop Bay and Swarm Drones. The Carrier Drone is controlled in flight by a Pixhawk 4 (PX4) microcontroller, which is responsible for controlling the motors, internal accelerometers and gyroscopes, global positioning system (GPS), barometer, and telemetry. The PX4 is in communication with an NVidia Jetson Nano Computer, which is responsible for Avionics, interfacing with the Multidrop inter-integrated circuit (i2c) link, and communicating by WiFi with the ground station.

The Multidrop bay is responsible for both holding the Swarm Drones during flight of the Carrier Drone, as well as deployment of Swarm Drones before the mission and recovering the Swarm Drones after the mission. The servos that facilitate the actuation are controlled by a microcontroller. This is then connected to the Carrier Drone and is in constant communication via an i2c link.

The Swarm Drones are the focus of the system, and are responsible for aerial drop deployment from the Multidrop Bay, as well as recovery with the Multidrop Bay after completing the missions. Like the Carrier Drone, the Swarm Drones are outfitted with PX4 microcontrollers which control the motors, internal accelerometers and gyroscopes, GPS, barometer, and telemetry. The PX4 is in communication with an NVidia Jetson Nano Computer, which controls avionics, the external camera used for computer vision during a precision land, and the copper contact sensing between the landing guides of the Multidrop Bay and the copper bottoms of the Swarm Drones.

During the mission, the subsystems of the Carrier Drone, Multidrop Bay, and Swarm Drones are viewable by the ground control. The ground control contains a graphical user interface (GUI) for overall system telemetry display, as well as options for user input. This is then connected by WiFi link to the Carrier Drone and Swarm Drone for constant communication.

The capstone project has many smaller subsystems which combine to form the overall system. To verify the subsystems, individual tests were developed to validate the Swarm Carrier's safety and functionality. These tests focus on smaller subsystems at first, and combine in later tests after validating the base concepts to scale up to a full system test. These tests were carefully developed following approved standard operating procedures (SOPs).

To validate and inform future design decisions on frame design, motor configuration, motor specification, and propeller type, a thrust test was developed. Using an off the shelf motor thrust

stand, the motor thrust, voltage, current, torque, and rpm are recorded. This data is used to measure both single rotor and coaxial propeller configurations to further inform design decisions.

To validate and inform future design decisions on software integration and hardware components of the Multidrop Bay and Swarm Drones, a precision land test was developed. This tests the fidelity and precision of the swarm drones to land in a set location using fully automated computer vision. The test involves one of the Swarm Drones taking flight from the ground, hovering over an ArUco marker, and landing on top of the marker. This validates that the Swarm Drones are capable of automatically landing inside of the Multidrop Bay without manual inputs.

To validate and inform future design decisions on the Swarm Drone and Multidrop Bay, a drop mode test was developed. This tests the ability of the Swarm Drone to arm and stabilize itself after dropping from the Multidrop Bay. This test involves dropping a single Swarm Drone from a high wall and testing whether the drone activates as expected. If the drone does not catch itself as intended, a safety net is in place below to prevent loss of the Swarm Drone. This validates the custom software developed to catch the drone after it is released from the Multidrop Bay, and it can then continue on its mission.

To validate and inform future design decisions on the Carrier Drone, an air frame test was developed. This tests the functionality of the frame as a whole, and sees if there are any vibration issues with the frame. The Carrier Drone takes off without any payloads, and its pitch, roll, and yaw performance are evaluated qualitatively by the pilots. The frame is also analyzed for vibration using the onboard sensors. This test validates design decisions for the current frame, which informs development of the second version of the frame.

To validate subsystem integration between all of the subsystems, a combined tests was developed. This tested the capability of the Carrier Drone to lift and transport the Multidrop Bay and three Swarm Drones, the ability of the Carrier-Drone-mounted Multidrop Bay to deploy and reintegrate the Swarm Drones, and the functionality of the Swarm Drones to successfully activate midair from a Carrier Drone deployment and autonomously land into the Carrier Drone. This final test validated the system as a whole and proved it met the goals defined in the problem statement.

### **7.3 Progress to Date**

This project is broken up into the subsystems of the Carrier Drone, the Swarm Drones, and the Multidrop Bay. Each subsystem has had its separate design, test, and iteration phases:

The Carrier Drone V1 was designed and manufactured using a custom-built 3 axis tube CNC. The electronics, including electronic speed controllers (ESC), flight controllers (FC), and power distribution boards (PDB) have all been mounted on the vehicle. Many of these electronics mounting plates have been laser-cut out of wood for prototyping purposes. Thrust tests were conducted to tabulate the motor characteristics of planar and coaxial motor configuration to develop the final Carrier Drone motor and propeller configuration. Construction for the Carrier Drone V1 with a quadcopter motor configuration was completed. This quadcopter Carrier was test flown and revealed several issues with the design such as static and dynamic torsion and flight control software. Following the V1 flight test, the Carrier Drone V3 was designed. Design improvements included reducing overall size to an octocopter motor configuration and adding cable tensioning to increase overall rigidity. The Carrier Drone V3 was successfully built and flight tested with superior flight dynamics. The flight test proved that the Carrier Drone was capable of carrying the Swarm Drones

and Multidrop Bay for the desired flight duration.

The Multidrop Bay V3 has been manufactured and tested to work with the linkage mechanisms. The V3 has had modifications done to the slots of the linkages to ensure consistent operations. These iterations to the linkage system have produced a system capable of consistently operating with the full weight of a Swarm Drone resting on them. The copper contact sensing on the bay has also been tested. This provides feedback to the swarm drone during landing as to when it has made physical contact with the Multidrop bay. The passive landing geometries have been iterated several times to allow for larger landing position variance.

The Swarm Drones V3 have had three vehicles fitted with the new PX4 FCs and shielding on their cabling to reduce electric and magnetic field (EMF) noise. Custom TPU and copper contact sensing landing gear were mounted on the Swarm Drone fleet for an electronic feedback for when they make physical contact with the Multidrop Bay. The precision landing feature was first tested alone and worked proving the aspect of autonomy to land within a small area only using onboard sensors of the Swarm Drone. Once proven successful, the precision landing feature was tested while landing inside the Multidrop Bay successfully proving the recovery aspect of the project. In these same tests for the Swarm Drone V3s, the GUI has been proven to be very successful, allowing users in the field to view PX4 parameters. Drop mode for the Swarm Drones has been successful in simulations, drops from a high wall, as well as deployments from the Carrier Drone. The successful deployments proved the feasibility of the deployment method used in this project.

This summary encapsulates the total progress of the Swarm Carrier capstone project.

## 7.4 Individual Contributions

**Table 3: IP team member contributions**

Team Member	Discipline	Airframes	Payloads	Interface	Autonomy
John Buczek	EE, Power Systems	Thrust validation, electronics debugging, configuration, and test pilot	Developing contact sensing electronics for the Multidrop Bay. Integrating sensing solutions for telemetry on all vehicles	Evaluating ROSBoard and developing test methods	Interfacing sensors with current software architectures and supporting tests
Erik Little	ME	Designing fixtures, connectors, mechanisms, and the new octo-motor configuration for the Carrier Drone. Helping with development of Swarm Drone V3s	Completing assembly, tolerance stack-up mitigation, and phase-in changes for the Multidrop bay	Assisting with tests and shaping design requirements around software functionality	Assisting with tests and shaping design requirements around software functionality
Michael Tang	ME, Mechatronics	Designing fixtures, connectors, mechanisms, and the new octo-motor configuration for the Carrier Drone.	Assisting with assembly of Multidrop Bay, phase in changes, and testing of Swarm Drone to Multidrop interface	Carrying out Pixhawk 4 configuration and parameter debugging	Assisting with tests and shaping design requirements around software functionality
Blake McHale	CE, Vision/ML/Algos	Conducting simulations of all airframes using Gazebo. Modeling real world dynamics to test algorithms	Developing architectures for precision landings around excising hardware capabilities. Interfacing with sensors and actuators with higher level actions	Researching methods of communication between the Pixhawk, computer, and vehicle network. Executing and debugging simulated and real-world tests	Developing precision land, drop-mode, and collaborative searching, queuing, and recovery methods
Josh Field	CE, Vision/ML/Algos	Developing search metrics for swarm autonomy given the operational ranges of airframes	Developing architectures for precision landings around excising hardware capabilities. Interfacing with sensors and actuators with higher level actions	Developing ROSBoard as Swarm Carrier's GUI, aiding in the development of communication between the Pixhawk, computer, and network	Developing precision land, drop-mode, and collaborative searching, queuing, and recovery methods
Noah Ossanna	ME, Mechatronics	Developing motor configurations, connector design, and electronics organization for the Carrier Drone. Releasing the Swarm Drone V3 design with new fixtures, sensors, and electronics	Conducting phase-in changes on the Multidrop Bay and helping with assembly. Testing collision detecting sensing methods and planning test procedures	Assisting with the configuration, calibration, and debugging of Pixhawk flight controllers and sensors	Managing the connection between hardware and software development of high level tasks

## 7.5 Future Work

Having validated the proposed method of Swarm Drone transportation, deployment, and recovery, the Swarm Carrier team has no future plans to continue work outlined by the provided problem statement. The team expects that many future project will stem from the research that they have provided. Future projects may entail using more robust wireless communication than WiFi such as Software Defined Radios, usage of active alignment techniques of the landing geometries, or implementation of the system into specific Swarm Drone applications.

## 8 References

- [1] A. Gajeski, “The right drone for your department.” <https://botlink.com/blog/2018/7/9/the-right-drone-for-the-job>, Jul 2018.
- [2] G. F. Miller, “Persistent Surveillance Unmanned Aerial Vehicle and Launch/Recovery Platform System and method of using with secure communication, sensor systems, targeting systems, locating systems, and precision landing and stabilization systems ,” U.S. Patent 10,890,927, Jan. 2021.
- [3] H. Chin and K. Carraha, “Airborne Drone Launch and Recovery Apparatus,” U.S. Patent 10,179,648, June 2016.
- [4] A. Bondyra, S. Gardecki, P. Gąsior, and W. Giernacki, “Performance of Coaxial Propulsion in Design of Multi-rotor UAVs,” in *Challenges in Automation, Robotics and Measurement Techniques* (R. Szewczyk, C. Zieliński, and M. Kaliczyńska, eds.), (Cham), pp. 523–531, Springer International Publishing, 2016.
- [5] “Introducing alta x.” <https://freedflysystems.com/alta-x>, May 2021.
- [6] S. Garrido and S. Nicholson, “Detection of aruco markers.” <https://docs.opencv.org/3.4.15/d5/dae/tutorialarucodetection.html>.
- [7] M. Colledanchise and P. Ögren, *Behavior Trees in Robotics and AI*. CRC Press, 1st ed., 2018.
- [8] L. Meier, “Overview.” <https://docs.qgroundcontrol.com/master/en/index.html>, Aug 2021.
- [9] L. Meier, “RTSPS/DDS interface: PX4-Fast RTSPS(DDS) bridge.” <https://docs.px4.io/master/en/middleware/micrortsp.html>, Jun 2021.
- [10] P. Doherty and P. Rudol, “A uav search and rescue scenario with human body detection and geolocalization,” in *AI 2007: Advances in Artificial Intelligence* (M. A. Orgun and J. Thornton, eds.), (Berlin, Heidelberg), pp. 1–13, Springer Berlin Heidelberg, 2007.
- [11] F. Afghah, A. Razi, J. Chakareski, and J. D. Ashdown, “Wildfire monitoring in remote areas using autonomous unmanned aerial vehicles,” *CoRR*, vol. abs/1905.00492, 2019.
- [12] J. Ornato, A. You, G. McDiarmid, L. Keyser-Marcus, A. Surrey, J. Humble, S. Dukkupati, L. Harkrader, S. Davis, J. Moyer, D. Tidwell, and M. Peberdy, “Feasibility of bystander-administered naloxone delivered by drone to opioid overdose victims,” *The American Journal of Emergency Medicine*, vol. 38, 06 2020.
- [13] F. Mancini, M. Dubbini, M. Gattelli, F. Stecchi, S. Fabbri, and G. Gabbianelli, “Using unmanned aerial vehicles (uav) for high-resolution reconstruction of topography: The structure from motion approach on coastal environments,” *Remote Sensing*, vol. 5, no. 12, pp. 6880–6898, 2013.

- [14] J. Buczek, L. Bertizzolo, S. Basagni, and T. Melodia, "What is a wireless uav? a design blueprint for 6g flying wireless nodes," WiNTECH'21, (New Orleans, LA, USA), Association for Computing Machinery, 2021.
- [15] P. Pounds, R. Mahony, and P. Corke, "Modelling and control of a quad-rotor robot," 12 2006.
- [16] M. S. Bradbury, "Drone Deployment Apparatus for Accommodating Aircraft Fuselages ," U.S. Patent 10,578,398, Mar. 2020.
- [17] W. Heinzmann, "Apparatus for Recovery of Unmanned, Reusable Aircraft," U.S. Patent 5,109,788, May 1992.
- [18] M. Grubb, "Locking Line Capture Devices for Unmanned Aircraft, and Associated Systems and Methods," U.S. Patent 10,967,987, April 2021.
- [19] S. K. McGann and N. McGaha, "Unmanned Aerial Vehicle (UAV) Recovery System," U.S. Patent 10,800,547, Oct. 2020.
- [20] C. H. F. Foo and H. L. Hsi, "Apparatus and Method for Aerial Recovery of an Unmanned Aerial Vehicle," U.S. Patent 10,589,859, Mar. 2020.
- [21] J. Peverill, A. Woodworth, B. Freudberg, and D. Cottrell, "Capturing Hook for Aerial System ," U.S. Patent 10,308,375, June 2019.
- [22] D. Davidson, " Methods and Apparatus to Deploy and Recover a Fixed Wing Unmanned Aerial Vehicle via a Non-Fixed Wing Aircraft ," U.S. Patent 10,133,272, Nov. 2018.
- [23] T. S. McKee and S. C. Roden, "UAV Launch and Recovery ," U.S. Patent 9,969,505, May 2018.
- [24] M. Yoffe, " Point Take-off and Landing of Unmanned Flying Objects ," U.S. Patent 9,637,245, May 2017.
- [25] R. C. Melish, K. J. Neeld, and R. L. Orner, " Unmanned Air Vehicle Recovery System ," U.S. Patent 9,527,604, Dec. 2016.
- [26] M. C. Allen, D. D. Hallerberg, and G. P. Timm, "Method for Recovering a UAV," U.S. Patent 9,527,603, Dec. 2016.
- [27] J. Goldie, N. Vitale, G. A. Downey, K. Leary, and W. Hafer, "Unmanned Aerial Vehicle(UAV) Recovery System," U.S. Patent 8,464,981, June 2013.
- [28] G. H. Lovell, E. C.-K. Hui, and M. K. Umbreit, "Stabilized UAV Recovery System," U.S. Patent 8,172,177, May 2012.
- [29] J. Snediker, M. A. Watts, and G. W. Corboy, "UAV Arresting Hook for use with UAV Recovery System ," U.S. Patent 7,143,976, Dec. 2006.

- [30] J. W. Lim, K. W. McAlister, and W. Johnson, "Hover performance correlation for full-scale and model-scale coaxial rotors," *Journal of the American Helicopter Society*, vol. 54, no. 3, p. 32005–3200514, 2009.
- [31] H. Otsuka and K. Nagatani, "Thrust loss saving design of overlapping rotor arrangement on small multirotor unmanned aerial vehicles," in *2016 IEEE International Conference on Robotics and Automation (ICRA)*, pp. 3242–3248, 2016.
- [32] "Matrice 300 rtk –built tough. works smart.." <https://www.dji.com/matrice-300?site=developer>.
- [33] Skydio, "Skydio x2 autonomous drone - skydio inc.." <https://www.skydio.com/skydio-x2>.
- [34] "Corvus one drone." <https://www.corvus-robotics.com/corvus-one>.
- [35] T. M. Cabreira, L. B. Brisolara, and P. R. Ferreira Jr., "Survey on coverage path planning with unmanned aerial vehicles," *Drones*, vol. 3, no. 1, 2019.
- [36] J. Malecha, "Drone operations over 55 pounds." <https://www.faa.gov/uas/resources/events/calendar/archive/2019uassymposium/media/HowToDroneOperationsOver55lbs.pdf>, 2021.
- [37] FAA, "Uas certification." <https://www.faa.gov/uas/advancedoperations/certification/>, Nov 2020.
- [38] G. Inc., "Pyrofil mr60h 24k." [https://www.rockwestcomposites.com/media/downloads/MR60H-24K\(02-2008\).pdf](https://www.rockwestcomposites.com/media/downloads/MR60H-24K(02-2008).pdf).
- [39] "Pyrofil hr50." <https://www.rockwestcomposites.com/media/downloads/HR40-14008-Fiber.pdf>, author=Grafil Inc.
- [40] Stromkalkylator, "Continuous current carrying capacity of a trace." <http://www.skottanselektronik.com/currenten.html>.
- [41] B. Prasad, "Busbar size and calculation." <https://bralpowerassociate.blogspot.com/2013/10/busbar-size-and-calculation.html>, Oct 2013.
- [42] D. Faonte, "Behaviortree/behaviortree.cpp: Behavior trees library in c++. batteries included.." <https://github.com/BehaviorTree/BehaviorTree.CPP>.
- [43] "Export a solidworks assembly to urdf." <https://wiki.ros.org/swurdfexporter/Tutorials/Export%20an%20Assembly>.
- [44] "Multicopter pid tuning." <https://docs.px4.io/master/en/configmc/pidtuningguidemulticopter.html>.
- [45] *Federal Aviation Administration, Docket No. FAA-2015-0150*. 2015.
- [46] *Federal Aviation Administration, Docket No. FAA-2019-0364*, vol. 84. 2019.